

INTEGRATING TRANSACTIVE ENERGY AND MACHINE LEARNING FOR RE-
ENERGIZING WASTEWATER TREATMENT PLANTS

by

Shriyank Somvanshi, B. Tech.

A thesis submitted to the Graduate Council of
Texas State University in partial fulfillment
of the requirements for the degree of
Master of Science
with a Major in Engineering
May 2023

Committee Members:

Tongdan Jin, Chair

Keisuke Ikehata

Emily Zhu Fainman

COPYRIGHT

by

Shriyank Somvanshi

2023

DEDICATION

Dedicated to my father, family, friends, and all those who have supported me throughout this journey. Their unwavering encouragement and belief in me has been the driving force behind my success. I am grateful for their constant love and support.

ACKNOWLEDGMENTS

I would like to express my sincere gratitude to my supervisor Dr. Tongdan Jin, for his guidance, encouragement, and support throughout my research work. His expertise, insightful feedback, and patience were instrumental in shaping my research ideas and in guiding me through the challenging phases of this project.

I would also like to thank the members of my thesis committee Dr. Keisuke Ikehata and Dr. Emily Zhu Fainman for their valuable guidance and expertise on domain knowledge of wastewater treatment and machine learning algorithms, respectively, which have greatly contributed to the quality and rigor of this thesis.

I am grateful to Industrial Engineering and Civil Engineering programs at Texas State University, for providing me with the financial support to conduct the cutting-edge research, and for providing the necessary resources and facilities to carry out numerical experiments. I would like to thank my colleagues for their stimulating discussions and for creating a supportive work environment that made this research experience enjoyable and fulfilling.

Finally, I want to express my heartfelt appreciation to my family, for their love, encouragement, and unwavering support throughout my academic journey. Without their constant encouragement and sacrifices, this achievement would not have been possible.

Thank you all for being a part of my journey and for contributing to the successful completion of my master's thesis.

TABLE OF CONTENTS

	Page
LIST OF TABLES	vii
LIST OF FIGURES	viii
LIST OF ABBREVIATIONS.....	x
ABSTRACT.....	xii
CHAPTER	
1. INTRODUCTION AND LITERATURE REVIEW	1
1.1 Background and Motivation	1
1.1.1 Wastewater Properties	1
1.1.2 Types of Wastewater Treatment	2
1.2 The State of the Art.....	3
1.2.1 Wastewater Treatment Technologies.....	3
1.2.2 Energy Sources in Wastewater Treatment.....	9
1.2.3 Energy Consumption in Wastewater Treatment.....	12
1.2.4 Machine Learning in Wind Speed Forecasting.....	16
1.3 Research Objectives and Contributions	17
2. RENEWABLE ENERGY AND POWER DEMAND OF WWTP	20
2.1 Renewable Energy Enabled Potable Water Reuse System.....	20
2.1.1 System Setting	20
2.2 Power Load Profile	21
2.2.1 Wastewater Treatment Plant	21
2.2.2 Water Treatment Plant	37
3. MACHINE LEARNING APPROACH TO SHORT-TERM WIND SPEED FORECASTING	45
3.1 Characterizing Wind Generation	45
3.1.1 Wind Power Generation Model	45
3.2 Wind Speed Forecasting using Machine Learning	48
3.2.1 Machine Learning in Forecasting Time Series Data.....	48
3.2.2 Data description of San Marcos	49
3.2.3 Forecasting Performance Metrics	51
3.3 Regression Models.....	53

3.3.1 Recurrent Neural Network.....	53
3.3.2 Long Short-Term Memory.....	62
3.3.3 Ensemble Model	68
3.4 Comparison of Regression Models.....	72
4. TRANSACTIVE ENERGY OPERATIONS IN WWTP FACILITY	76
4.1 Transactive Energy Trading as Emerging Market	76
4.1.1 Transactive Energy Market Mechanism	76
4.1.2 Best industry practices	78
4.2 Estimating Onsite Wind Turbine Power Generation	79
4.3 Transactive Energy Trading over 24 Hours in WWTP	84
4.4 Transactive Energy Trading for San Marcos Water Treatment Plant.....	89
4.5 Carbon Footprint Analysis.....	92
4.5.1 Calculation of Carbon Footprint of 3MW Wind Turbine	92
4.5.2 Calculation of Carbon Footprint of 1MW Wind Turbine.....	94
4.6 Life Cycle Cost Analysis	94
4.6.1 Quantification of Cost Elements.....	96
4.6.2 Payback Period.....	98
4.7 Wind Turbine Spacing	99
5. CONCLUSION AND FUTURE WORK	101
5.1 Conclusion	101
5.2 Future Work	103
APPENDIX.....	105
REFERENCES	138

LIST OF TABLES

Table	Page
Table 1.1 Principal components of concerns in wastewater treatment.....	2
Table 1.2 Bar screen classes	4
Table 1.3 Most used secondary waste-water treatment methods (aerobic)	6
Table 1.4 Most used secondary waste-water treatment methods (anaerobic)	7
Table 1.5 Disinfection methods with benefits and drawbacks	8
Table 1.6 Comparison of existing and proposed studies	15
Table 2.1 Power consumption in major processes.....	21
Table 2.2 WWTP with onsite solar and/or wind generation.....	22
Table 2.3 Descriptive statistical report for box plot of Melbourne WWTP	25
Table 2.4 Equipment level energy consumption in SMAT WWTP in Italy.....	36
Table 2.5 Descriptive statistical report for Monroe WTP.....	40
Table 3.1 Explanation of San Marcos wind speed data	50
Table 3.2 Comparison of MSE, MAE and R^2 errors at different consideration times	58
Table 3.3 Architecture of the model	59
Table 3.4 Comparison of MSE, MAE and R^2 errors at different consideration times	65
Table 3.5 Architecture of the model	66
Table 3.6 Comparison of error scores for first ensemble model in 24-hour ahead forecasting.....	73
Table 3.7 Comparison of error scores for second ensemble model in 24-hour ahead forecasting	73
Table 4.1 Approximate wind shear exponent range in the USA	81
Table 4.2 Output power of RNN, LSTM and ensemble models on 03/16/2018 with 1MW WT..	82
Table 4.3 Output power of RNN, LSTM and ensemble models on 03/16/2018 with 3 MW WT.	83
Table 4.4 Energy consumption of different WWTP.....	84
Table 4.5 Estimated surplus energy from 3 MW wind turbine for April 2018	88

LIST OF FIGURES

	Page
Figure 1.1 Flow chart of wastewater treatment plant	3
Figure 1.2 Energy distribution in conventional AS systems.....	13
Figure 2.1 Renewable energy enabled potable water reuse (REPWR) infrastructure.....	20
Figure 2.2 Daily power demand of Melbourne wastewater treatment plant from 2014-2021	23
Figure 2.3 Yearly box plot for power demand of Melbourne WWTP.....	24
Figure 2.4 Mean comparison of power demand of Melbourne WWTP	26
Figure 2.5 Histogram showing power demand of the Melbourne WWTP from 2014 to 2021	28
Figure 2.6 Probability plot of 2014 power demand	29
Figure 2.7 Probability plot of 2015 power demand	30
Figure 2.8 Probability plot of 2016 power demand	31
Figure 2.9 Probability plot of 2017 power demand	31
Figure 2.10 Probability plot of 2018 power demand	32
Figure 2.11 Probability plot of 2019 power demand	33
Figure 2.12 Probability plot of 2020 power demand	34
Figure 2.13 Probability plot of 2021 power demand	35
Figure 2.14 Machine level energy consumption SMAT WWTP in Italy	35
Figure 2.15 Daily power demand of Monroe water treatment plant from 2010-2019	37
Figure 2.16 Yearly box plot for power demand of Monroe WTP (2010-2019)	39
Figure 2.17 Mean comparison chart of power demand of Monroe WTP.....	41
Figure 2.18 Histogram of power demand of Monroe WTP (2010-2017).....	43
Figure 2.19 Histogram of power demand of Monroe WTP (2018-2019).....	44
Figure 2.20 Process level energy consumption in a water treatment plant in USA.....	44
Figure 3.1 A typical wind power curve	46
Figure 3.2 Weibull wind speed distributions	48
Figure 3.3 Wind speed profile for San Marcos (2011-2019).....	49
Figure 3.4 Boxplot for variation of hourly wind speed from 2011 to 2019.....	50
Figure 3.5 RNN architecture (the sequence {start-update loop-end}).....	54
Figure 3.6 RNN architecture (the update loop)	55
Figure 3.7 RNN learning curve.....	59
Figure 3.8 RNN prediction curve (2011-2019).....	61
Figure 3.9 Last 7 days RNN prediction curve (2011-2019)	61
Figure 3.10 LSTM cell architecture.....	63
Figure 3.11 LSTM learning curve	67
Figure 3.12 LSTM prediction curve (2011-2019)	67
Figure 3.13 Last 7 days LSTM prediction curve (2011-2019)	68
Figure 3.14 A simple ensemble architecture.....	69
Figure 3.15 Ensemble prediction curve (2011-2019)	71
Figure 3.16 Last 7 days ensemble prediction curve (2011-2019).....	72
Figure 3.17 Last 7 days all model predictions (2011-2019)	74
Figure 4.1 A transactive energy setup involving prosumers.....	78
Figure 4.2 Daily power consumption analysis with 1 MW turbine (April 2018).....	85
Figure 4.3 Daily power consumption analysis with 3 MW turbine (April 2018).....	86

Figure 4.4 Peak demands in Melbourne WWTP87
Figure 4.5 Daily power consumption analysis with 3 MW turbine (Mar -Aug. 2019)89
Figure 4.6 Daily Energy consumption Analysis of San Marcos WTP with a 3 MW turbine.....90
Figure 4.7 Daily Energy use of San Marcos WTP with two 3 MW turbines (2019).....91

LIST OF ABBREVIATIONS

Abbreviation	Description
A/A/O	Anaerobic-Anoxic-Oxic
A/O	Anoxic Oxidation
AS	Activated Sludge
AD	Anaerobic Digestion
ANN	Artificial Neural Network
AWPF	Advanced Water Purification Facility
ACUA	Atlantic County Utilities Authority
AI	Artificial Intelligence
BES	Battery Energy Storage
BPTT	Back-Propagation Through Time
BOD ₅	Five-Day Biochemical Oxygen Demand
BOD	Biochemical oxygen demand
CO ₂	Carbon Dioxide
CHP	Combined Heat and Power
DWT	Discrete Wavelet Transform
DG	Distributed Generation
HVAC	Heating, Ventilation and Air Conditioning
KDE	Kernel Density Estimation
IQR	Interquartile Range
LSTM	Long Short-Term Memory
MGD	Million Gallons Per Day

MSE	Mean Squared Error
MAE	Mean Absolute Error
ML	Machine Learning
PV	Photovoltaic
R^2	R^2 or Coefficient of Determination
RNN	Recurrent Neural Network
REPWR	Renewable Energy Enabled Potable Water Reuse
RBC	Rotating Biological Contractor
SSR	Sum Of Squares Regression
SST	Sum Of Squares Total
SBR	Sequencing Batch Reactor
SQP	Sequential Quadratic Programming
SARIMA	Seasonal Auto-Regressive Integrated Moving Average
THM	Trihalomethanes
UASB	Up-flow Anaerobic Sludge Blanket
UV	Ultraviolet
WSP	Waste-stabilization Pond
WWTP	Wastewater Treatment Plant
WTP	Water Treatment Plant
WT	Wind Turbine

ABSTRACT

A large wastewater treatment plant (WWTP) typically consumes 300-500 MWh of electricity per day and often relies on the grid power generated by burning fossil fuels. Wind- and solar-based distributed generation emerged as a clean energy solution to achieve environmental sustainability and net-zero performance. This study investigates power consumption trends in WWTP facilities using six and nine years of data, respectively. The study leverages machine learning algorithms for wind speed and power load forecasting. Particularly, recurrent neural network (RNN), long short-term memory (LSTM), and ensemble models are adopted as intelligent computing tool for generation forecasting. A regression model was developed to forecast the power output of onsite wind turbines. Managerial insights were obtained regarding the most effective model for wind power forecasting and load prediction of the WWTP in Melbourne, Australia, and the water treatment plant in San Marcos, Texas. The following research findings are obtained. First, when multiple criteria along with forecasting wind speed are considered, the RNN model provides much better prediction than the LSTM and ensemble models. Second, when integrated with two or more low performance neural network models, the ensemble model can yield more accurate results by collectively increasing their predicting accuracy. Third, the integration of renewable transactive energy and blockchain technology has the potential to realize peer-to-peer energy trading, in which electricity is sold directly between prosumers and consumers without the intermediaries. Future research could investigate other machine learning algorithms, such as convolutional neural networks, for improving wind speed or solar irradiance forecasting, and extend the machine learning based computing tools to residential, commercial, and other industrial prosumers.

1. INTRODUCTION AND LITERATURE REVIEW

1.1 Background and Motivation

The proper treatment of wastewater is necessary to meet discharge standards, and it requires a large amount of energy. According to Crawford, (2010), wastewater contains carbon, nutrients like sulfur, nitrogen, and phosphorous, as well as reusable water that can be recycled and reused. First-level strengthening treatment methods include high load activated sludge (AS) process, pre-stage process of adsorption biodegradation (AB) method, and pre-stage process of hydrolysis aerobic process. Second-level treatment methods involve the use of oxidation ditch process, hydrolysis aerobic method, AS process, AB method, biological filter method, and the process of sequencing batch reactor (SBR), as reported by Akhouni and Nazif (2018) and others, including Liu et al. (2018); Qiao and Zhang (2018); and Rott et al. (2018). To eliminate contaminants with carbon source during phosphorous and nitrogen elimination strengthening, the Anaerobic-Anoxic-Oxic (A/A/O) technique or the Anoxic Oxidation (A/O) approach can be used for secondary strengthening treatment (Mehr et al., 2018). There are various types of wastewater treatment plants, each with their own set of advantages and disadvantages. The following section provides an overview of the conventional wastewater treatment process with essential details.

1.1.1 Wastewater Properties

According to various sources such as Asano et al. (1996), Muttamara (1996), and Secretariat (2015), industrial, agricultural, commercial, and domestic sources are all common types of wastewater. Stovell (2007) identified several biological components found in wastewater, including pathogens, protozoa, viruses, and bacteria. Chemical components such as heavy metals, dissolved organics, and nutrients are also present in wastewater. Table 1.1 summarizes these elements and the reasons for their removal.

Table 1.1 Principal components of concerns in wastewater treatment (Crites and Tchobanoglous, 1998)

Elements	Causes
Heavy metals	Generated by industrial and commercial activity, their eradication is must.
Pathogens	A variety of illnesses such as typhoid, cholera etc. can be transmitted to animals and humans by pathogens.
Biodegradable organics	The establishment of septic conditions and the depletion of natural oxygen resources can occur because of biological stabilization. BOD is a frequent unit of measurement.
Nutrients	Development of unwanted plants can be promoted by phosphorous and nitrogen.
Suspended Solids (SS)	Anaerobic condition and sludge deposits can be caused by SS.

1.1.2 Types of Wastewater Treatment

Wastewater treatment is generally composed of three stages: primary, secondary, and tertiary treatment. The main objective of the preliminary treatment is to eliminate solids that may become trapped in the treatment plant and damage equipment. The main treatment process aims to minimize the amounts of solids or inorganic matter that settles or floats in the tanks. In primary treatment, approximately 60 percent of SS and 35 percent of Five-Day Biochemical Oxygen Demand (BOD₅) are typically removed (Davis and Cornwell, 2008). The subsequent secondary treatment process targets the removal of soluble BOD₅ or dissolved organic matter. Removing nutrients such as phosphorus and nitrogen is an optional process carried out during tertiary treatment. Throughout the primary and secondary treatment, sludge is generated and subsequently treated in the following step.

Figure 1.1 depicts a flowchart of the wastewater treatment process, which presents a graphical representation of the sequences in which various unit processes and operations are carried out for

the treatment of sewage.

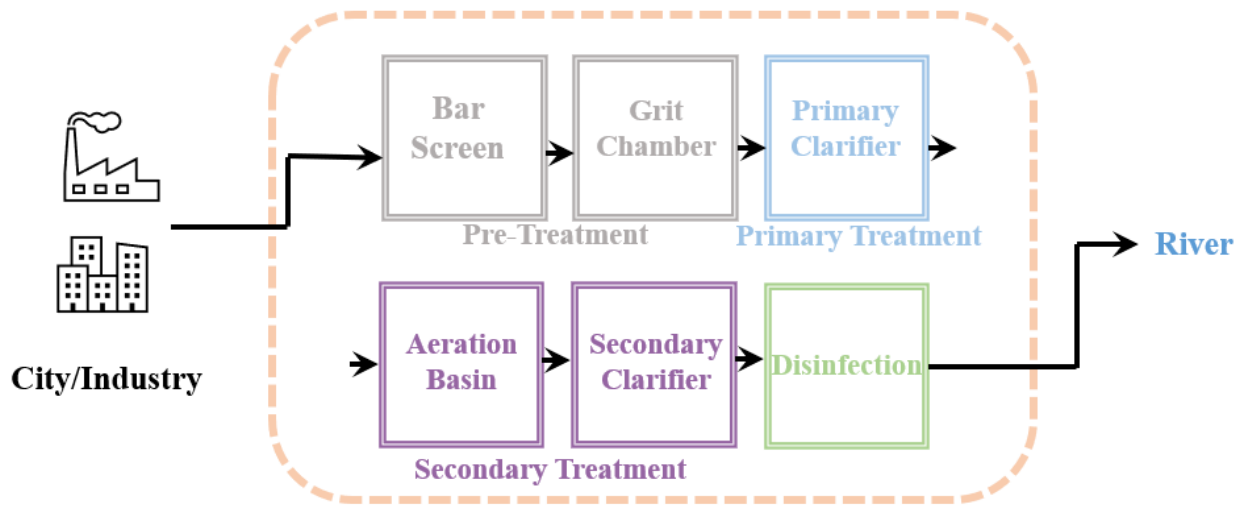


Figure 1.1 Flow chart of wastewater treatment plant

1.2 The State of the Art

1.2.1 Wastewater Treatment Technologies

The Elimination of inorganic matter or large materials is the purpose of the preliminary treatment, to safeguard the machinery of the treatment plant as they might damage or clog the pumps, pipes and other equipment (Davis and Cornwell, 2008). Although, as this process only removes a small amount of BOD₅ it is called pretreatment. Grit removal and bar screen are the several devices that are used in this step. Fine and coarse screen are the primary forms of screen. Table 1.2 shows the specifics of these screens.

Wastewater treatment plants (WWTPs) heavily rely on purchased electricity from the grid. However, there have been ongoing efforts to investigate potential solutions to reduce energy consumption and increase renewable energy generation in these plants. Some of the examples of these solutions include installing wind turbines to generate renewable energy, upgrading aeration systems to increase energy efficiency, using high-efficiency motors and pumps to reduce energy

consumption, and developing energy recovery systems to capture and utilize waste heat generated in treatment processes. Energy is the second largest cost of operation in wastewater treatment plants, after labor. Direct and indirect energy consumption are the two categories that can be used to classify the electricity use in wastewater treatment. Direct energy consumption refers to the electricity required to operate the return pumps, lift pumps, aeration blower, and other similar devices. The use of chemicals for sludge dewatering and chemical phosphorus elimination is classified as indirect energy usage (Pan et al., 2018).

Table 1.2 Bar screen classes

Classes	Details
Coarse Screen	
Bar or bar racks screen	Cleaned mechanically or manually.
Woven wired media screen	To filter the tiny particulates disk, basket, flat or cage type screens are used
Sewage grinders	They grind the particles held by the screens.
Fine Screen	
Band screen	It has higher and lower rollers that comprise of an infinite perforated band. To clean the remained residue on the screen a brush is installed, and the trash is flushed using a stream of water.
Shovel or wing screen	Horizontal axis has gently revolving ventilated circular radial vents.
Drum or strainer screen	It has a revolving cylinder with a screen around the circumference of the drum.

Now, we will discuss the three primary stages of a standard wastewater treatment facility, including primary, secondary, and tertiary treatment processes. The primary sedimentation tank utilizes the force of gravity to effectively remove settleable organic and inorganic materials that may remain in wastewater following pretreatment procedures (Davis and Cornwell, 2008). Two fundamental shapes of primary sedimentation tanks are rectangular and circular, while different types include inclined plate and horizontal flow tanks. Scrapers are utilized to remove settled solids

or sludge from the sedimentation tank, while skimming devices assist in the removal of floating materials. The subsequent sludge management operations continually treat the solids in the wastewater. Approximately 30-40% of BOD5 and 50-70% of SS can be eliminated through this process (Qasim, 2017).

The process of using microorganisms to remove contaminants from wastewater is known as biological treatment. The primary aim of this procedure is to eliminate soluble organic materials present in the sewage, along with coagulating any settleable colloidal particles and stabilizing organic materials. Crites and Tchobanoglous (1998) highlighted that the secondary objectives of biological treatment could include eliminating nutrients such as phosphorous and nitrogen, depending on the local conditions. To ensure optimal microbial activity during the secondary stage of wastewater treatment, it is crucial to maintain ideal temperature, sufficient time for the microbial process, favorable environmental conditions, such as oxygen availability, and effective bacterial contact (Davis and Cornwell, 2008). The most widely used secondary treatment methods include trickling filters and AS process. Table 1.3 provides an overview of the most popular techniques, along with the advantages and drawbacks of commonly used wastewater treatment methods.

Table 1.3 Most used secondary waste-water treatment methods (aerobic)

Methods	Process	Benefits Drawbacks
Aerobic		
Tricking filter	The sewage is treated by flowing through a porous stone layer with the help of microorganisms present on it. Oxygen is taken from atmosphere during the bacterial aerobic process	Benefits: High BOD removal, no mechanical aeration, simple Operation and maintenance, small land application. Drawbacks: Dependence on temperature, sludge production need for further treatment, high construction cost, sensitive to toxic, less flexible than AS.
AS Process	Microorganisms are fed with oxygen in the wastewater	Benefits: High resistance, flexible effective, less odor, low land requirement. Drawbacks: Complicated process, possibility of environmental challenges, large sludge produced.
Rotating biological contractors (RBC)	A surface is provided for growth of bacteria on clusters of upright plates. Standard aerobic therapy is being used.	Benefits: Short retention time and contact, low operating cost, high removal efficiency Drawbacks: possible system failure, maintenance cost high.
Up-flow anaerobic sludge blanket (UASB)	In order to remove pollutants, a covering of bacteria is used in the anaerobic process.	Benefits: No power required, low sludge produced, low operation and maintenance cost, little land used, suitable for hot countries, low construction cost. Drawbacks: Slow process startup, sensitive to toxic, odors problems, Ineffective process.
Oxidation ditches	Mechanical aeration in oval shaped duct.	Benefits: Easy to operate compared to AS, less land required compared to WSP, higher treatment power. Drawbacks: energy consumption is high.
Waste-stabilization Pond (WSP)	It has a shallow pond with a large surface. Microbes were utilized to treat sewage, while algae's photosynthesis mechanism was exploited to produce oxygen.	Benefits: No power required, effective in treatment of pathogenic microorganisms, simple, resistant, low operation and maintenance cost, suitable for hot climates, low construction cost. Drawbacks: Odor problems, depends on temperatures, large area, inflexible, fair removal efficiency.

Table 1.4 Most used secondary waste-water treatment methods (anaerobic)

Methods	Process	Benefits Drawbacks
Anaerobic		
Anaerobic filters	Particles in wastewater are retained on a filter while passing through it and the active biomass adhering to the filter material decomposes the active biomass.	Benefits: Resistance, flexibility, similar benefits to UASB. Drawbacks: Clogging problems, drawbacks like UASB, treating is confined to low SS influent, SS present in high proportion with inferior effluent quality
Natural Treatment		
Construct wetland	Here roots of plants and soil are used for the treatment. Wastewater was made to flow across a reed bed.	Benefits: System stable under peak loads, oxygen not needed, maintenance and operating cost is low, pathogen eradication is efficient Drawbacks: Climate reliance
Aquacultures	Maintained ammonia levels and aerobic conditions are required for this treatment. This step combines aquaculture with wastewater treatment.	Benefits: Contaminant's removal very efficient, edible fish and vegetables can be cultured, fertilizers, and animal fodder. Drawbacks: High maintenance and operation cost, health hazards, huge area requirement, expensive installation
Land treatments	Processing wastewater is done in a safe environment with soil.	Benefits: Easy operation and maintenance, construction is cheap, coliform and BOD removal rate is higher, resilience to sewage fluctuations, zero sludge generation. Drawbacks: High area requirement, contaminants extraction rate is less, climate dependance, odor, potential of ground water pollution.

Various disinfection technologies such as chlorination, ozone, and ultraviolet (UV) can be employed in the disinfection process, which involves the removal of microorganisms and pathogens. Chlorination is a popular method due to its cost-effectiveness and efficiency. However, it may also have negative impacts on beneficial microbial populations and can pose toxicity risks to marine and aquatic organisms. Residual chlorine is effective in eliminating targeted microorganisms. Table 1.5 provides a summary of the advantages and disadvantages of each

disinfection method.

Table 1.5 Disinfection methods with benefits and drawbacks (Qasim, 2017)

Methods	Benefits	Drawbacks
UV	Comparatively requires less space than other approaches, User friendly, effective, No lasting chemical influence, fast treatment time	Some organisms can sustain and reverse the harmful UV effects, highly priced compared to chlorine, routine maintenance required.
Ozone	Enhances the dissolved oxygen, trihalomethanes (THMs) production is less, requires less contact time, much efficient than chlorine.	Requires non-corrosive materials, costly instruments, complex, elimination or recycling of surplus ozone, least effective with rise in SS, high energy requirement, can be toxic to humans.
Chlorine	Removes ammonia, inexpensive than other methods, effective on large range of bacteria, helps in removal of grease and scum and regulated foaming and bulking.	Causes dissolved salts accumulation, synthesis of possibly halogenated, carcinogenic organic compounds can be formed, due to toxicity requires de-chlorination following chlorination procedure

Advanced wastewater treatment or tertiary treatment processes are typically used to remove moderate-level contaminants such as heavy metals, phosphorus, and nitrogen. Wastewater containing ammonia can be toxic to aquatic animals. Nitrifying bacteria can transform ammonia into nitrate through the nitrification process, and denitrification can remove nitrate from wastewater by transforming it into nitrogen gas. Overabundance of nitrate in river bodies can cause eutrophication as it acts as a nutrient, which is similar to phosphorus that aids in the growth of algae. An improved biological phosphorus removal technique can help remove phosphorus and produce biosolids that can be used as agricultural compost. By addressing these nutrient issues, useful sustainable resources can be created, and improved effluent quality can be achieved.

During the wastewater treatment process, sludge is generated which requires appropriate treatment. There are several methods available such as dewatering, thickening, and stabilization

used for sludge treatment. The three most popular methods of sludge stabilization are anaerobic, aerobic, and chemical digestion. According to Qasim (2017), the stabilization process can help to eliminate odor problems, remove germs, and minimize sludge. The use of anaerobic digestion is a good option as it can recover energy for use as electricity in facilities. To reduce the cost of sludge relocation, wastewater treatment plants can reduce the sludge bulk through thickening and dewatering procedures. The cheapest option for sludge disposal is land disposal. The most environmentally friendly method of sludge recycling is converting it to other useful applications such as components of brick, fertilizer, and others. Landfilling or incineration of sludge is possible, but these methods could be costly.

1.2.2 Energy Sources in Wastewater Treatment

- **Solar Energy:** A good solar irradiance, or the power received per unit area from the sun, promotes a location's on-site solar electricity generation. Solar Photovoltaic (PV) system is a dependable, stable, and cost-effective technology. Solar PV systems contributed just 0.1 percent of total world power output in 2010 but are expected to provide 11 percent of global electricity consumption by 2050. According to the report (Energy and Food Nexus, 2019), the utilization of renewable energy sources, such as wind and solar energy, in wastewater treatment plants could potentially reduce up to 2.2 gigatons of CO₂ emissions by 2030. The report highlights that such renewable energy sources have the potential to cut energy-related emissions by 90% in the wastewater industry. (Xu et al., 2017) reported that using monocrystalline cells, a wastewater treatment plant (WWTP) in China could potentially generate about 80% of its energy needs through solar power alone. However, the installation of approximately 9,000 m² of solar panels would be necessary to achieve this, which could be costly and require a

significant amount of space. Therefore, while this approach has potential benefits, it is important to consider the associated expenses and spatial requirements.

- **Wind Energy:** Wind energy is a popular source of renewable energy compared to other sources, such as water, geothermal, and mineral energy. According to (Eftekhari et al., 2022), wind turbines can be utilized differently based on the load and local conditions to maximize the transformation of wind energy into mechanical energy. Despite being pollution-free and eco-friendly, wind energy has its limitations as it varies with weather conditions and requires adequate space for installation. Gomes and Cardoso (2011) found that locating the ground anemometer station at a similar height to the wind turbine's rotor can improve the efficiency of wind energy generation.
- **Combined heat and power (CHP):** CHP are a state-of-the-art technology that can be used in various settings such as industrial, commercial, multi-family, and residential buildings, as well as wastewater treatment facilities. When implemented in wastewater treatment plants (WWTP), CHP enables the simultaneous generation of electricity and thermal energy (i.e., cooling and/or heating) using a single energy source. Another term used for CHP is cogeneration. One of the key advantages of utilizing CHP in WWTP is that it enables the efficient utilization of on-site biogas generation. During the wastewater treatment process, biogas, which mainly consists of methane and carbon dioxide, is produced and can be utilized as a fuel source for CHP systems. This results in a cost-effective and environmentally friendly approach to energy generation. According to Trendewicz and Braun (2013), system cost estimates indicate that the unit installed cost per kilowatt (\$/kW) decreases as the system size increases. For instance, the unit installed cost is \$5780/kW for a small system with a capacity of 330 kW, while it becomes \$3584/kW for a larger system with a capacity of 6 MW.

- **Hydro energy:** Hydroelectric power generation in WWTPs involves converting the potential energy of water flowing through a pipe or channel into electrical energy. This is typically accomplished by using a turbine that is driven by the water flow. The turbine drives a generator that produces electricity. The amount of electricity that can be generated depends on the amount of water flowing through the turbine, which is determined by the head pressure and flow rate of the effluent. In WWTPs, there are two primary sources of water flow that can be used to generate hydroelectric power. The first is the flow of effluent leaving the treatment process, which typically has a relatively low head pressure but a high flow rate. The second source is the flow of water entering the treatment process, which may have a higher head pressure but a lower flow rate. (Power et al., 2014) stated that head pressure and effluent flow rate are the two main factors to consider when developing a hydroelectric plant, and larger plants with higher flow rates are better suited for hydroelectric energy generation. Bousquet et al. (2017) observed that the type of system used for hydroelectric power generation in WWTPs depends on various site-specific factors, including urban settlement design and available infrastructure. The authors suggested that an algorithm of upstream operations using untreated water may provide a general screening for the potential of hydropower at a particular site, but results may vary depending on cost issues such as penstock assumptions. The water industry is increasingly focusing on developing sustainable solutions for energy independence due to climate change concerns and stringent effluent standards. Chae and Kang (2013) found that hydro power plants in WWTP may be attractive because they can operate year-round without creating negative environmental impacts.
- **Biogas:** It is primarily composed of methane (CH₄), is first collected and purified to remove impurities such as water and carbon dioxide. The purified biogas can then be burned in an

engine or a turbine to generate electricity. The heat produced by combustion can be used to generate steam or hot water, which can be used for space heating or to meet the digester's heat requirements. Biogas is a sustainable method for converting biological waste into energy and fertilizer. However, its use in wastewater treatment plants (WWTPs) in the United States is currently limited. According to (Bachmann and Cour, 2015), biogas can be produced in municipal WWTPs and used to improve energy efficiency along with other sustainable techniques. Larger plants can achieve higher energy independence using biogas, and those with populations under 100,000 can easily attain electricity autonomy at 37 percent and heat autonomy at 90-100 percent. In plants with populations over 100,000, electricity independence can reach 68-100 percent, but complete energy independence is only achieved in very large and complex facilities. Despite the benefits of biogas, (Shen et al., 2015) found that it receives less attention compared to alternative renewable sources like solar or wind. Currently, biogas is mainly used on site for electricity and heat co-generation or burned in most WWTPs in the US.

1.2.3 Energy Consumption in Wastewater Treatment

Many studies (Lindtner et al., 2008; Masłoń et al., 2018; and Moss et al., 2013) have shown that energy is a significant expense for WWTPs, second only to labor costs, in providing wastewater treatment services to the public. Qiao and Zhang (2018) discovered that more than 70% of the total energy consumption in the treatment process is used in secondary treatment, biological treatment, and sludge disposal. Specifically, about 10-20% of energy is consumed by the sewage lift pump, 50-70% by biological treatment, and 10-25% by sludge disposal. As shown in Figure 1.2, the majority of energy use in a traditional AS system is related to the aeration process, accounting for approximately 60% of the total energy consumed.

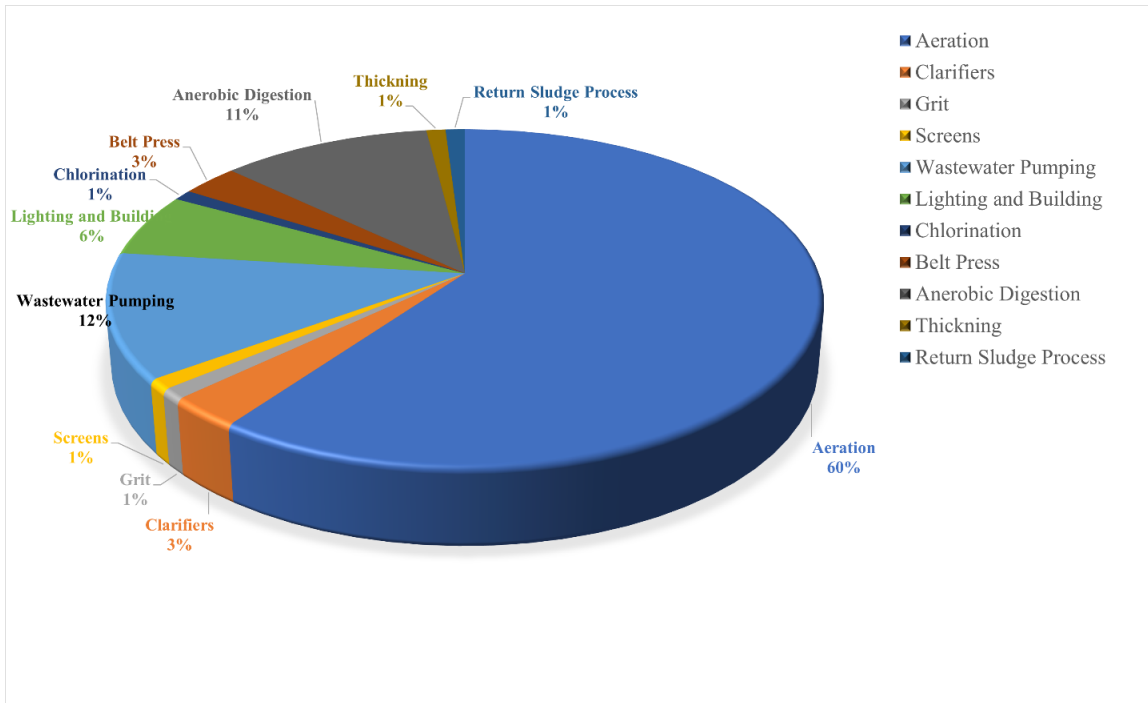


Figure 1.2 Energy distribution in conventional AS systems (Gu et al., 2017)

Energy consumption in WWTPs can be reduced through a variety of strategies. One approach is to improve the efficiency of the treatment processes themselves, such as using more advanced aeration systems or optimizing biological nutrient removal. Another approach is to implement energy recovery systems, such as using biogas generated from anaerobic digestion of wastewater solids to fuel turbines or cogeneration systems. This can reduce the need for external energy sources and even generate surplus energy that can be sold back to the grid.

Other energy-saving strategies include optimizing the operation and maintenance of equipment, implementing energy-efficient lighting and heating, ventilation and air conditioning (HVAC) systems, and reducing energy losses through insulation and air sealing. In addition, WWTPs can explore the use of renewable energy sources such as wind, solar, and hydropower.

Bertanza et al., (2018) conducted an extensive analysis on the potential benefits of upgrading existing WWTPs, and concluded that achieving energy self-sufficiency was feasible,

especially if the system had both primary sedimentation and anaerobic digestion (AD), with minimal technological and economic significance. To improve energy efficiency, regular monitoring of electricity consumption is crucial. Marner et al., (2016) recommended conducting energy assessments using a systematic approach to obtain accurate data on a WWTP's energy usage profile. To achieve energy self-sufficiency in WWTPs, all available options should be utilized. However, the electricity produced from different types of effluent is often inadequate to achieve energy self-sufficiency. Therefore, it is necessary to explore alternative sources of sustainable energy from outside the WWTP to achieve power balance. The use of sustainable energy sources seems to offer a greater opportunity for WWTPs to achieve energy neutrality.

Shizas and Bagley (2004) utilized a bomb calorimetry method to evaluate the amount of biological energy present in municipal sewage. The findings from these experiments revealed that the biological energy content in sewage is approximately ten times greater than the energy required to treat it, as also noted in studies by Jasper et al., (2013) and Moss et al., (2013). However, Parry (2014) challenged this idea by demonstrating that due to the low-quality electricity generated with less thermal efficiency, not all the electricity generated in WWTPs can be effectively utilized for achieving energy neutrality or even a positive outcome. Therefore, a highly efficient operation is necessary to achieve a positive energy outcome in WWTPs.

Strazzabosco et al. (2019) found that there is no clear correlation between the size of WWTPs and the size of the onsite solar photovoltaic (PV) system installed. In California, the most common size of installed solar array is 1 MW, and the presence or absence of rebate schemes affects the adoption of solar PV in both the wastewater industry and other non-residential sectors. Half of the WWTPs with flow rates of 5 to 50 million gallons per day (MGD) have a solar PV system installed, and 80 percent recovered biogas is for energy use.

Table 1.6 Comparison of existing and proposed studies

Reference	Integration into Industry	Renewable Energy	ML Models	Transactive Energy	Blockchain Energy	Product and Energy Market Integration
AlHajri (2007)	No	distributed generation (DG)	Sequential Quadratic Programming (SQP)	No	No	No
Malato (2009)	Yes	solar PV	No	No	No	No
Bazen (2009)	Yes	solar PV	No	No	No	No
Gomes (2011)	Yes	wind	No	No	No	No
Chae and Kang (2013)	Yes	solar PV, hydro energy, sewage heat recovery	No	No	No	No
Li et al. (2013)	Yes	wind	No	No	No	No
Moss et al. (2013)	Yes	solar PV, wind	No	No	No	No
Mo and Zhang (2013)	No	wind, solar PV, CHP	No	No	No	No
Luo (2013)	Yes	NA (vegetable industry)	SARIMA	No	No	No
Shen (2015)	Yes	biogas	No	No	No	No
Power (2016)	Yes	hydro energy	No	No	No	No
Fang (2016)	No	NA (heat demand forecast)	Linear regression models, SARIMA	No	No	No
Bousquet (2017)	Yes	hydro energy	No	No	No	No
Mehr et al. (2018)	Yes	combined cooling heating and power	No	No	No	No
Madan (2018)	Yes	NA (Internet Traffic)	Discrete Wavelet Transform (DWT), ARIMA, RNN	No	No	No
Musbah et al. (2019)	No	NA (electrical load)	SARIMA	No	No	No
Wang (2019)	Yes	NA (passenger volume)	LSTM	No	No	No
Le et al. (2019)	No	NA (flood forecast)	LSTM	No	No	No
Strazzabosco et al. (2019)	Yes	solar PV	No	No	No	No
Bukhary et al. (2020)	Yes	solar PV	No	No	No	No
Ma (2020)	No	NA (stock Price)	ARIMA,	No	No	No

Wahbah (2020)	No	forecast) solar irradiance	ANN, LSTM Kernel density estimation (KDE)	No	No	No
Eftekhari (2022)	No	wind	No	No	No	No
This Paper	Yes	Wind	RNN, LSTM, Ensemble	Yes	Yes	Yes

However, it is not cost-effective for WWTPs with flow rates less than 5 MGD to recover biogas for energy use. According to Bazen and Brown, (2009), the main drawback of onsite solar or wind technology is the high financial investment, and the suitability may be limited by weather conditions and the location of WWTPs. The US Department of Energy provides wind and solar potential maps on their website to evaluate the economic feasibility of onsite wind and solar technologies. According to Elliott et al (2011), Texas, Nebraska, Kansas, North Dakota, South Dakota, and Iowa have the highest wind energy potential. Despite the significant energy generation potential of onsite wind power, it is not commonly used in the United States. Table 1.6 compares the existing studies with the current study.

1.2.4. Machine Learning in Wind Speed Forecasting

Many countries have experienced an electricity deficiency owing to a lack of sufficient infrastructure and resources. WWTP consumes around 30 TWh of energy every year in the US, which costs approximately \$2 billion (Lemar, 2017), and the electricity is frequently acquired from the power grid. According to Li et al. (2013), solar and wind energy are among the cleanest forms of energy and may be utilized without emitting hazardous gases or hurting the environment. Wind energy is pollution-free and environmentally benign, but it changes with the weather, making it difficult to dispatch. Rodrigues Moreno et al. (2020) observed that the ground anemometer station in a wind turbine should be situated at a comparable height to the wind turbine's rotor for the best forecasting results.

However, due to the intermittent and unpredictable nature of wind speed, reliable

generation forecasting is difficult to make (Liu et al., 2018). Machine learning is a powerful multidisciplinary subject that may be used to improve wind speed predictions. Many researchers (Ma, 2020; Memarzadeh and Keynia, 2020; Rodrigues Moreno et al., 2020; Wang et al., 2020) explain using ANN to develop regression models to anticipate wind speed and power. In recent decades, ML has been widely used to handle time series problems, with neural network models being the most popular approach. Neural networks have been proved to be capable of evaluating time series data in past studies. Recently a substantial amount of effort has been devoted to developing algorithms for recurrent neural networks (RNN) and their variant, long short-term memory (LSTM). Both RNN and LSTM are shown to be more accurate than conventional statistical models for modeling time series data in several fields and have produced impressive results (Greff et al., 2017; Liu et al., 2018).

1.3 Research Objectives and Contributions

This thesis proposes to integrate onsite wind generation into the design and operations of WWTP for achieving long-term, eco-friendly operations in water-energy nexus. Using onsite renewables lowers the wastewater treatment facility's energy costs as well as reducing the carbon footprint. The research aims to achieve the following objectives:

- Performing WWTP power load analytics. The daily power load profiles of several WWTP and WTP are analyzed to understand the demand variability and uncertainty of various stages using data from six and nine years, respectively. The energy consumption and demand of different treatment processes is scrutinized each day.

This study involved developing a machine learning approach to forecast wind speeds based on a 9-year time series of meteorological data from San Marcos, TX. Various machine learning models, such as LSTM, RNN, and ensemble models, were explored to determine the most effective ones.

The meteorological time series dataset for wind speed prediction utilized in this study was obtained from Austin Airport between 2011 and 2019 because it is approximately 40 km from the city of San Marcos, Texas. The dataset includes 14 attributes, including temperature, wind speed, dew point, and precipitation. The performance of the regression models was evaluated using different metrics, including mean square error (MSE), mean absolute error (MAE), and coefficient of determination (R^2 score), in addition to analyzing their learning curves, prediction scores, and prediction speeds.

- Introducing edge computing and blockchain technology in transactive energy market. The thesis explored blockchain and edge intelligence, and presented real-world examples to demonstrate how these enabling technologies can be utilized to establish a peer-to-peer renewable energy trading system that is more transparent, decentralized, efficient, and trustworthy for prosumers.
- Managing transactive energy trading with main grid and estimating the power output of onsite wind turbine. The thesis also investigates the use of transactive energy trading to facilitate the exchange of wind-generated electricity among prosumers and customers in a transactive energy network. Additionally, the thesis explores methods for estimating the power output of onsite wind turbines using a regression model involving the data from the previous three NN and ensemble models, which can help determine the amount of power that can be supplied by the turbine.

The research contributions can be described to the following aspects:

- The study analyzes power consumption patterns in WWTP and WTP and shows that energy demand varies daily and seasonally across different processes and equipment in treatment

facilities. This highlights the necessity of implementing targeted energy-saving strategies to minimize the power usage and utility bill.

- The study's contribution lies in utilizing various machine learning models, including RNN, LSTM, and ensemble models, to forecast day-ahead (i.e., 24-hour ahead) forecast of wind speed for the city of San Marcos, TX based on 11-year hourly meteorological data. Different regression models were used to determine the most precise wind speed predictions.
- The study examines how enabling technologies including blockchain and edge computing could facilitate renewable energy integration and trading that is more transparent, decentralized, efficient, and trustworthy, using real-world examples. Additionally, it aims to determine how blockchain technology can promote decentralized, affordable, and sustainable renewable energy trading.
- Additionally, the research estimates the power output of the wind turbine based on the non-linear power curve with the help of a regression models which utilizes the forecasted wind speeds of the neural network and ensemble model. Case studies on 1 and 3 MW turbine are made to compare their actual electricity generation with the electricity consumption data of a WWTP.

2. RENEWABLE ENERGY AND POWER DEMAND OF WWTP

2.1 Renewable Energy Enabled Potable Water Reuse System

2.1.1 System Setting

We design a renewable energy enabled potable water reuse (REPWR) system, which processes wastewater to potable level and then circulates back to residential water system. To achieve the potable water reuse, an additional infrastructure called advanced water purification facility (AWPF) is required in addition to WWTP (Ikehata et al., 2013). An AWPF takes influent water from WWTP and uses a series of energy intensive processes such as reverse osmosis, ultraviolet, and ozone to produce potable water (Ikehata et al., 2018). Depending on various cost-effectiveness and climatic conditions, AWPF is expected to offer multiple economic and environmental benefits to municipalities like the City of San Marcos. Meanwhile renewable distributed generation (DG) units, such as WT, PV, and battery energy storage (BES), are installed on site to power AWPF, WWTP, WTP, and auxiliary equipment such as pumps. Figure 2.1 depicts the architecture and the working principle of the proposed REPWR infrastructure.

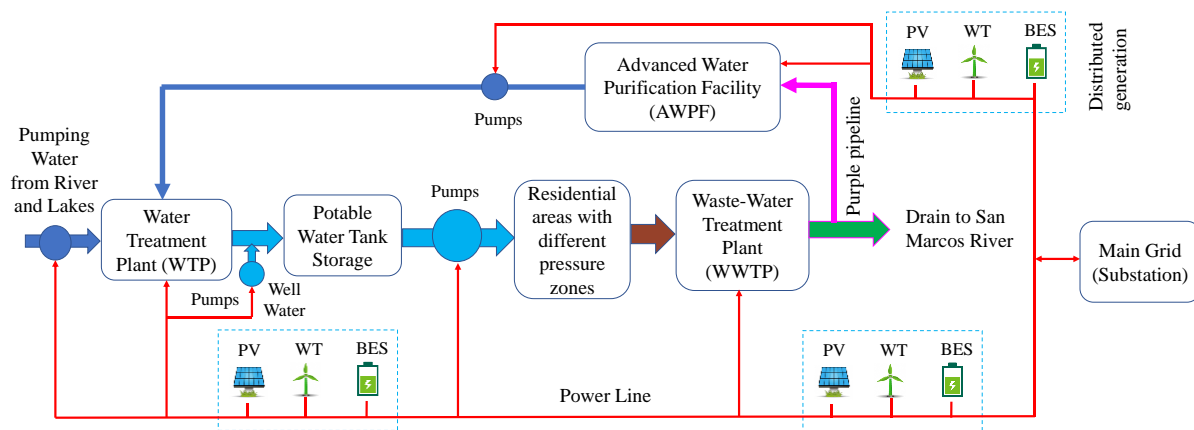


Figure 2.1 Renewable energy enabled potable water reuse infrastructure (Jin et al., 2021)

Since REPWR can intake residential reclaimed water for treatment, without using surface water, the system is drought resistant, and can be applied in many arid and semi-arid regions of the world.

A possible solution to these challenges is the use of treated reclaimed water as a source of potable water supply (i.e., potable water reuse). The REPWR provides a sustainable solution to balance water supply and demand in urban areas. Reclaimed water reduces the consumption of fresh water, and a secondary network is needed to distribute the reclaimed water to residential areas. This is a long-term decision over several decades, therefore many uncertainties and challenges arise from the system planning and operations. For example, population growth or migration, climate changes, extreme weather events, and seasonal weather variations. Texas has one of the highest wind potentials compared to other states, hence wind-based water-energy nexus will turn our public water supply systems more circular, sustainable, and cost-effective.

2.2 Power Load Profile

2.2.1 Wastewater Treatment Plant

For estimating the power demand, a WWTP in eastern part of China was selected having an area of 716 acres which serves a population of 2.5 million people. The WWTP's long-term treatment capacity will be approximately 725.748 thousand cubic meters per day. The WWTP employs hydrolysis acidification, modified A/A/O, and coagulation sedimentation filtration technique. The sample WWTP had a daily flow of 57,938 m³/d on average. Table 2.1 shows the power consumption of the major processes in this plant.

Table 2.1 Power consumption in major processes (Xu et al., 2017)

Stages	Power consumption (kW)	Percentage share (%)
Primary treatment	6,771	22.9
Secondary treatment	17,635	59.7
Advanced treatment	4,229	14.3
Sludge treatment	915	3.1
Total	29,550	100

In Table 2.2 a list of state-of-the-art WWTP in United States with onsite solar and wind technology were shown with their power generation capacity, solar/wind integration and the electricity use in the plant.

Table 2.2 WWTP with Onsite Solar and/or Wind Generation (Mo and Zhang, 2013)

Facility	Treatment Capacity (thousand m ³ /day)	State	Source	Capacity	Comments	Reference Source
Atlantic County Utilities Authority	151.4	New Jersey	Wind Solar	7.5 MW of wind, 500 kW of PV	Provide 70% of facility needs Provide 660,000 kWh of energy to the facility per year	ACUA, 2011
Browning WWTP	0.9464	Montana	Wind	40 kW	Displace grid electricity used at the facility	Browning, 2001
Boulder WWTP	75.708	Colorado	Solar	1 MW	Provide 15% of facility needs	Boulder, 2012
Oroville WWTP	24.6	California	Solar	520 kW	Provide 80% of facility needs	SPGSolar, 2012

In Figure 2.2, a time series plot illustrates the total power usage of Melbourne Water’s wastewater treatment facility (East), the largest WWTP in Melbourne, which can treat 440 thousand cubic meters per day. This data is collected from January 2014 to January 2021 from Melbourne water database, (2021), covering eight years of daily electricity consumption (kW) data. The data set is open to everyone for research purposes and was collected using revenue quality meters and Melbourne Water-owned power meters at 15-minute intervals. To compute the total electricity consumption, data from feeders 1 and 2 were combined, and total electricity generation was added to it. The daily power demand was then estimated by dividing total electricity consumption by 24 hours. Figure 2.2 shows various dips, which may be due to atmospheric changes, such as

temperature and rainfall patterns, in the area.

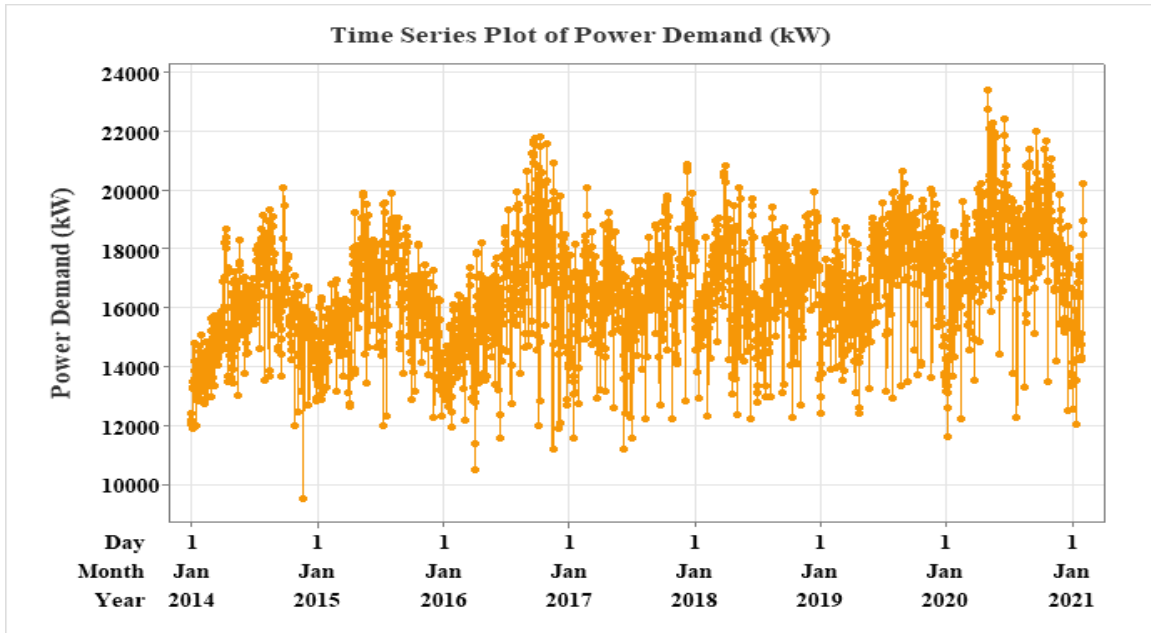


Figure 2.2 Daily power demand of Melbourne wastewater treatment plant from 2014-2021

Looking closely at the data provided in Figure 2.3, it becomes apparent that the energy usage of the WWTP has increased steadily in a linear fashion from 2014 to 2020, as shown by the red line. The cause of this increase could be attributed to various factors, such as the population growth of the area or an increase in the concentration of pollutants in the influent, or possibly both. Although there appears to be a dip in energy consumption in 2021, it would be unfair to compare it with the previous years as only one month's worth of data is available for that year. The gradual increase in energy consumption can also be seen in the mean energy consumption figures, which have gone up from 15,605 kW in 2014 to 17,926 kW in 2020. Outliers are more frequent in 2017 and 2020 than in other years, and the interquartile ranges (IQR) differ significantly between years. The smaller IQR sizes of 2014, 2015, 2017, and 2018 indicate that the power demand was more concentrated during these years, whereas the larger IQR range of 3,062 kW in 2016 suggests that the power demand was less concentrated for 50 percent of that year. In other words, there was a

greater variability in power demand during that period.

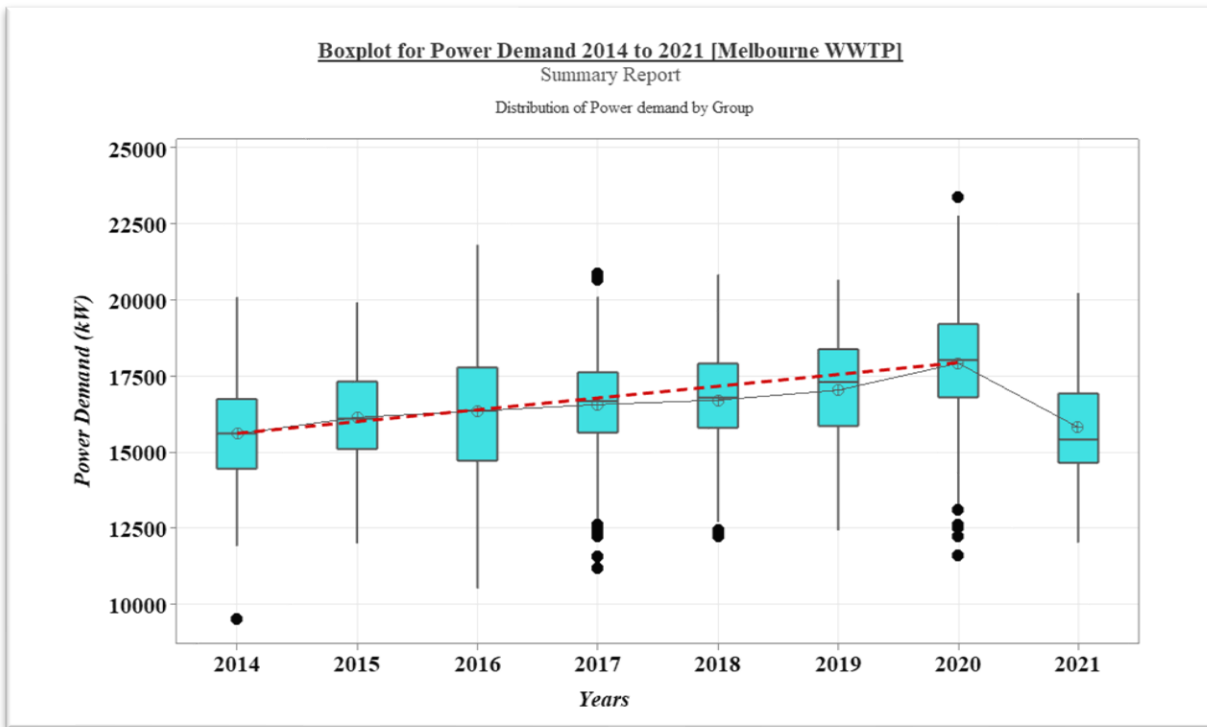


Figure 2.3 Yearly box plot for power demand of Melbourne WWTP

Table 2.3 presents a descriptive statistical analysis of the power demand for the WWTP facility, with information on the number of days, mean, standard deviation, minimum, and maximum power demand for each year. Table 2.3 also includes an additional row that shows the power fluctuation for the facility. Power fluctuation refers to the loss or damage caused by factors such as voltage dips, power surges, outages, inadequate current, or improper voltage. These voltage fluctuations can cause instability in the facility’s operation and affect equipment performance. However, voltage fluctuations below 10% do not affect electrical equipment. We calculated the voltage fluctuations of the facility’s power demand by dividing the standard deviation of each year by the mean of each year. The results indicate that power fluctuations were within the safe limits of 10% or below, except for 2016 and 2020, which exceeded 13.58% and 11.12%, respectively.

High voltage fluctuations can cause increased vibrations, leading to reduced mechanical strength and a shorter lifespan for facility equipment and motors.

Table 2.3 Descriptive statistical report for Box plot of Melbourne WWTP (Unit: kW)

Year	2014	2015	2016	2017	2018	2019	2020	2021
Number (N)	366	365	366	365	365	365	366	30
Mean	15605	16150	16363	16570	16716	17043	17926	15824
St. Dev	1639.5	1610.5	2222.5	1616.0	1630.8	1682.6	1992.8	1749.0
Minimum	9547.1	12010	10537	11214	12264	12443	11637	12036
Maximum	20103	19926	21819	20892	20837	20663	23389	20231
Voltage Fluctuation	10.51%	9.97%	13.58%	9.75%	9.76%	9.87%	11.12%	11.05%

Figure 2.4 depicts a one-way ANOVA analysis for the daily power demand of Melbourne WWTP. The P-value obtained in the analysis is less than 0.05, indicating that the differences between the means are significant. In statistical hypothesis testing, a P-value less than 0.05 implies that the null hypothesis can be rejected, and the alternative hypothesis is correct. The mean value represents the average of all the data. The mean values for the years 2014 to 2020 are 15614 kW, 16149 kW, 16363 kW, 15823 kW, 16570 kW, 16716 kW, 17042 kW, and 17925 kW, respectively. Therefore, we can conclude from Figure 2.4 that the average daily power demand of this plant is different

during the seven-year period.

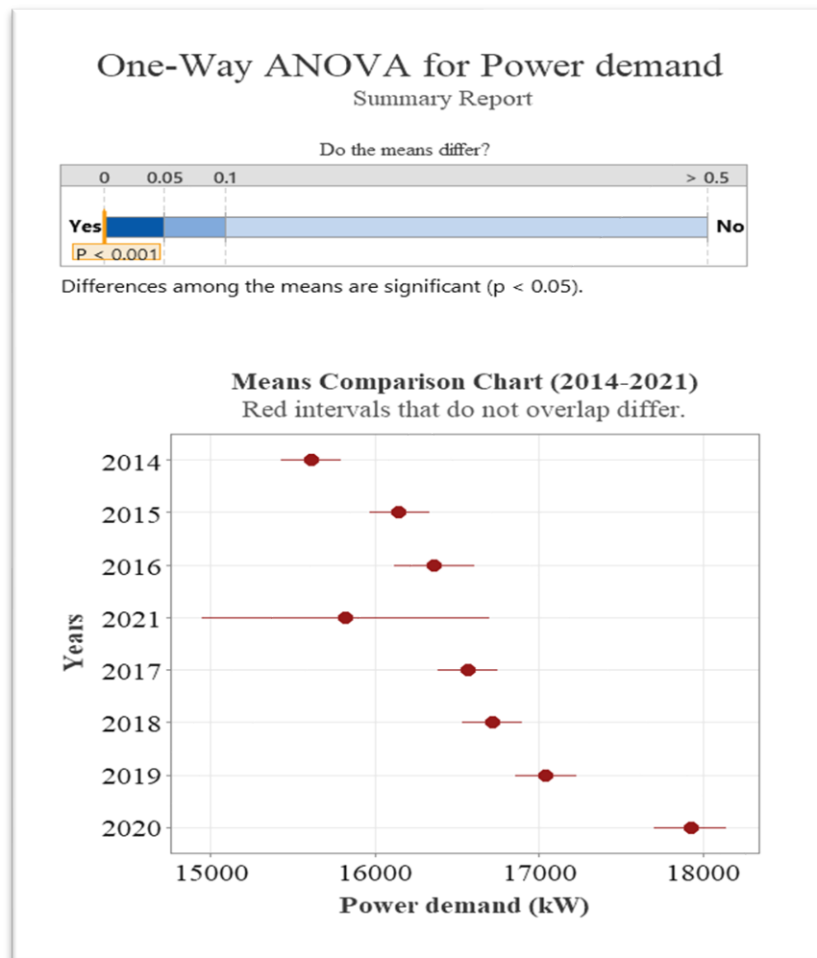


Figure 2.4 Mean comparison of power demand of Melbourne WWTP

The histograms presented in Figure 2.5 display the power demand of Melbourne WWTP on an annual basis, providing a visual representation of the data from 2014 to 2021. The histogram for 2014 demonstrates a bell-shaped distribution that is evenly distributed. The most frequent power demand for the year was 14,750 kW with a frequency of 48 days, while the mean value was 15,614 kW with a frequency of 45 days. The lowest and highest power demand values for this year were 9,547 kW and 20,103 kW, respectively. For 2015, the histogram also exhibited a roughly bell-shaped curve, with the highest frequency (45 days) of power demand being 14,750 kW and a mean

value of 16,150 kW. The minimum and maximum power demand values for this year were 12,010 kW and 19,926 kW, respectively. In 2016, the histogram similarly displayed a normal distribution, with a power demand value of 16,750 kW appearing most frequently for 36 days. This year's minimum and maximum power demand values were 10,537 kW and 21,819 kW, respectively, and the standard deviation was the highest at 2,222 kW when compared to the previous years.

In 2017, the histogram did not fall below the normality curve, and the most common power demand value was 16,750 kW with a frequency of 58 days. The minimum and maximum power demand values for this year were 11,214 kW and 20,892 kW, respectively. The histogram for 2018 exhibited a right-skewed shape and did not appear to be normally distributed. The most frequent power demand value for this year was 17,250 kW for 48 days, and the minimum and maximum power demand values were 12,264 kW and 20,837 kW, respectively.

Similarly, the histogram for 2019 appeared to be skewed to the right and was not normally distributed. This year's minimum and maximum power demand values were 12,443 kW and 20,663 kW, respectively. For 2020, the histogram showed several data points outside the normality curve on the right side, and the standard deviation was the second highest at 1992 kW. This year's minimum and maximum power demand values were 11,637 kW and 23,389 kW, respectively. As there is only 30 days of data available for 2021, we cannot forecast the histogram for this year. Based on the available data, the minimum and maximum power demand values for this year were 12,036 kW and 20,231 kW, respectively.

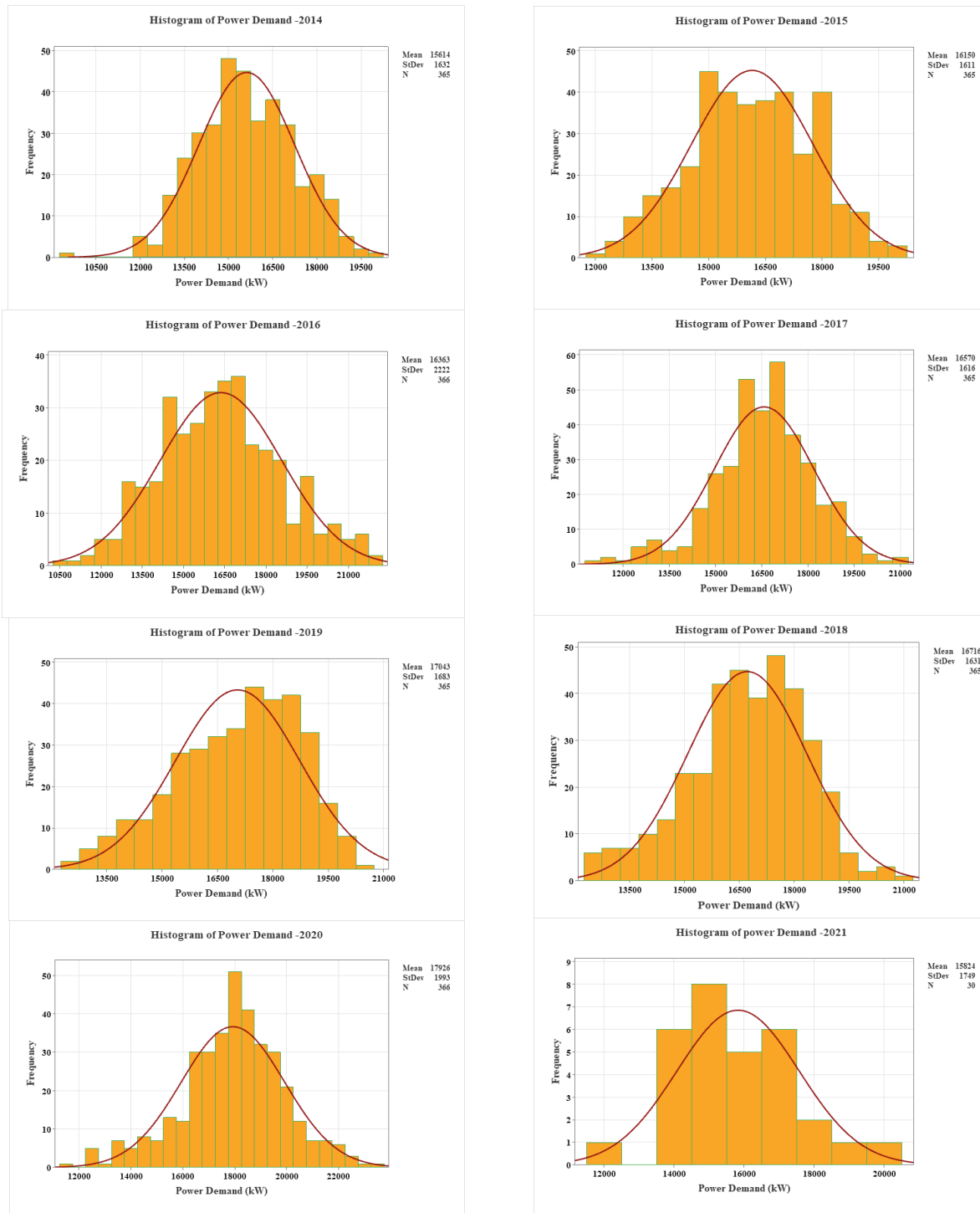


Figure 2.5 Histogram showing power demand of the Melbourne WWTP from 2014 to 2021

In order to assess the normality of the data for 2014, we utilized a single probability plot, displayed in Figure 2.6. The Normality test was conducted using this plot. All the pink dots on the plot fall on the red line, except for one data point located at 10,000 kW. Moreover, the P-value obtained from the test is 0.325, which is greater than the significance level of 0.05. These results indicate that the power demand data for 2014 follows a normal distribution.

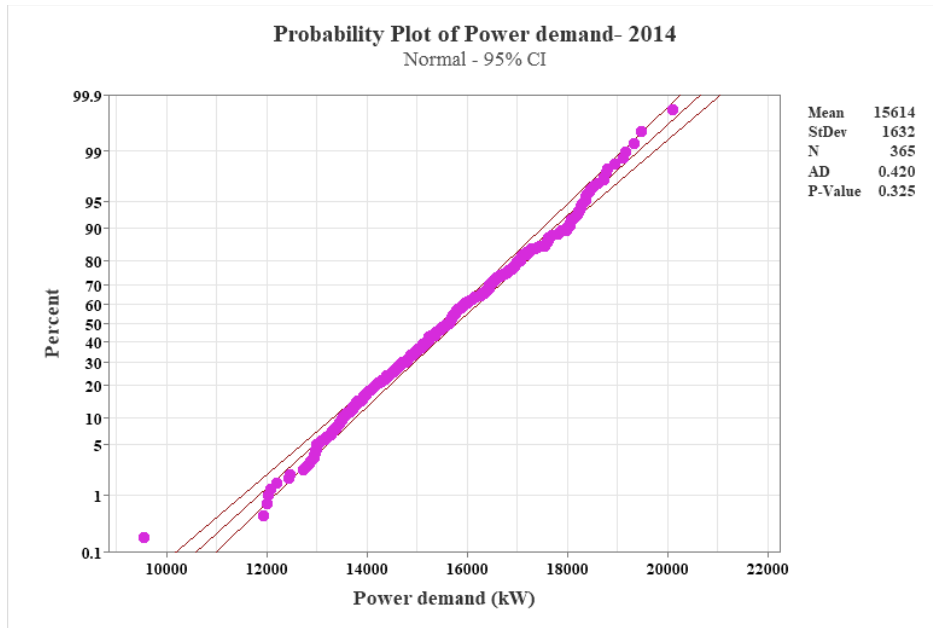


Figure 2.6 Probability plot of 2014 power demand

Figure 2.7 illustrates that the power demand data for 2015 follows the red line, except for one data point located at 20,000 kW. All the pink dots representing the power demand for 2015 are aligned with the red line. Moreover, the P-value for the power demand data for 2015 is 0.209, which exceeds 0.05. Thus, we can infer that the power demand data for 2015 is normally distributed.

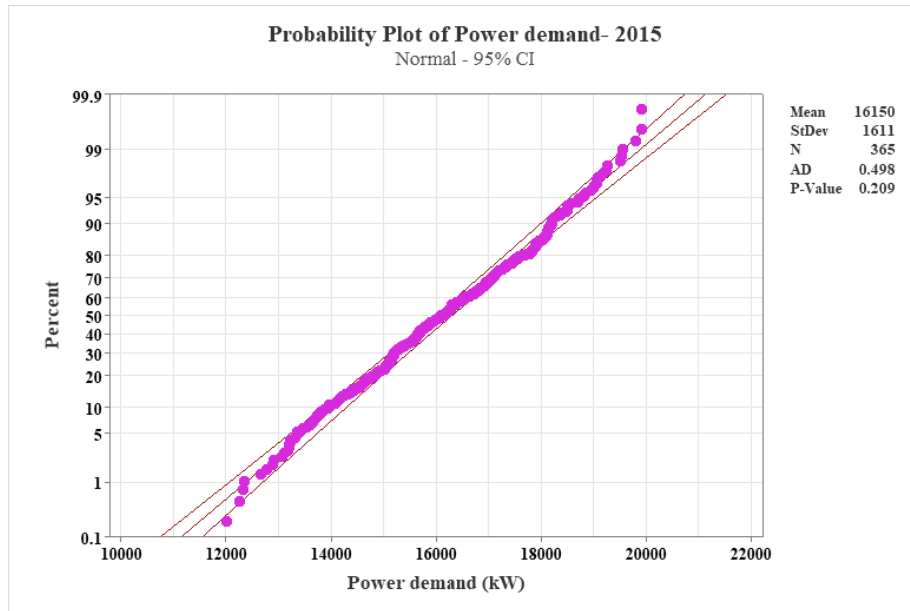


Figure 2.7 Probability plot of 2015 power demand

To test the normality of the data for 2016, Figure 2.8 displays a probability plot with pink dots representing data points. We can observe that all the pink dots follow the red line, except for one point at around 21,500 kW. The P-value for this test is greater than 0.05, indicating that the power demand data for 2016 is normally distributed.

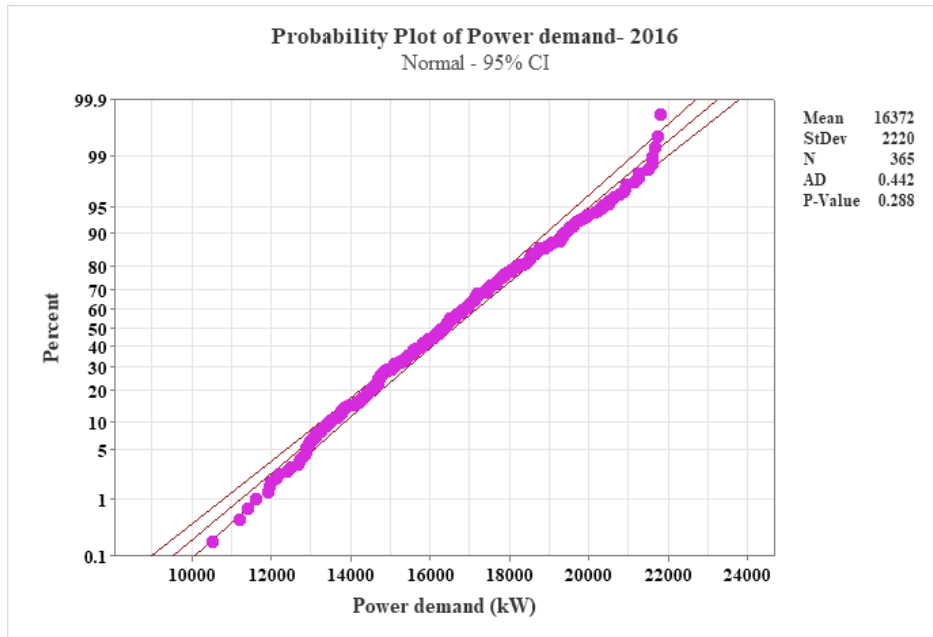


Figure 2.8 Probability plot of 2016 power demand

Figure 2.9 shows that a majority of the pink dots representing the power demand in 2017 are far away from the red lines. This suggests that the data for 2017 is not normally distributed. Additionally, the P-value is less than 0.005, which confirms that the data is not normally distributed.

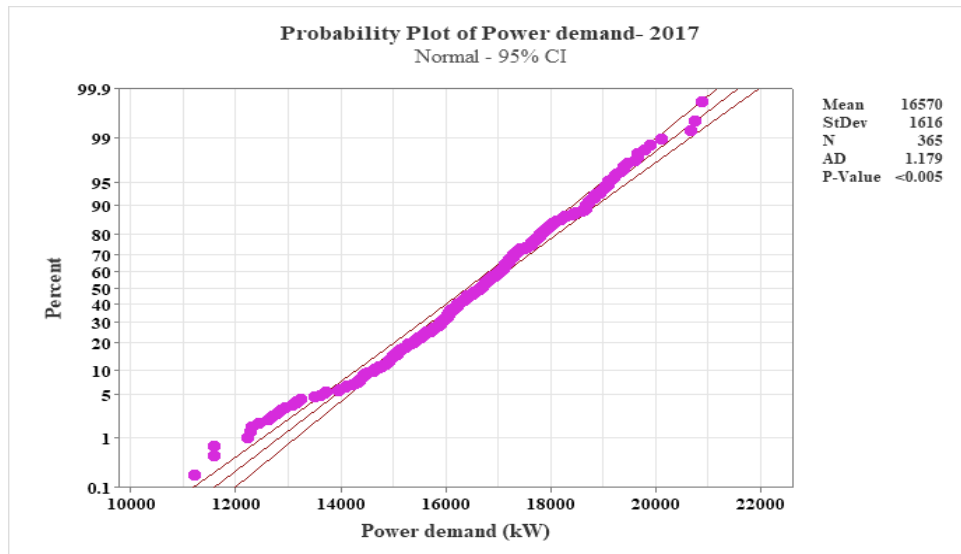


Figure 2.9 Probability plot of 2017 power demand

The non-normality of the 2018 data is evident from Figure 2.10 where several data points are located far from the red lines. Additionally, the P-value is less than 0.005, further confirming that the power demand data for 2018 is not following a normal distribution.

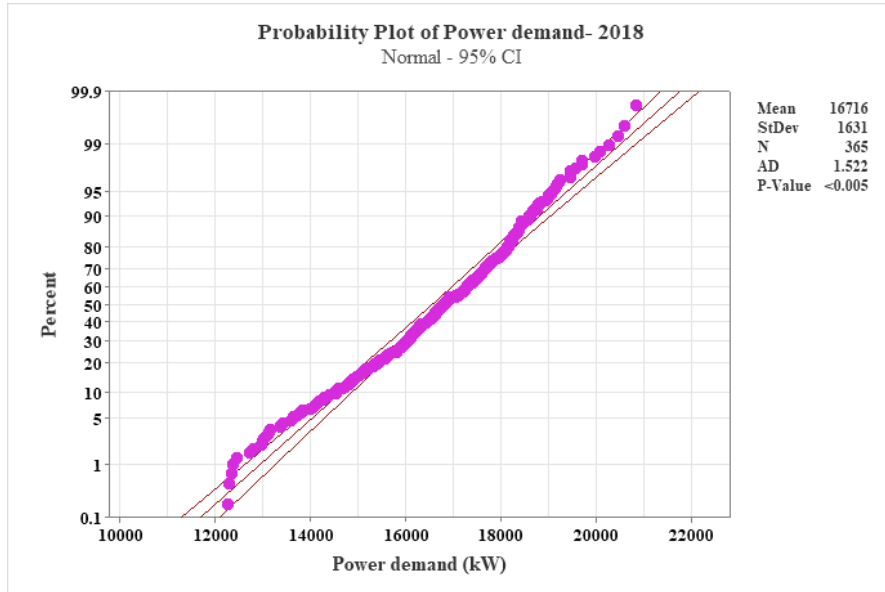


Figure 2.10 Probability plot of 2018 power demand

To put it differently, it can be seen from Figure 2.11 that a significant number of data points represented by pink dots lie beyond the two red lines' bounds, particularly in the top half of the probability plot. This suggests that the data is not distributed normally. This is also supported by the P-value of the plot, which is less than 0.005.

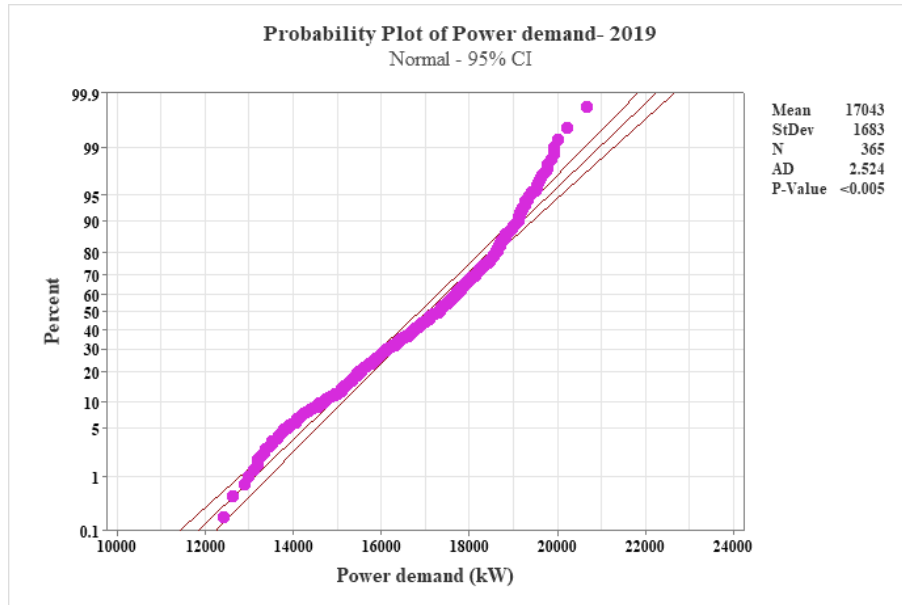


Figure 2.11 Probability plot of 2019 power demand

To describe Figure 2.12, we can observe that most of the pink dots representing the 2020 power demand data are far from the red lines, particularly in the lower part of the probability plot. This suggests that the data is not normally distributed. Additionally, the P-value of the plot is less than 0.005, which further supports the conclusion that the data is not normally distributed.

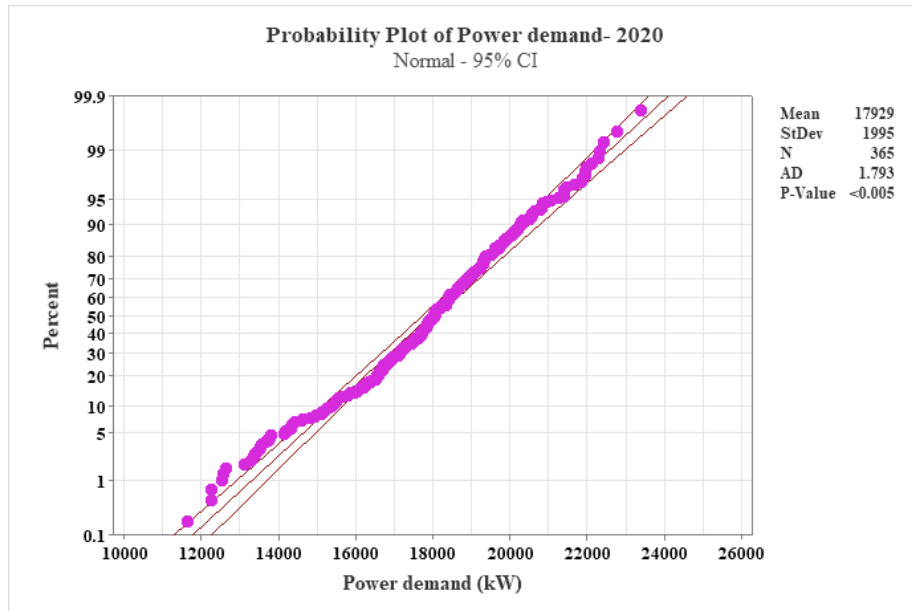


Figure 2.12 Probability plot of 2020 power demand

Figure 2.13 displays a wider distribution of data points for the 2021 power demand compared to other years, but they are still within the red lines. This could be attributed to the limited data available for that year. Additionally, the P-value is greater than 0.05, indicating that the 2021

power demand data is normally distributed.

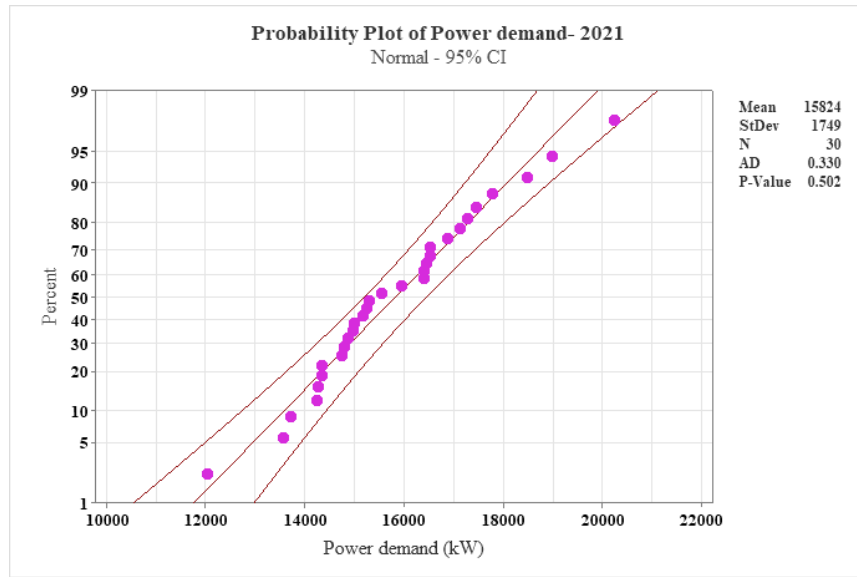


Figure 2.13 Probability plot of 2021 power demand

Figure 2.14 presents data on the power consumption at Società Metropolitana Acque Torino (SMAT) WWTP in Italy.

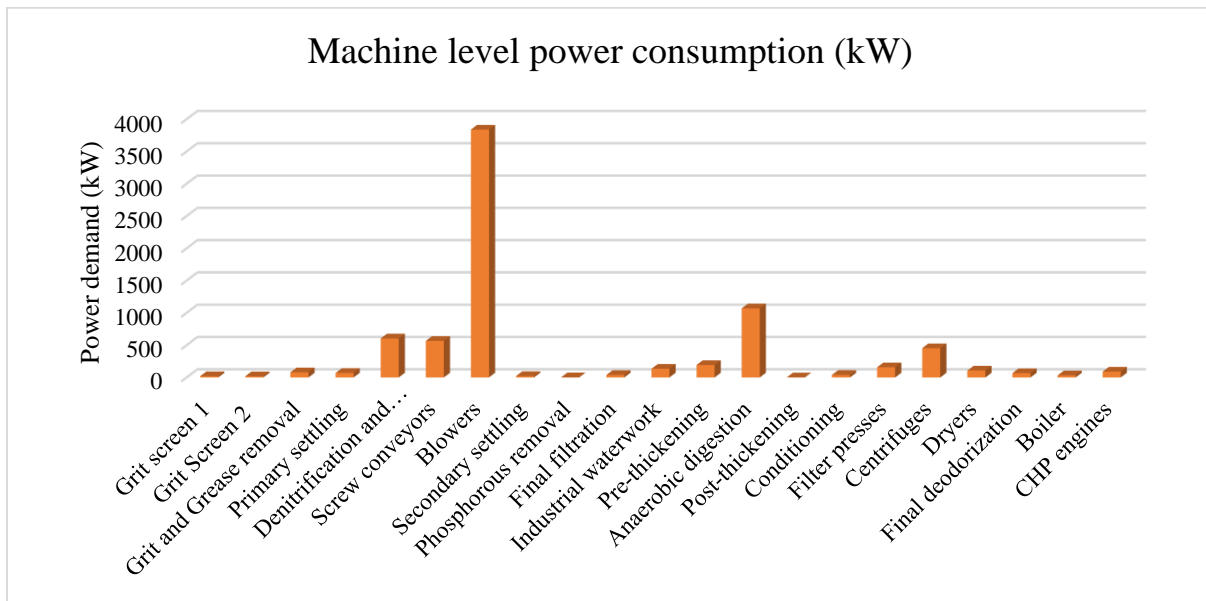


Figure 2.14 Machine level energy consumption SMAT WWTP in Italy (Panepinto et al., 2016)

This facility has a treatment capacity of 615 thousand cubic meters per day for municipal and industrial wastewater, which is equivalent to an organic load potentiality of 2.7 million equivalent inhabitants. The author of the study calculated the total power demand of the plant and found that approximately 50% of the energy is consumed in the oxidation tank during the aeration process. The figure also shows that the blowers consume a significant amount of energy in comparison to other equipment.

Table 2.4 Equipment level load in SMAT WWTP in Italy (Panepinto et al., 2016)

Water Line		
Equipment	kWh/day	Power demand (kW)
Grit screen 1	485	20.208
Grit Screen 2	446	18.583
Grit and Grease removal	1929	80.375
Primary settling	1665	69.375
Denitrification and biological oxidation	14,498	604.083
Screw conveyors	13,581	565.875
Blowers	92,102	3837.583
Secondary settling	518	21.583
Phosphorous removal	59	2.458
Final filtration	921	38.375
Industrial waterwork	3230	134.583
Sludge Line		
Equipment	kWh/day	Power demand (kW)
Pre-thickening	4629	192.875
Anaerobic digestion	25,682	1070.083
Post-thickening	54	2.25
Conditioning	951	39.625
Filter presses	3780	157.5
Centrifuges	10,880	453.333
Dryers	2556	106.5
Final deodorization	1608	67
Boiler	785	32.708
CHP engines	2160	90
Total	182,951	7622.958

2.2.2 Water Treatment Plants

Figure 2.15 depicts a time series plot created using Minitab software to display the total power demand of the Monroe water treatment plant situated in Bloomington, Indiana, USA. The graph shows the daily power demand over a period of approximately ten years, from January 2010 to April 2019. The data was obtained from the publicly available AmeriGEOSS Community Platform Datahub (2019) through the Google Datasets search engine. The Monroe water treatment plant serves a population of over 145,000 in Bloomington, IN. The plot in Figure 2.15 demonstrates a clear decreasing trend in electricity consumption at the facility. Specifically, the power demand decreased from 835 kW in September 2010 to approximately 625 kW in March 2019. Additionally, there is a similar trend in the initial years from 2010 to 2012, where the power demand increased during similar periods of the year (January to March, August to October, and December).

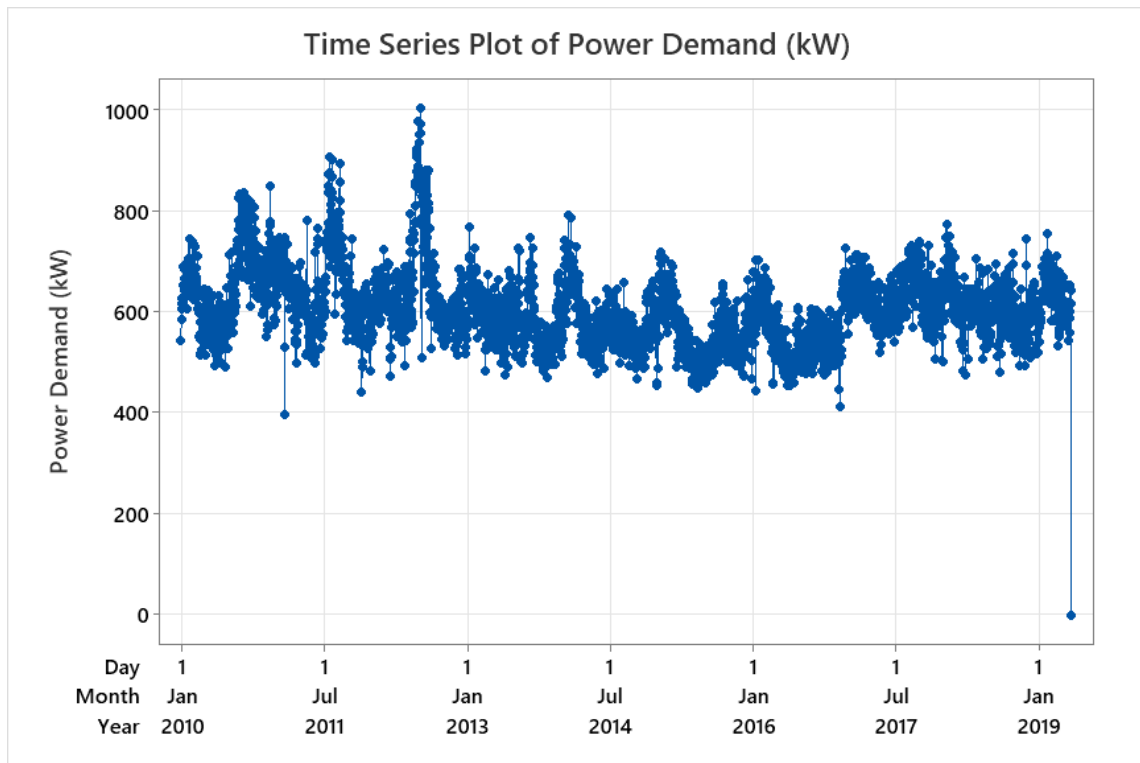


Figure 2.15 Daily power demand of Monroe water treatment plant from 2010-2019

To further analyze the data of Monroe water treatment plant from 2010 to 2019, a box and whisker plot has been generated in Figure 2.16. The mean power demand has shown a gradual decrease during this period, unlike the WWTP. This reduction in power demand may be attributed to a decrease in pollution concentration in Lake Monroe. The mean power demand was 649 kW in 2010 and decreased to 630 kW in 2019, except for a slight increase in 2017. However, comparing the data of 2019 with previous years is not appropriate because it contains only 4 months of data instead of the usual 12 months. The boxplot indicates a high number of outliers in 2011 and 2012, which could be due to sampling of the data, data entry errors, natural variation, or mechanical faults in the equipment. Additionally, the IQR of 2010 and 2011 is much larger than the remaining years, indicating higher variability in power demand during these two years. Conversely, 2017 and 2018 have the lowest variability in their power demand, with the least IQR of 58 kW and 60 kW.

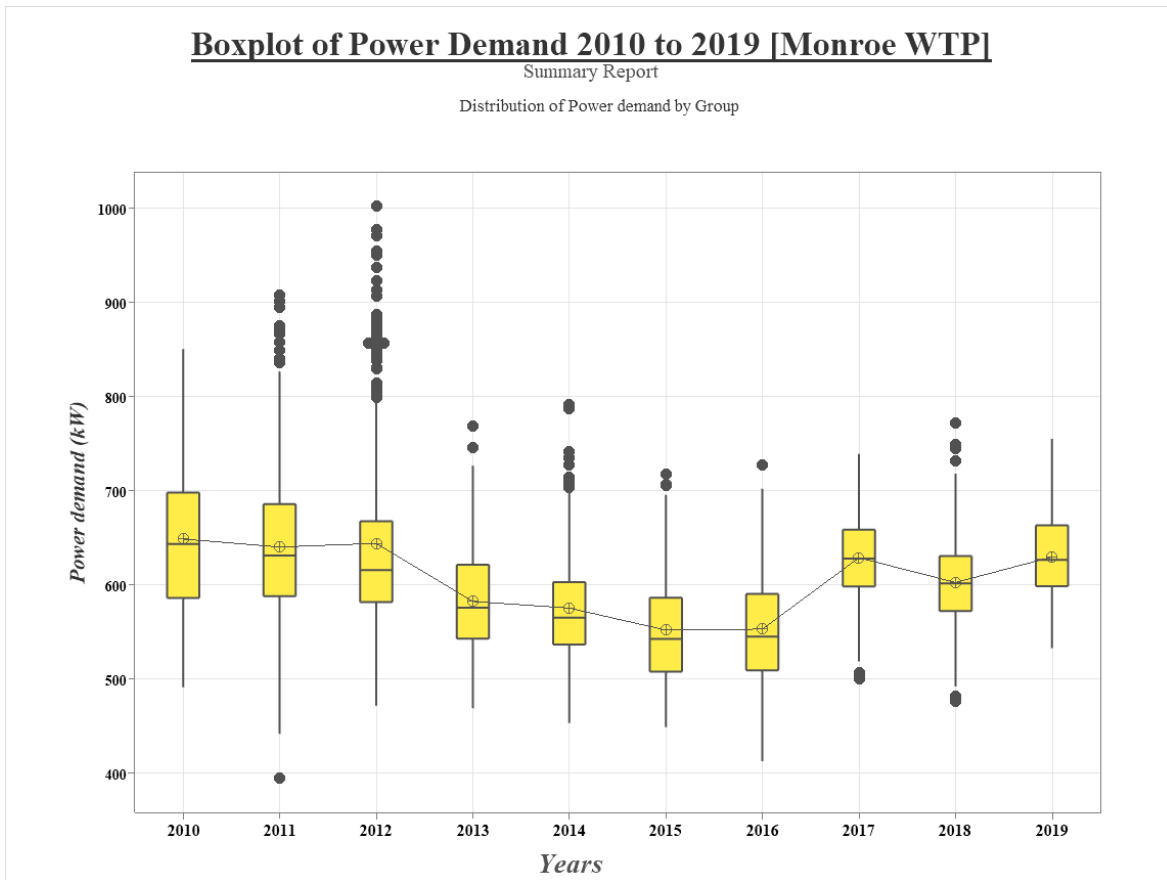


Figure 2.16 Yearly box plot for power demand of Monroe WTP (2010-2019)

Table 2.5 provides a descriptive statistical analysis of the power demand data for the Monroe WTP, showing the number of days, mean, standard deviation, minimum, and maximum values for each year. Additionally, a column has been added to show the power demand fluctuation, which is calculated by dividing the standard deviation of each year by its corresponding mean. It is worth noting that electrical equipment is not affected by voltage fluctuations under 10%. In the initial years, there were high voltage fluctuations, particularly in 2012 with a percentage of 15.17%, followed by 2011 and 2010 with 12.57% and 12.08%, respectively. However, there is a decreasing trend in the power fluctuations from 2010 to 2019, with a decrease from 12.08% to 6.77%. This decrease in fluctuations can potentially increase the lifespan of motors used in the water treatment facility.

Table 2.5 Descriptive statistical report for Monroe WTP (Unit: kW)

Year	Number (N)	Mean	St. Dev	Minimum	Maximum	Voltage Variation
2010	365	648.55	78.376	491.25	850.05	12.08%
2011	365	640.13	80.466	395	906.95	12.57%
2012	366	643.97	97.710	471.85	1001.8	15.17%
2013	365	582.34	54.792	468.95	768.1	9.41%
2014	365	575.34	55.383	453.4	791.5	9.63%
2015	365	551.95	56.906	448.85	717.3	10.31%
2016	366	553.04	57.199	412.75	726.75	10.34%
2017	365	628.71	44.505	500.6	738.75	7.08%
2018	365	602.49	47.929	475.85	771.85	7.96%
2019	120	629.56	42.619	532.7	754.9	6.77%

Figure 2.17 displays the results of a one-way ANOVA conducted on the daily power demand data of the Monroe WTP. The obtained P-value is less than 0.05, indicating that there are significant differences between the mean values. When the P-value is less than 0.05, it indicates that the null hypothesis is rejected, which means that the alternative hypothesis holds true. The mean power demand values for the years 2010 to 2019 are 648 kW, 640 kW, 684 kW, 582 kW, 575 kW, 552 kW, 553 kW, 628 kW, 602 kW, and 629 kW, respectively. Hence, we can infer from Figure 2.17 that the daily power demand of the Monroe WTP varies significantly over the 10-year period.

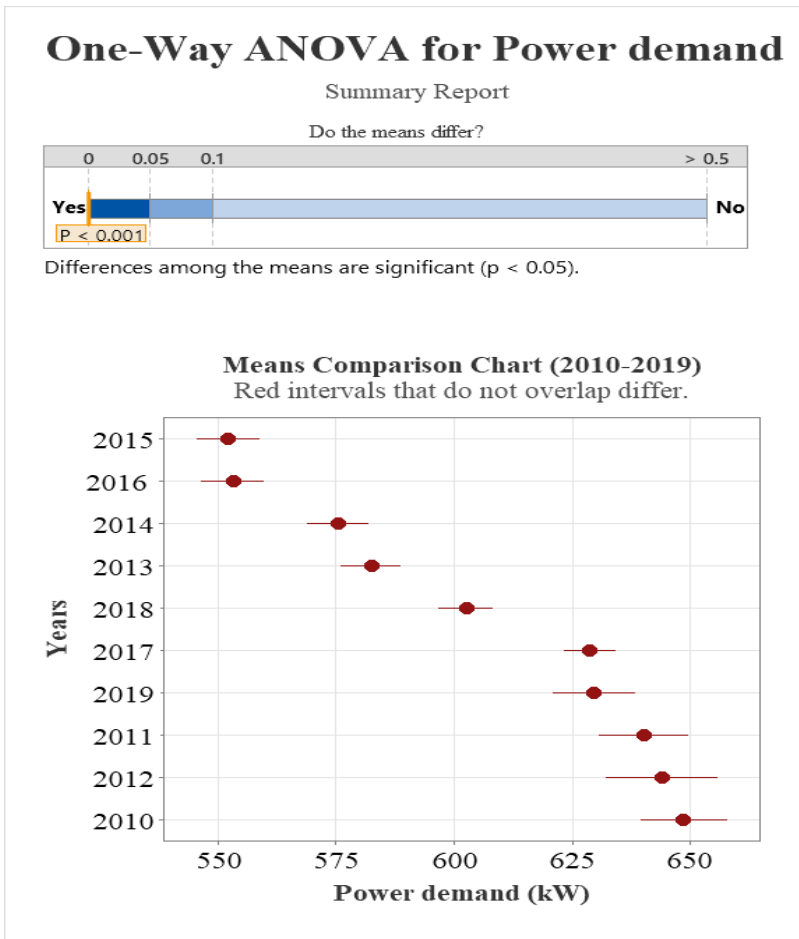


Figure 2.17 Mean comparison chart of power demand of Monroe WTP

We constructed histograms for each year from 2010 to 2019 to gain a better understanding of the power demand trends at Monroe WTP. Figure 2.18 illustrates the histogram for 2010, which displays a normal distribution and a bell-shaped curve. The most frequent power demand value in this year was 610 kW, occurring for 36 days, followed by a mean value of 648.6 kW with a frequency of 34 days. The lowest and highest readings for this year were 490 kW and 850 kW, respectively. The histogram for 2011 did not deviate below the normality curve. The most frequent power demand value for this year was 640 kW, with a frequency of 48 days, and the average value was 640.1 kW. The minimum and maximum readings for this year were 430 kW and 900 kW,

respectively. In contrast, some data points in 2012 were outside the normality curve on the left side. The most common power demand value for this year was 600 kW, with a frequency of 67 days, and the lowest and highest readings were 460 kW and 980 kW, respectively. The standard deviation for 2012 was the highest among all previous years at 97.71 kW. The histogram for 2013 revealed a bell-shaped and evenly dispersed electricity demand. The most common power consumption level in this year was 580 kW, occurring for 40 days, and the lowest and highest values were 450 and 765 kW, respectively. In contrast, the data for 2014 was skewed to the left and not normally distributed, with the minimum and maximum values of 450 kW and 800 kW, respectively. Similarly, the histograms for 2015 and 2016 were also skewed to the left and not evenly distributed, with lowest and highest values ranging from 450 kW to 720 kW. In 2017, some data points were outside the normality curve in the center, and the lowest and highest power demand levels were 500 kW and 400 kW, respectively. The histogram for 2018 in Figure 2.19 was also not regularly distributed in the middle, with the minimum and maximum values ranging from 480 kW to 770 kW. The histogram for 2019 is not available since we only have 120 days of data, compared to 365 days for previous years. Nonetheless, the minimum and maximum values for 2019 were 550 kW and 760 kW, respectively, based on the available data.

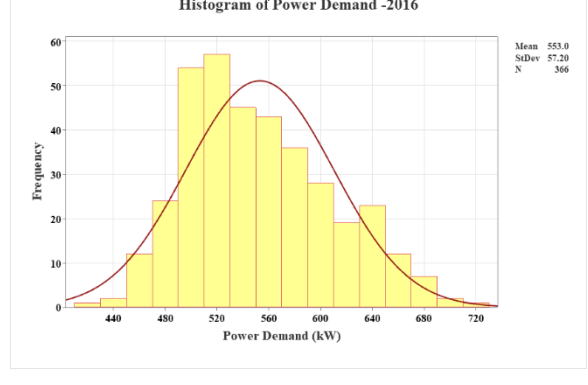
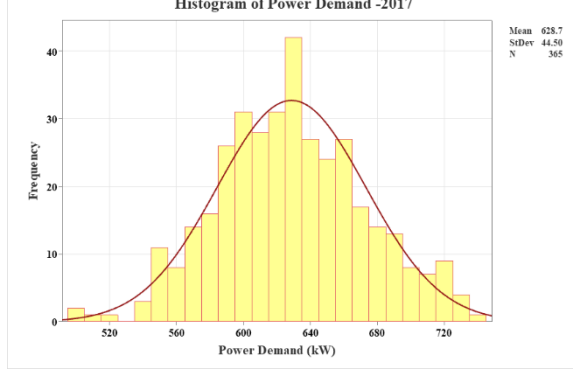
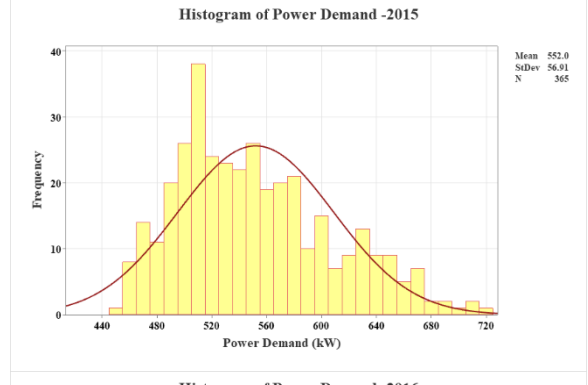
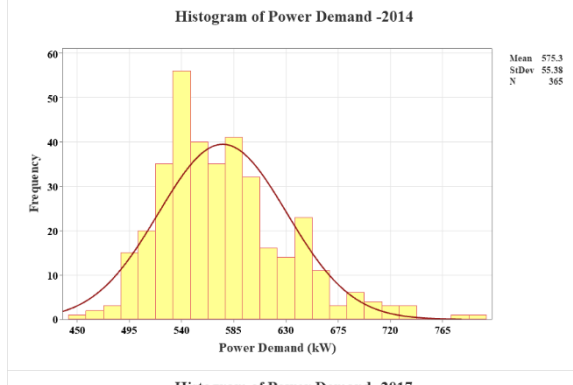
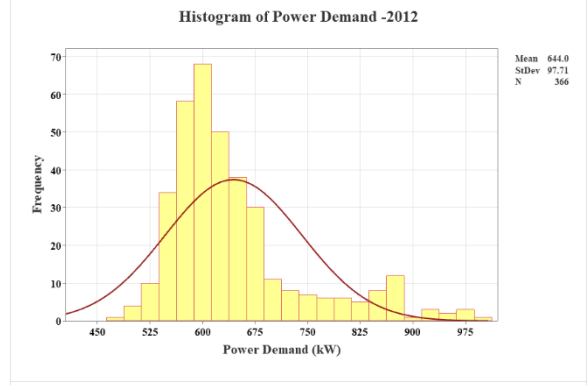
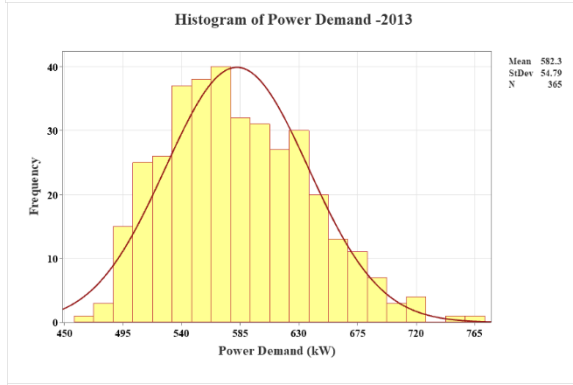
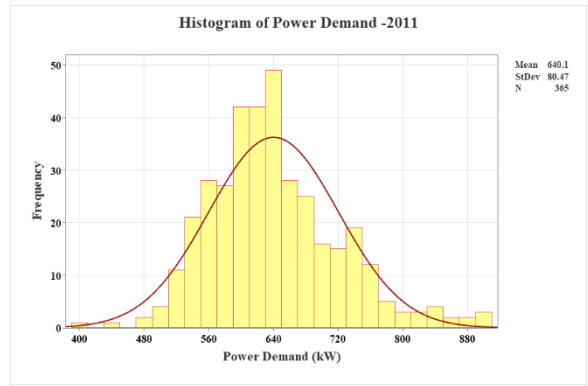
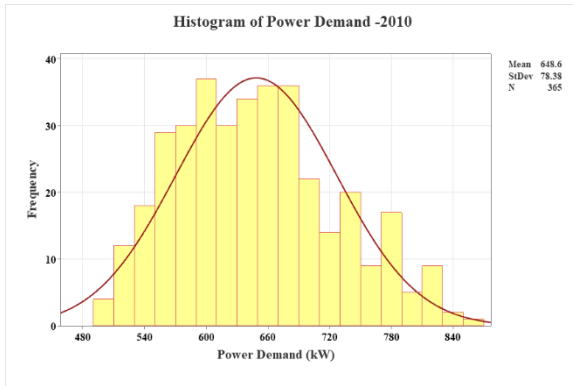


Figure 2.18 Histogram of power demand of Monroe WTP (2010-2017)

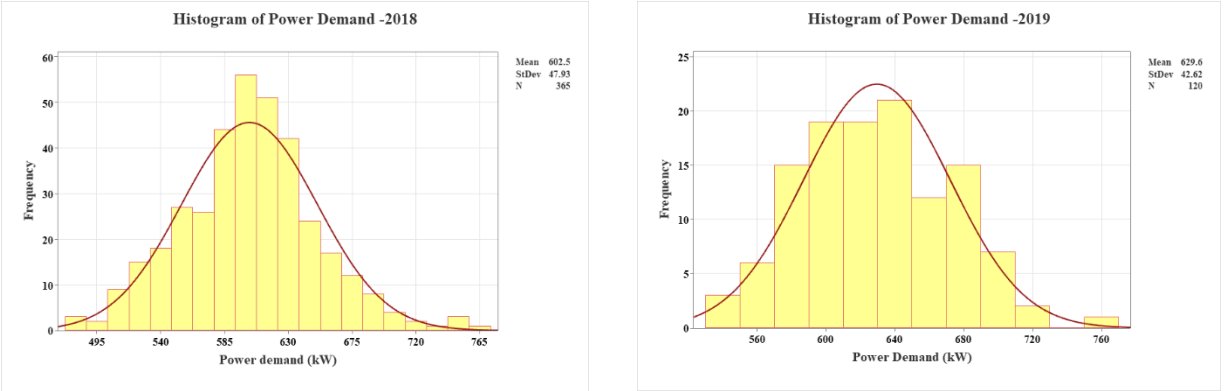


Figure 2.19 Histogram of power demand of Monroe WTP (2018-2019)

Figure 2.20 displays data on the energy consumption at the process level for a small drinking water treatment plant that treats groundwater for a city with a population of less than 10,000. The plant is located in the southwestern region of the US, but its specific location is not disclosed to maintain confidentiality. This data was reported by (Bukhary et al., 2020).

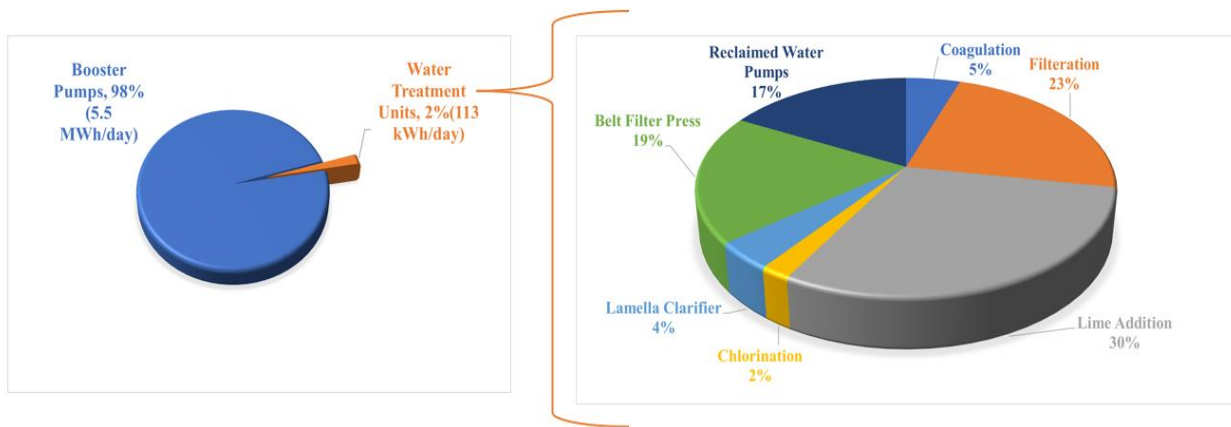


Figure 2.20 Process level energy use in a water treatment plant in USA (Bukhary et al., 2020)

The southwestern region has ideal solar conditions for photovoltaic (PV) installation and energy generation. At the water treatment plant, the booster pump accounts for approximately 98% of the energy consumption, while the other water treatment units consume the remaining 2%. Of this 2%, about 30% is used for lime addition and 23% for filtering procedures. Booster pumps play a critical

role in improving flow rate, water pressure, and transferring groundwater to the treatment plant. Without booster pumps, there is a risk of stagnant sewage buildup, which could pose health hazards. However, the high energy consumption of booster pumps presents an opportunity for wind or PV system installation to reduce the facility's energy cost and environmental impact.

3. MACHINE LEARNING APPROACH TO SHORT-TERM WIND SPEED FORECASTING

3.1 Characterizing Wind Generation

3.1.1 Wind Power Generation Model

The cubic function is commonly used to characterize the instantaneous power output of a wind turbine (WT) (AlHajri and El-Hawary, 2007). In fact, cubic wind power function is frequently used for optimal distribution generation sizing via fast sequential quadratic programming. Let $P_w(v)$ be the WT output power at wind speed v , then,

$$P_w(v) = \begin{cases} 0 & 0 < v < v_c, \text{ or } v > v_s \\ \gamma v^3 & v_c \leq v \leq v_r \\ P_m & v_r \leq v \leq v_s \end{cases} \quad (3.1)$$

where, P_m is the rated power or the turbine capacity in unit of MW or kW depending on the size, and $\gamma = P_m/v_r^3$. Note that v_c is the cut-in wind speed, v_r is the rated speed, and v_s is the cut-off speed, respectively. The value of v_c varies between 2.5 to 3.5 m/s. The value of v_r is around 10 to 12 m/s. The cutting off speed v_s is often set as 25 m/s.

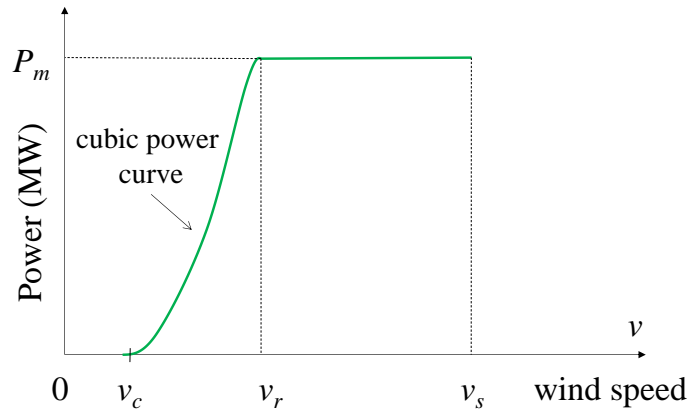


Figure 3.1 A typical wind power curve

Let V be the random wind speed. The mean and the variance of $P_w(V)$ can be estimated as follows (Jin and Tian, 2010).

$$E[P_w(V)] = \gamma \int_{v_c}^{v_r} v^3 f_w(v) dv + P_m(F_w(v_s) - F_w(v_r)), \quad (3.2)$$

$$E[P_w^2(V)] = \gamma^2 \int_{v_c}^{v_r} v^6 f_w(v) dv + P_m^2(F_w(v_s) - F_w(v_r)), \quad (3.3)$$

$$Var(P_w(V)) = E[P_w^2(V)] - (E[P_w(V)])^2, \quad (3.4)$$

where $F_w(v)$ and $f_w(v)$ are the cumulative distribution and the probability density functions of wind speed, respectively. Based on the local meteorological data, V can be fitted by Weibull, normal or other parametric distributions. In general, the characteristics of wind velocity often favor the fitting of a Weibull distribution in wind speed analysis (Tuller and Brett, 1984). For the Weibull model, the cumulative distribution function (CDF) and probability density function (PDF) are given below, respectively.

$$F_w(v) = 1 - e^{-(v/c)^k} \quad (3.5)$$

$$f_w(v) = \frac{k}{c} \left(\frac{v}{c}\right)^{k-1} e^{-(v/c)^k} \quad (3.6)$$

where c and k are scale and shape parameters. The larger the scale parameter ‘ c ’, the higher the average wind speed. Figure 3.2 shows a typical Weibull wind speed distribution with different values of c and k . Given the wind speed distribution and WT power curve, we are able to estimate the mean and variance of output power based on equations (3.2) and (3.4), respectively. Hence characterizing wind profile and forecasting its future behavior are the key to manage wind power generation and dispatch.

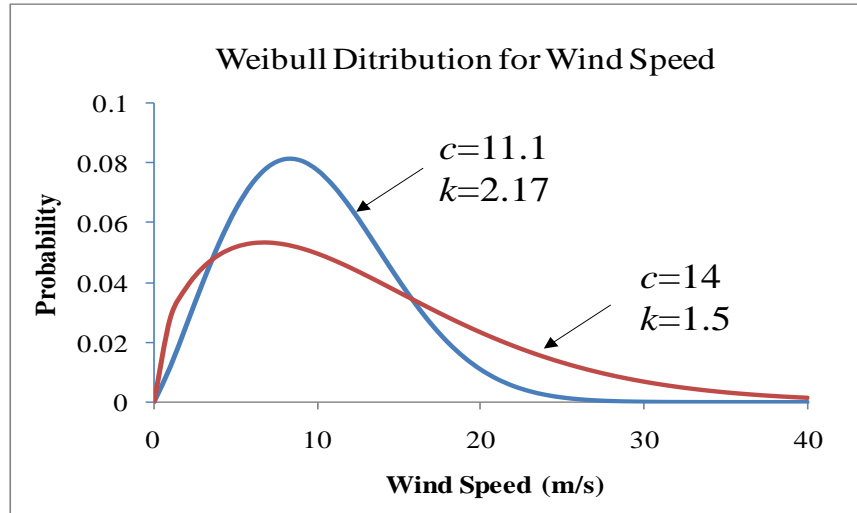


Figure 3.2 Weibull wind speed distributions (Jin and Tian, 2010)

3.2 Wind Speed Forecasting using Machine Learning

3.2.1 Machine Learning in Forecasting Time Series Data

In this section we will discuss the machine learning (ML) algorithms that will be used for the wind speed forecasting in our study. Wind speed forecasting is a type of regression problem in which wind speed is used as an input variable or predictor, and output variable is produced as predicted wind speed. In addition to wind speed, other meteorological attributes are temperature, humidity, weather condition, wind direction, and precipitation. Wind speed records also belong to a time series dataset. A time series is defined as a sequence of random variables, x_1, x_2, \dots, x_n , where x_1 represents the first-time stamp in the series, x_2 represents the second time stamp, and so on until time n , where n is a discrete integer (Shumway and Stoffer, 1982). A time series, in general, is made up of n consecutive observations collected from a fundamental stochastic process. ML is a collection of statistical methodologies designed to learn from recorded data, i.e., to construct a mathematical model for anticipating future data or observations. The primary objective of ML is to establish a data-driven, automated computation of models that do not require human decisions.

There are various methods that are available for the forecasting of time series data. In this

thesis three types of ML models will be used: recurrent neural network (RNN), long short-term memory (LSTM), and ensemble model. In the following subsections these models will be mathematically explained.

3.2.2 Data description of San Marcos

Typically, data obtained from international airport weather stations is suitable for research. The meteorological time series dataset for wind speed prediction utilized in this study was obtained from Austin Airport between 2011 and 2019 for the city of San Marcos, Texas because the distance between two sites is about 40 km. The airport station collects the meteorological data on an hourly basis, making it very reliable, and future data requests can be met easily. The average wind speed of San Marcos throughout the 9-year period as show in Figure 3.3. It is evident from this figure that San Marcos has a variable wind speed because of unpredictability of the weather in Central Texas. Temperature, wind speed, dew point, and precipitation are among the 14 attributes included in the dataset.

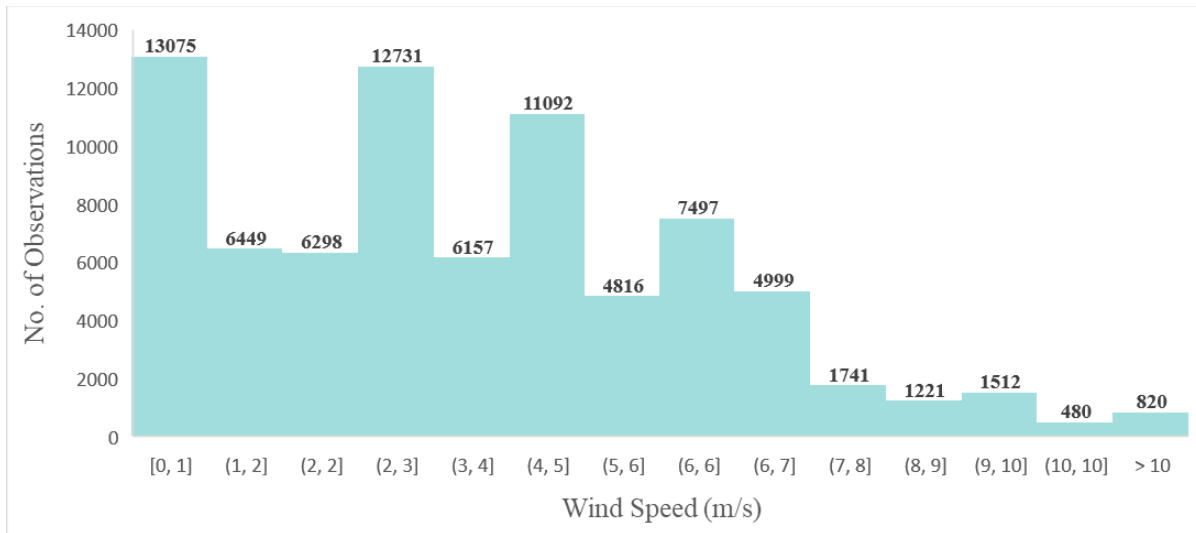


Figure 3.3 Wind speed profile for San Marcos (2011-2019)

This research considers hourly observations of wind speed in meters per second (m/s), yielding around 78,000 recordings. The total number of observations, including the mean, standard

deviation, minimum and maximum wind speed of the dataset is explained in Table 3.1.

Table 3.1 Explanation of San Marcos wind speed data (unit: m/s)

Location	Sample size	Mean	Std. Dev.	Min	25%	50%	75%	Max
San Marcos	78888	3.611	2.531	0.000	2.240	3.580	5.360	18.330

One of the requirements of time series models is that they need continuity and sufficiency of historical data. In addition to being continuous, data must also be stationary, which is also a requirement of machine learning models. Stationary data consists of time series with no trend or seasonality. That is, the data has a constant mean and variance that does not vary over time, as this can add seasonality to the models. The box plot in Figure 3.4 depicts the monthly variability of wind speed from 2011 to 2019.

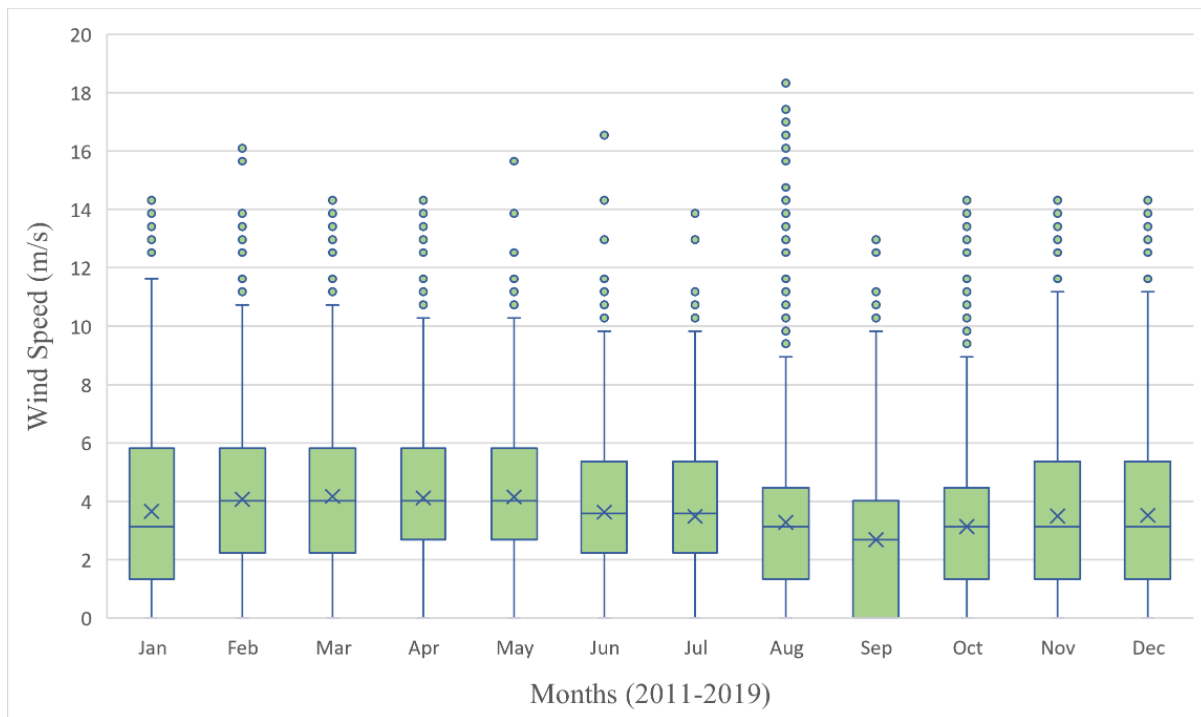


Figure 3.4 Boxplot for variation of hourly wind speed from 2011 to 2019

The whiskers of the boxplot clearly show that the maximum range of wind speed in San Marcos

is from 0 to 19 m/s. To comprehend these box and whisker plots, consider the box plot for the month of February, which has a range of 0 to around 16 m/s. The midline of the box represents the median. The top and bottom boundaries of the box are referred to as the third and first quartiles, respectively. The first quartile represents the median for the lower half of the data, while the third quartile represents the median for the upper half of the data.

The 'X' above the median represents the mean of the data set. Furthermore, the middle line of the boxes reflects the nine-year median of wind speed, indicating that the median appears to fluctuate from month to month, which can be a factor in the ML models. Furthermore, the wind speed is comparatively higher from January to July as compared to the wind speed in August to December. It is important to note that outliers increase rapidly from August to December as winter approaches and then decrease from January to July for the rest of the year. The boxplot clearly shows that the average wind speed at San Marcos is between 3 and 4 m/s.

3.2.3 Forecasting Performance Metrics

To compare the various regression models utilized in this thesis, several error metrics such as mean squared error, mean absolute error, and R-squared values will be employed. The next section will define these error metrics. These error ratings assist us in determining the accuracy of the predictions made by various models.

A. Mean Squared Error:

Now we will define the formula of the mean squared error (MSE) estimator. For supervised learning, regression models are used to predict the dependent variable, while MSE can be used to measure the model performance. Statistically speaking, MSE represents the average squared error between the observation and predicted value. It is sensitive to outliers and penalizes large errors. Though a zero MSE is preferred, it can range from 0 to infinity, with lower value indicating a more

efficient model. The MSE is defined as follows:

$$MSE = \frac{1}{n} \sum_{i=1}^n (y_i - \tilde{y}_i)^2 \quad (3.7)$$

Where:

n = number of observations

y_i = actual output value

\tilde{y}_i = predicted output value

B. Mean Absolute Error:

Mean absolute error (MAE), is calculated without taking into account their direction in a group of forecasts. Given all the individual deviations have equal weights, the average is calculated using the absolute differences between the predicted and the actual observation. Therefore, MAE is defined as the average absolute error between actual and the forecasted values. MAE is defined as follows:

$$MAE = \frac{1}{n} \sum_{i=1}^n |y_i - \tilde{y}_i| \quad (3.8)$$

The value of MAE also ranges from 0 to infinity, where lower MAE scores denote a more accurate forecast from the model.

C. R squared Score:

R squared (R^2 or the coefficient of determination) is a statistical metric used to assess prediction model effectiveness. It has a scale of 0 to 100 percent. R^2 indicates how well the regression models fit the observed and anticipated data, often known as the goodness of fit. R^2 calculates the proportion of the dependent variable's variation that can be explained by the independent variable. It is defined as a ratio of sum of squares regression (SSR) to sum of squares total (SST) as shown

in the following equations:

$$R^2 = 1 - \frac{SSR}{SST} \quad (3.9)$$

$$R^2 = 1 - \frac{\sum(y_i - \tilde{y}_i)^2}{\sum(y_i - \bar{y})^2} \quad (3.10)$$

Where:

SSR = total variance of all the predicted values obtained on the regression line from the mean value of all response variable values

SST = entire variance of original data from the mean value of all response variables

\bar{y} = mean value of output

3.3 Regression Models

3.3.1 Recurrent Neural Network

Recurrent Neural Network (RNN) uses time series or sequential data and is a type of artificial neural network (ANN). Essentially, the output from one step is used as input for the next step. RNN is a state-of-the-art algorithm for sequential data analysis and also used by Google voice search and Apple's Siri (Beaufays, 2015; Donges, 2022).

From a given set of data points with predefined outputs, neural networks can self-adapt and learn, which allows them to model and predict the complex pattern of the data (Madan and Mangipudi, 2018). RNN is considered one of the most powerful neural networks due to its internal memory, and it falls under the umbrella of Artificial Intelligence (AI). The recurrent edges in RNN span neighboring time steps. These edges have the potential to form cycles, incorporating the concept of time into the model. The weights and biases of the neurons or units in RNN models are modified based on the error scores backpropagated from the last to the first timestamp, with unrolling of all timestamps. This is referred to as back-propagation through time (BPTT). Calculating the error for each timestamp allows us to update the weights. Backpropagation is an

algorithm that returns errors from output nodes to input nodes. As a result, it is known as backpropagation (Donges, 2022).

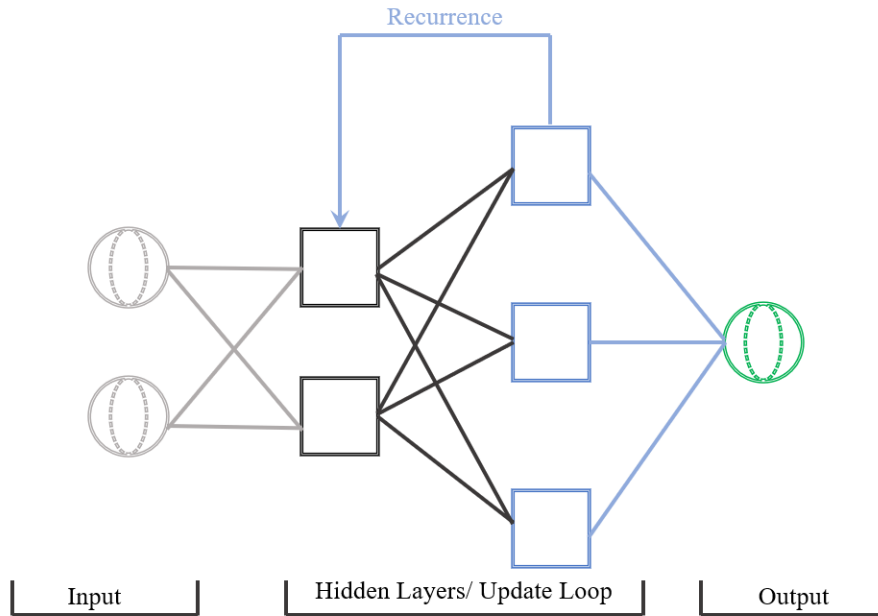


Figure 3.5 RNN architecture (the sequence {start-update loop-end})

In Figure 3.5 the input variable is x , and the output variable is y . The data is fed with the help of an input variable at time t , denoted as x_t , which is multiplied with its equivalent weight (W). The sum of the products is measured and then output y is generated after passing the sum through a non-linear activation function. NN models employ activation functions to generate output from input variables that are fed into the next layer. These activation functions also add non-linearity to the NN. Some typical activation functions used in NN models are sigmoid or logistic activation function, tanh activation function (hyperbolic tangent), and ReLU (rectified linear unit) activation function. A sigmoid function (S) takes any real number as its input and returns a value between 0 and 1, which is commonly used when forecasting the output as a probability. A sigmoid function is defined as (Sharma, 2017):

$$S(x) = \frac{1}{(1+e^{-x})} \quad (3.11)$$

In contrast to sigmoid functions, tanh activation functions have an output range of -1 to 1. As tanh functions produce a zero-centered output, the output may be translated as highly positive, highly negative, or neutral. A tanh function is described as:

$$\tanh(x) = \frac{e^x - e^{-x}}{e^x + e^{-x}} \quad (3.12)$$

A *relu* (R) performs effective backpropagation as a result of its derivative function. As compared to tanh and sigmoid functions, the *relu* function has greater computational efficiency. A *relu* function can be described as:

$$R(x) = \begin{cases} x, & x > 0 \\ 0, & x \leq 0 \end{cases} \quad (3.13)$$

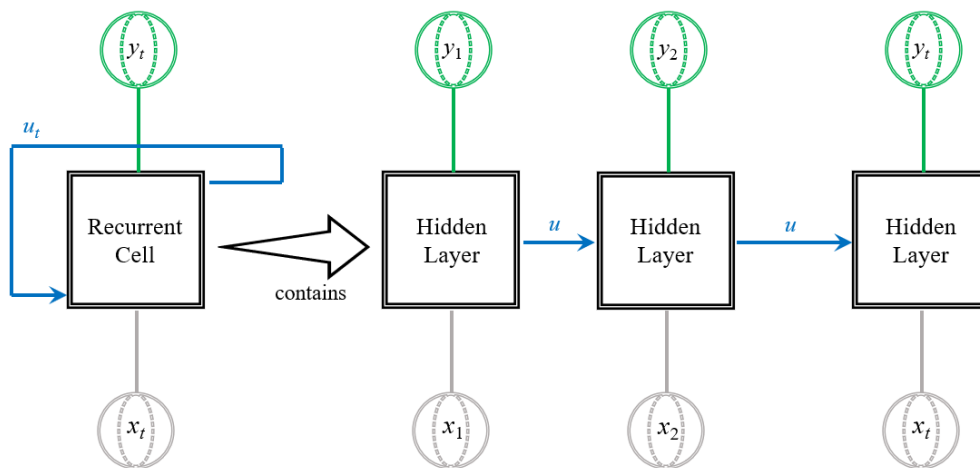


Figure 3.6 RNN architecture (the update loop) (Le et al., 2019)

In Figure 3.6 a local state update function u is generated from the network. This update function is basically used to review the previous input data and generate different outputs considering the previous data. RNN has hidden layers between its input and output layers. This local state update, u is a function of the current input data x and the previous u and occurs with every recurrent step of the hidden layers as the time evolves.

It is possible to think of recurrent neural networks as multiple copies of feedforward networks, each sending a message to the successor. The RNN receives the current value as input as well as a state vector indicating what the network has observed in previous time steps at each time step. At time step t , the input is determined by the output at time step $t-1$ (Dontas, 2010). The working principle of an RNN model can also be further understood from the following equation:

$$h_t = \sigma(W_x^T x_{t-1} + W_y^T y_t + \mathbf{v}) \quad (3.14)$$

where:

x = input variable

y = target or output variable

σ = sigmoid, tanh or relu functions

\mathbf{v} = bias vector of hidden units

W_x = input weight at the current time stamp

W_y = Output weight for previous time stamp

In the RNN model, the data is forwarded with the help of input variable, and every input has a respective weight W . A bias vector is also included to shift the function according to the problem.

Some **pros and cons** of the RNN model are elaborated below.

Pros:

- Model size is not affected even if the data size is large.
- Can process inputs of any length.
- The weights can be shared across the time steps.
- It can remember all the information fed to them, which is very helpful in any time-series predictor.

- Can use the internal memory for processing arbitrary series of inputs which is not the case with feed forward NN.

Cons:

- Computation time is prolonged because of its recurrent nature.
- While using Relu or Tanh as activation function, it becomes very difficult to process long sequences.
- RNN models can be difficult to train since they are not feedforward neural networks, which only move signals in one direction (Stoltzfus, 2022).
- Vanishing gradient and exploding gradient are the two major problems of RNN.

Model Explanation:

For our project hourly wind speed data of nine years between 2011 and 2019 of San Marcos, TX are used. For the RNN model we have first imported the dataset and parsed the date into a date time format. Parsing is important as different entities need the data in different forms. It allows us to transform the data in a way that can be understood by specific software. Then the first five values of the data are printed to check if the program is reading it. After this all the column names were printed and those which are not required are dropped. Then we have again printed the first five values to check if the columns have been dropped.

Then all the NULL or missing values are dropped using Pandas *dropna ()* function and the dataset was reshaped after this step. Then the *MinMaxScaler* function is used to scale down all the dataset values in the range of 0 to 1, without changing the shape of the original distribution. After scaling, the model has been trained with 80% values (6,3110) of the dataset. Test size is defined in the model by subtracting the training size from the original dataset. After this step a dataset has been

created in matrix format and X_t and Y_w are defined where X_t is the list of time stamp in hours and Y_w is the list of wind speed in m/s. Furthermore, a 'for loop' can be used to define the range of the function, and it ranges from 0 to i , where i is the length of the dataset subtracted by consideration time subtracted by one. Where C denotes the number of hours that the model will consider for predicting future wind speeds. Without loss of generality, six different horizons, i.e., 1, 3, 8, 12, 24, and 36 hours, are considered respectively for the time-period as shown in Table 3.2. Then an array A is introduced as a in the model containing sum of i and C . In the next step the value of A is appended to X_t and the sum of i and C is appended to Y_w . Append method is generally used to add a new element to any existing list. Then C is introduced again where we can input different consideration time for predicting the future wind speeds as shown in Table 3.2. The X training and testing values, as well as the Y training and testing values, were then used to create a dataset. In this instance, the X train values will range from 0 to X train size, and the Y train values will range from 0 to Y train size. In the next step input data has been reshaped into training and testing data.

Table 3.2 Comparison of MSE, MAE and R^2 errors at different consideration times

Hours	MSE	MAE	R^2
1	0.578	0.399	0.947
3	0.763	0.515	0.908
8	0.725	0.483	0.916
12	0.740	0.512	0.913
24	0.726	0.507	0.917
36	0.736	0.499	0.914

The model was created with the help of *SimpleRNN* model, which is a recurrent layer object in *Keras* deep learning library (Saeed, 2022). After this a layer has been added to this model with *relu* activation function, having 100 hidden units. Every hidden layer in RNN model is composed of multiple hidden units, these hidden units will always be an integer as they are the memory cells

that are used to store information. The *relu* activation function is preferred over other functions because it produces better results. A dropout layer is also added to prevent overfitting of the model. Overfitting is a condition when a model fits perfectly with the training data but fails to perform with the new data. The regression model uses two hidden layers to give better predictive performance including the dense layer. After this the mean squared error (MSE) is evaluated with the help of *adam* optimizer. The purpose of optimizers in deep learning models is to minimize the loss by updating the network parameters in a highly efficient manner.

Table 3.3 Architecture of the model

Layer (type)	Output Shape	Parameter Number	Comment
SimpleRNN	(None, 100)	10,200	<ul style="list-style-type: none"> • Total parameters: 10,301 • Trainable parameters: 10,301 • Non-trainable parameters: 0
Dropout	(None, 100)	0	
Dense	(None, 1)	101	

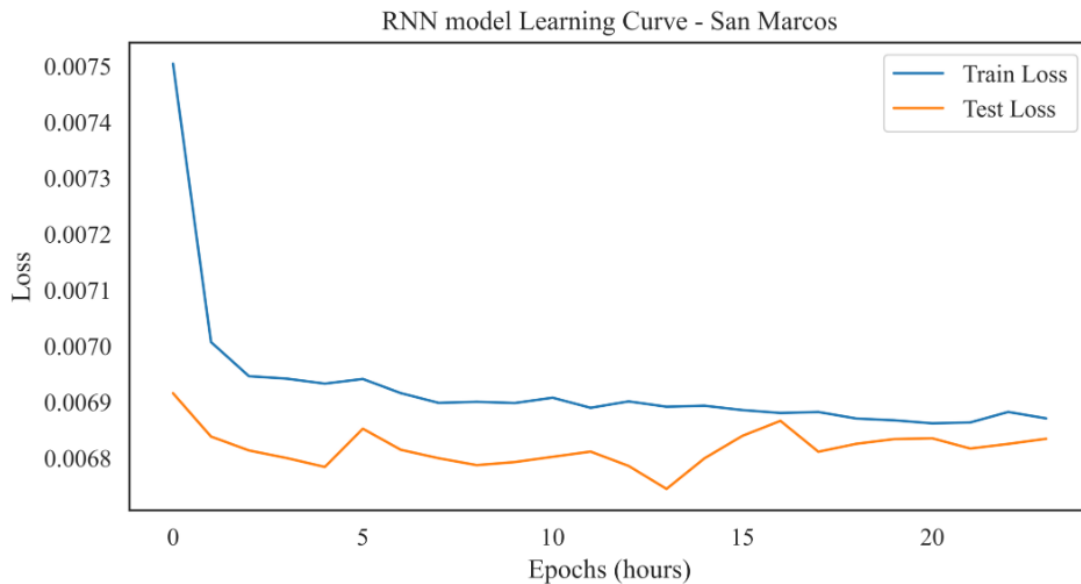


Figure 3.7 RNN learning curve

In the next step *EarlyStopping* is used to avoid overfitting of the training model with a patience level of 10. *EarlyStopping* is a regularization technique used to avoid overfitting in different ML models, in this case it allows 10 iterations before the model begins to overfit. Patience represents the number of epochs with no improvement after which the training will be terminated. The number of epochs reflects how many cycles the ML algorithm has made over the full training dataset. The exact amount of patience required varies from model to model. In our situation, patience is set to 10 because there has been no progress in the validation loss, and the learning curve has also begun to converge as shown in Fig 3.7. After this the model is fitted with X_{train} and Y_{train} values with 200 *epochs* and an output is generated as shown in Table 3.3.

Here the trainable and non-trainable parameters denote the weights W of this regression model. Weight is a NN parameter that modifies input data inside the network's hidden layers. In the next step the learning curve of the RNN model has been plotted as shown in Figure 3.7. A learning curve is a plot that depicts the progression of a ML model, indicating how well the model learns with training and testing data. It is found that the loss of training and test data struggles to catch up at first and then converges at the seventh epoch with some distortion for some time. It ultimately converges from 23 hours after a couple of epochs.

The MAE was then projected, and the prediction graph for training versus prediction data was plotted for our dataset across a 36-hour interval, also called as one and half day ahead forecasting, as shown in Figure 3.8.

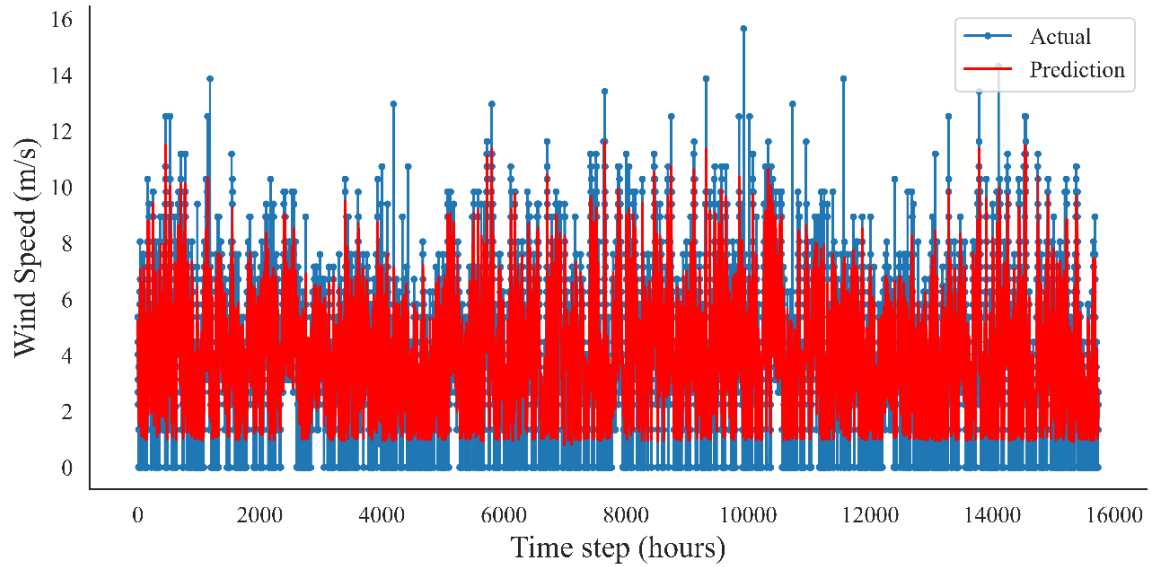


Figure 3.8 RNN prediction curve (2011-2019)

To better assess the aforementioned predictions in Figure 3.8, an expanded graph with only the last seven days (168 hours) of 2019 forecasts is displayed in Figure 3.9. We can observe that the projections fit the actual wind speed reasonably well. The results were then printed, and MSE, MAE, and R^2 values were obtained for various time steps. The details are referred to Table 3.2.

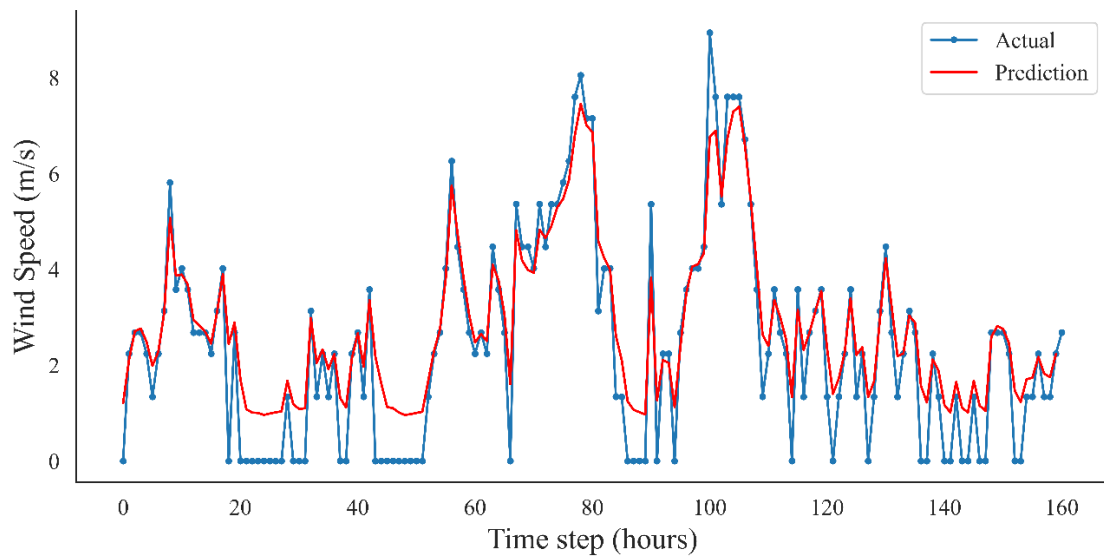


Figure 3.9 Last 7 days RNN prediction curve of December 2019

3.3.2 Long Short-Term Memory

A Long Short-Term Memory (LSTM) is a neural network that is analogous to a standard RNN. It has both long-term and short-term memories. The model was developed for solving the problem of ‘Long term dependency’, ‘vanishing gradient’ and ‘gradient explosion’ occurred in RNN models (Ma, 2020; Y. Wang et al., 2019). LSTM can have single or more modules in its basic units and these modules are like memory units which are used to store and transfer data in the system (Y. Wang et al., 2019). These memory units are also called hidden layers. As shown in Figure 3.10 the data are stored in memory units and gates, which are present in each module, including inputs, outputs, and forget gates that regulate the way the data is stored. An input gate decides what should be forwarded to the next activation. A forget gate decides what information should be omitted. An output gate is used to determine the value of the next hidden state. This state contains information of the previous inputs (Singhal, 2020).

The various terms used in Figure 3.10 include:

x_t = current input

C_{t-1} = memory transferred from last cell

h_{t-1} = output of last cell

C_t = new updated memory

h_t = current output

tanh = tanh layer

σ = sigmoid layer

b = bias

s_i = scaling of information

Since time series data might contain undetermined delays between critical events, LSTM networks are well suited for categorizing, processing, and generating predictions. In addition, LSTM is used

to handle complicated issues in speech recognition, machine translation, handwriting recognition, and modeling dynamic systems including time and order-dependent data, such as audio or video. (Beaufays, 2015; Breuel et al., 2013; Ren, 2020; Shewalkar, 2019; Smagulova and James, 2019).

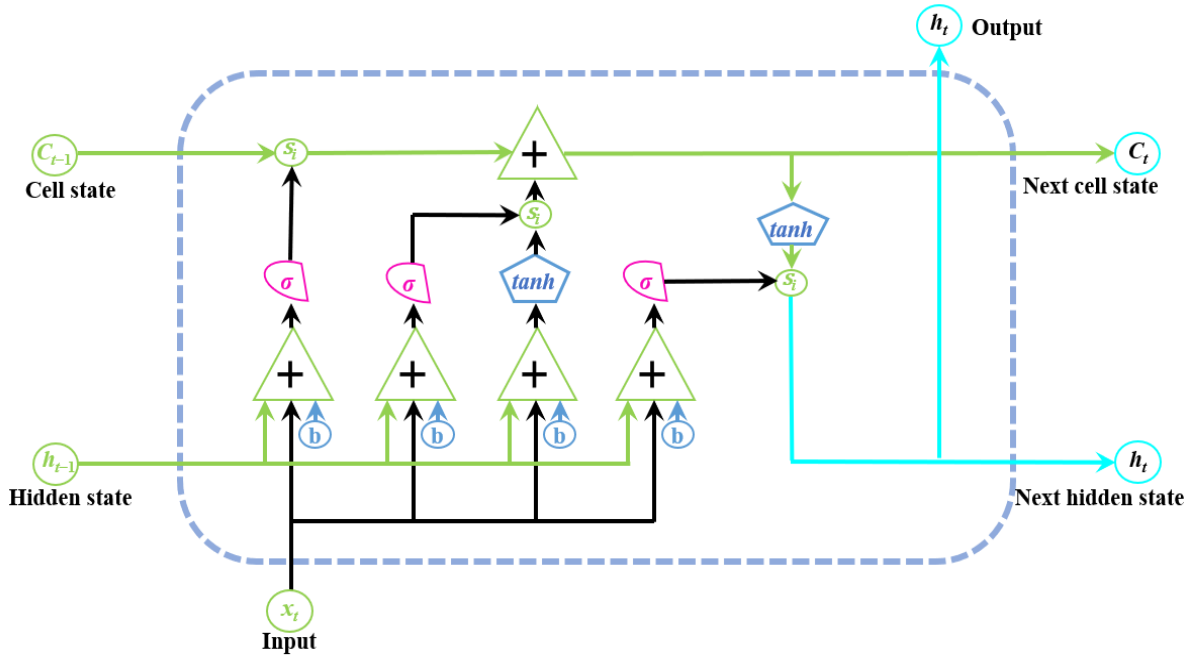


Figure 3.10 LSTM cell architecture (Le et al., 2019)

The working principle of an LSTM model can be further understood from the following equations (Memarzadeh and Keynia, 2020; Singhal, 2020).

Equation for the gates:

$$i_t = \sigma (W_i[h_{t-1}, X_t] + b_i) \quad (3.15)$$

$$f_t = \sigma (W_f[h_{t-1}, X_t] + b_f) \quad (3.16)$$

$$\sigma_t = \sigma (W_o[h_{t-1}, X_t] + b_o) \quad (3.17)$$

where:

i_t = input gate

f_t = forget gate

o_t = output gate

σ = sigmoid function

W_x = Weight of respective gate's neurons

h_{t-1} = output of previous LSTM cell at timestamp $t-1$

X_t = input at timestamp t or the current input

b_x = biases of respective gates

Equation for the cell, candidate cell and final output:

$$\hat{c}_t = \tanh (W_c[h_{t-1}, X_t] + b_c) \quad (3.18)$$

$$c_t = f_t \times c_{t-1} + i_t \times \hat{c}_t \quad (3.19)$$

$$h_t = o_t \times \tanh (c_t) \quad (3.20)$$

Where:

c_t = cell at time stamp t

\hat{c}_t = candidate for cell at time stamp t

LSTM also have some **pros and cons** given below (Aditianu, 2020).

Pros:

- LSTM can remove the vanishing gradient problems of RNN while training the model.
- Since LSTM has larger memory than RNN, they can readily recall data or predict data with longer time lags.
- The LSTM can be used to model a variety of variables, including input bias, output bias, and learning rate. Therefore, no precise adjustments are required. It is similar to BPTT that LSTM reduces the difficulty in updating each weight.

Cons:

- LSTM could solve the problem of vanishing gradients, though not fully remove it.
- Need high memory-bandwidth because of linear layers present in each cell for which the system usually fails to provide. Thus hardware-wise, LSTM has become quite inefficient.
- LSTM is affected by different random weight initialization and hence behaves quite similar to that of a feed-forward neural net.
- LSTM is prone to overfitting and difficult to apply the dropout algorithm to curb this issue. Dropout is a regularization method where input and recurrent connections to LSTM units are probabilistically excluded from activation and weight updates during the training.

Model Explanation:

For the LSTM model first, the dataset has been imported and parsed the date into a date-hour-minute format. After this the dataset is reshaped, scaled and appended similar to the RNN model explained above. Then C is introduced again for predicting the future wind speeds at different consideration time as shown in Table 3.4. The X training and testing values, as well as the Y training and testing values, were then used to create a dataset. In the next step input data has been reshaped into training and testing data.

Table 3.4 Comparison of MSE, MAE and R² errors at different consideration times

Hours	MSE	MAE	R ² (R-Squared)
1	0.553	0.348	0.952
3	0.690	0.465	0.924
8	0.690	0.465	0.925
12	0.682	0.538	0.926
24	0.744	0.510	0.912
36	0.744	0.527	0.912

The model was created with the help of *keras LSTM* layer, which was built by Hochreiter in 1997

(Team, n.d.). After this a layer has been added to this model with *tanh* activation function, having 100 hidden units. The *tanh* activation function was chosen above other functions because it produced better results. Each hidden layer in the LSTM model is composed of multiple hidden units, here the units will always be a positive integer. A dropout layer is also added to prevent overfitting of the model. The regression model uses two hidden layers to give better predictive performance including the dense layer. After this the loss function of MSE is evaluated with the help of *adam* optimizer.

In the next step *EarlyStopping* is used to avoid overfitting of the training model with a patience level of 10. After this the model is fitted with Xtrain and Ytrain values with 200 *epochs* and an output is generated as shown in Table 3.5.

Table 3.5 Architecture of the model

Layer (type)	Output Shape	Parameter Number	Comment
LSTM	(None, 100)	40,800	Total parameters: 40,901 Trainable parameters: 40,901 Non-trainable parameters: 0
Dropout	(None, 100)	0	
Dense	(None, 1)	101	

In the next step the learning curve of the RNN model has been plotted as shown in Figure 3.11 for 36-hour intervals. It can be observed that the train loss and test loss attempt to converge at around the 4th hour, but after a few iterations, they eventually converge at approximately the 53rd epoch. Train loss is a measure that indicates how well a deep learning model fits the training data. Likewise, test loss is a statistic that indicates how well a deep learning model matches the test data.

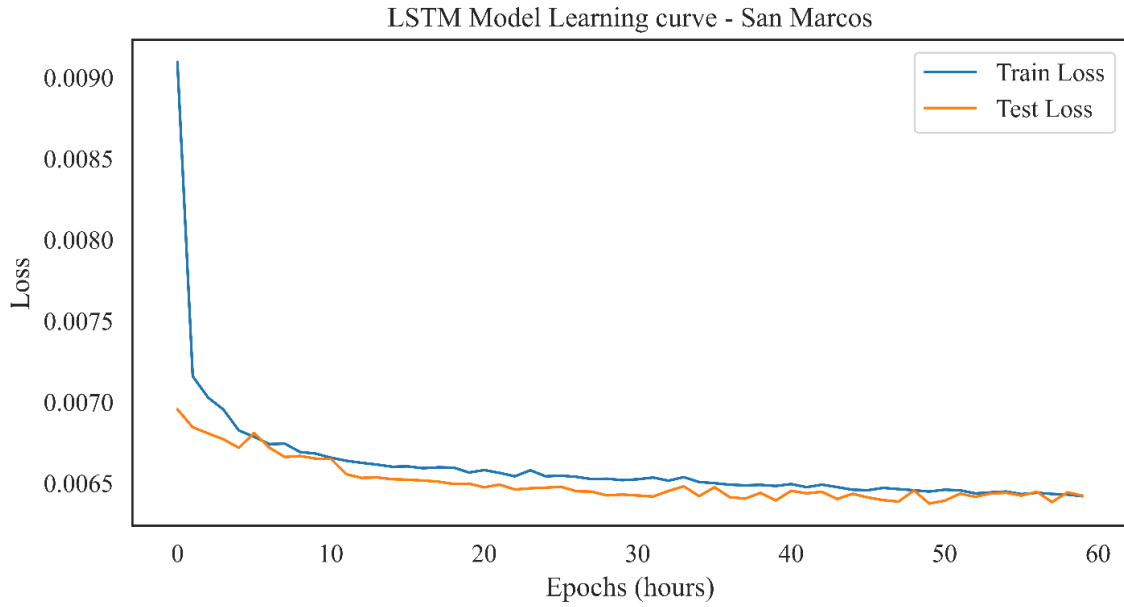


Figure 3.11 LSTM learning curve

Following that, the MAE was projected, and the prediction plot for training vs prediction data for the whole dataset was plotted, as shown in Figure 3.12.

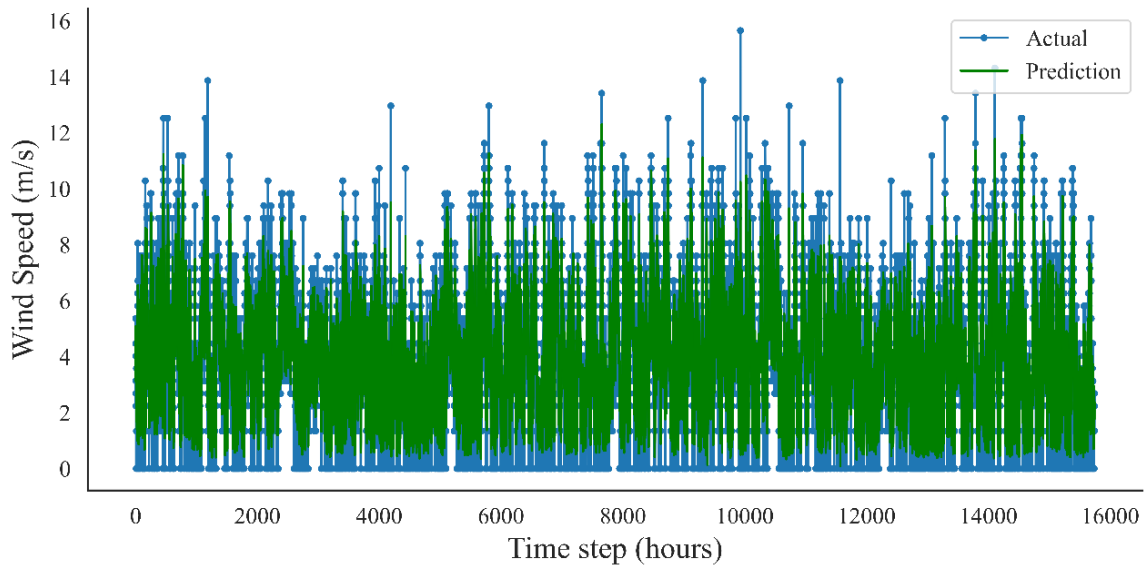


Figure 3.12 LSTM prediction curve (2011-2019)

In order to easily assess the aforementioned predictions in Figure 3.12, an expanded graph with

only the last seven days (168 hours) of forecasts has been displayed in Figure 3.13. We can clearly observe that the projections fit the actual wind speed.

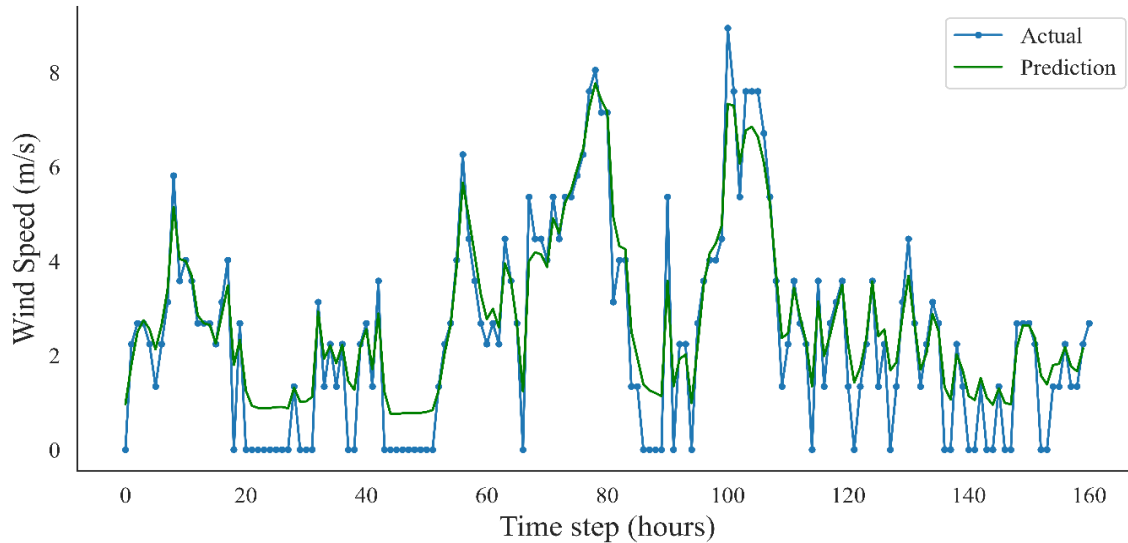


Figure 3.13 Last 7 days LSTM prediction curve of December 2019

The results were then printed, and MSE, MAE, and R^2 values were obtained for various time steps (see Table 3.4).

3.3.3 Ensemble Model

The process of ensemble modeling is running two or more separate analytical models to forecast the output, each using a different modeling approach. The basic idea behind an ensemble model is that the collective intelligence of multiple models is often better than the intelligence of a single model. The goal of integrating those projections is to increase the model's capacity for prediction. Ensemble learning models have showed promising possibilities in the ML area for improving the efficiency of a single model (Li et al., 2019; Wang, et al., 2018; Wang et al., 2018). Ensemble models work by training multiple models on the same dataset, using different algorithms or hyperparameters, and then combining the predictions of those models to make a final prediction.

Figure 3.14 shows a general architecture of an ensemble model.

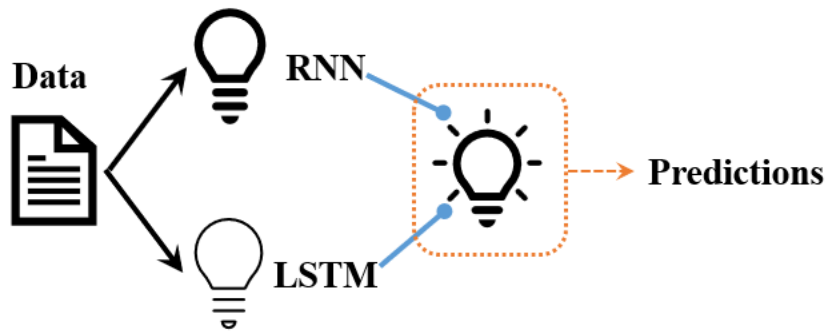


Figure 3.14 A simple ensemble architecture (Alhamid, 2022)

There are two main types of ensemble models: bagging and boosting (Wang et al., 2018)

- Bagging (Bootstrap Aggregating) is a technique that involves creating multiple independent models on different subsets of the data, with each model trained on a different subset of the data. The subsets are created by randomly sampling the training data with replacement. This means that some data points may appear in multiple subsets, while others may not appear at all. Each model produces a prediction for the target variable, and these predictions are combined through averaging or majority voting.
 - The most common example of a bagging ensemble model is the Random Forest algorithm. In this algorithm, multiple decision trees are trained on different subsets of the data, and the final prediction is made by aggregating the predictions of all the trees.
- Boosting is a technique that involves creating multiple models in sequence, with each model designed to correct the errors of the previous model. The models are created using a weighted sampling strategy, where the samples that were misclassified by the previous model are given higher weights in the next iteration. This means that the subsequent models focus more on the samples that were difficult to classify. The most common example of a boosting ensemble model is the Gradient Boosting algorithm. In this algorithm, a decision tree is trained on the

entire dataset, and subsequent trees are trained on the residuals of the previous tree.

Ensemble models offer both advantages and disadvantages, which are discussed below (Kapalko, 2019).

Pros:

- Ensemble models tend to outperform individual models, as they are able to capture more complex relationships between variables.
- Ensemble models are less likely to be affected by outliers or noisy data.
- Ensemble models can be used with a variety of machine learning algorithms, making them versatile and adaptable to different data types.

Cons:

- Ensemble models are often more complex than individual models, which can make them harder to interpret.
- Ensemble models require more computation time than individual models, as multiple models need to be trained and combined.
- If not implemented properly, ensemble models can be prone to overfitting, where the model performs well on the training data but poorly on the test data.

Model Explanation:

The ensemble model for time-series prediction using two pre-trained models (RNN and LSTM) is made with TensorFlow. To enhance the comparison of the three models, the RNN and LSTM models were merged to produce two ensemble models. The first ensemble model was formed by combining two well-performing models, while the second one was created by amalgamating two underperforming RNN and LSTM models. Firstly, the input shape of the model is defined based on the shape of the training data. Next, the output of each model in the list is obtained by passing

the input data to each of the models. These outputs are then averaged using the Average layer in TensorFlow, resulting in the ensemble output. The ensemble model is then defined by specifying the input and output layers. The model is trained on the training data, and the prediction is obtained for both the training and testing datasets. The predicted results are then transformed back to their original scales using the scaler. These values are saved in a dictionary, and the predicted and actual values are plotted using matplotlib, the prediction plot for training vs prediction data for the whole dataset was plotted, as shown in Figure 3.15

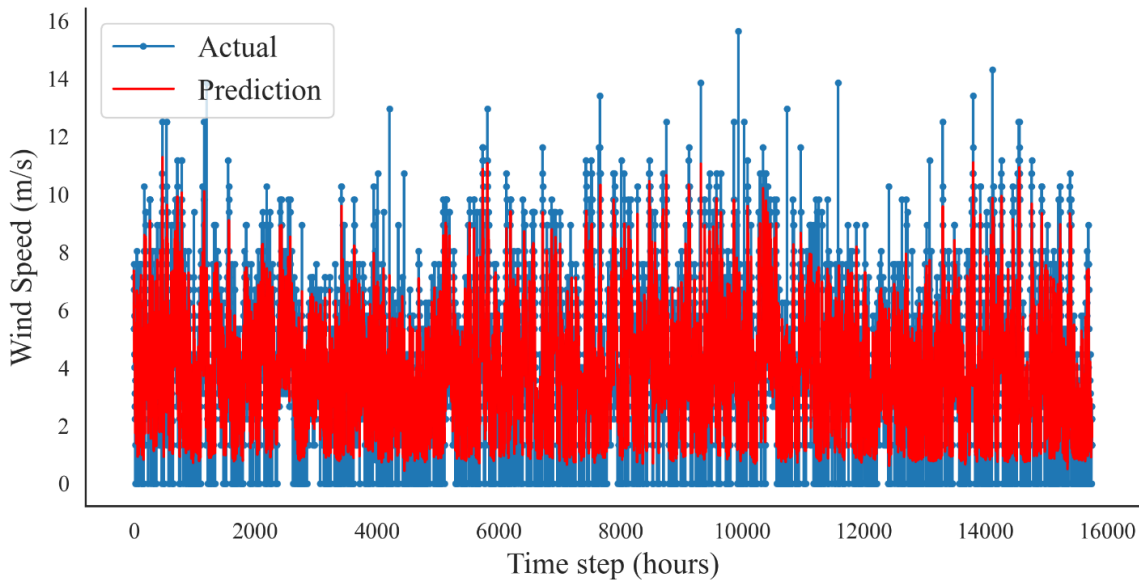


Figure 3.15 Ensemble prediction curve (2011-2019)

To facilitate the evaluation of the wind speed predictions shown in Figure 3.15, an enlarged plot displaying only the last 168 hours (7 days) of forecasts has been included in Figure 3.16. It is evident that the forecasted wind speeds align well with the actual values.

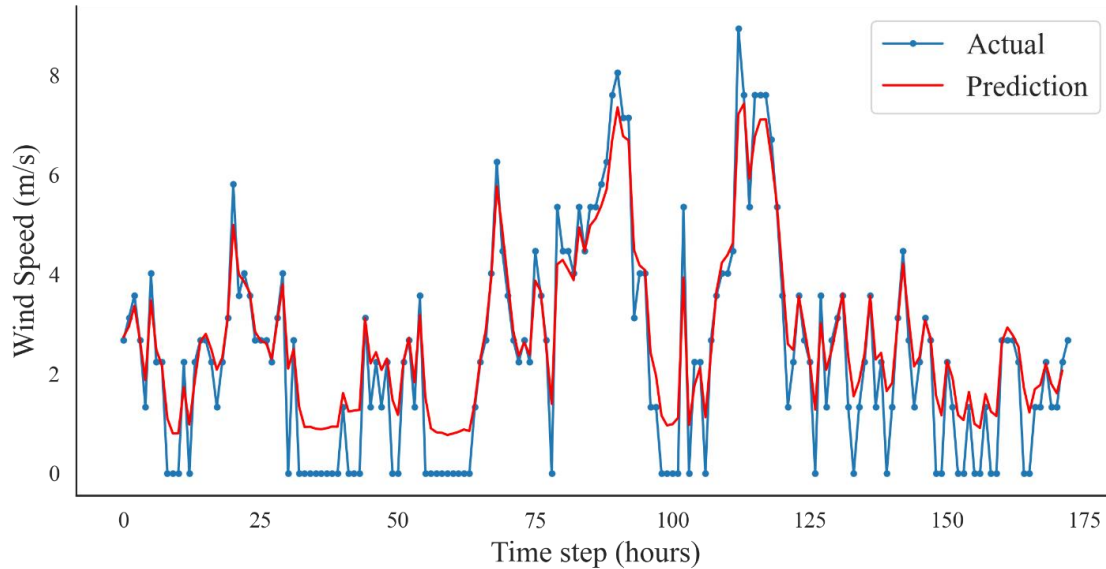


Figure 3.16 Last 7 days or 168 hours ensemble prediction curve of December 2019

Finally, the error scores were calculated for the training and testing data.

3.4 Comparison of the Regression Models

As far as the use of statistical measures in assessing a model is concerned, there is no universal rule. A metric's insights may vary depending on the context of the experiment or forecast. The performance scores of RNN, LSTM and ensemble models are compared in terms of error score, learning curve, and prediction speed (or computational load), and prediction accuracy.

- **Error scores:** The performance scores of RNN, LSTM and ensemble models can be seen in Tables 3.6 and 3.7 for the first ensemble (E^1) and second ensemble (E^2). All the results are compared on 24-hour horizon for the hourly windspeed data in San Marcos.

For the first ensemble model the error score for MSE and MAE are 0.8532 and 0.6705 which are very in between the error score of RNN and LSTM models. Moreover, the R^2 values of ensemble model is 0.8765 which is again in between the RNN and LSTM models which have R^2 scores of 0.8977, and 0.9190 respectively. The lower value of the MSE and MAE

scores usually implies a higher R^2 value, hence denoting a better predictive model. Out of all three models, LSTM has the lowest MSE and MAE scores and the highest R^2 values.

On the other hand, for the second ensemble model when two loosely fitted RNN and LSTM models were used the ensemble came out to be the best performing model with the lowest MSE and MAE scores and the highest R^2 score.

Table 3.6 Comparison of error scores for first ensemble model in 24-hour ahead forecasting

Error	RNN	LSTM	E ¹
MSE	0.8036	0.7148	0.8532
MAE	0.6310	0.4949	0.6705
R² (R-Squared)	0.8977	0.9190	0.8765
Performance	High	Best	Medium

Table 3.7 Comparison of error scores for second ensemble model in 24-hour ahead forecasting

Error	RNN	LSTM	E ²
MSE	1.512	1.4635	0.8464
MAE	1.562	1.1131	0.6606
R² (R-Squared)	0.6382	0.6606	0.8865
Performance	Medium	High	Best

- **Learning curve:** Because the ensemble model does not use iterations, it is not feasible to depict the learning curve for this model; however, we can see the learning curves for the RNN and LSTM models in Figures 3.7 and 3.11.

The learning curve indicates how well the predictive models learn from training and testing data. As shown in Figure 3.7, the testing model of the RNN has difficulty capturing the pattern of the training model. The LSTM model, on the other hand, Figure 3.11 has a smoother learning curve that depicts the testing model readily replicating the pattern of the training model.

- Prediction Speed:** Several parameters are necessary to configure the ML models, however computational time is also a significant factor to consider when choosing a model for a certain task. During the model training, it was discovered that the RNN model required less time to train and had a quicker processing speed of approximately 5 minutes. On the other hand, the LSTM model took around 22 minutes, E1 took around 26 minutes, and E2 took about 23 minutes to train.
- Predictions Accuracy:** Figures 3.9, 3.13 and 3.16 show the last seven days of forecasts from all models. The predictions in all the models are extremely closely fitting with the the testing data, and it's difficult to discern which is producing more accurate results as can be seen in Figure 3.17

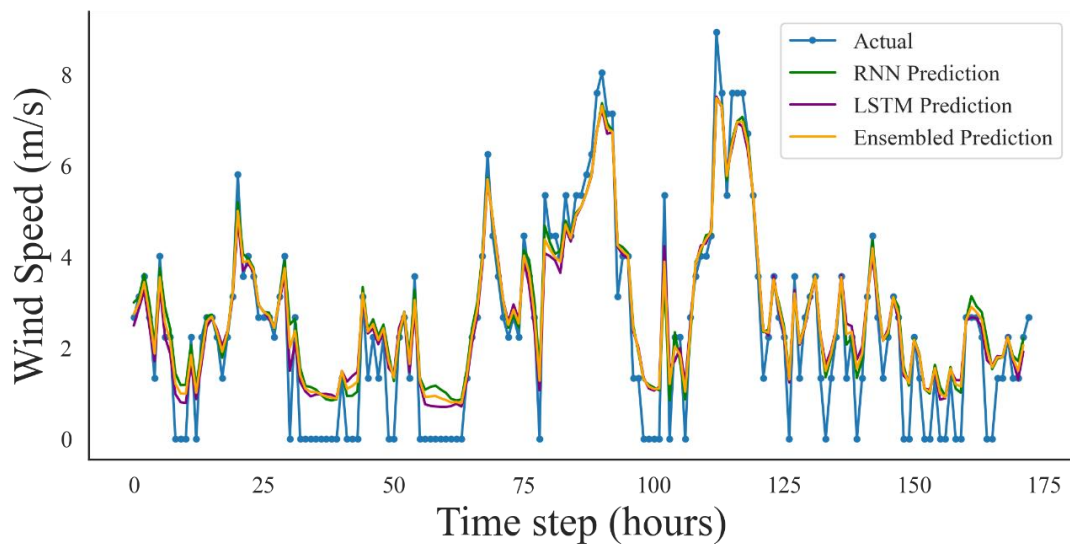


Figure 3.17 Last 7 days all model predictions of December 2019

Furthermore, the RNN, LSTM and ensemble models forecasting curve only predict 1 m/s approximately and not zero m/s, but this can be ignored since it is still below the threshold of the cut-in speed of a wind turbine of 2.5 to 3.5 m/s. As a result, this forecast will not affect electricity generation since it is still forecasting below the cut-in speed.

Precise wind speed prediction is crucial when installing wind turbines in WWTPs to aid grid operators in balancing electricity generated from other sources like coal, natural gas, geothermal, and hydroelectricity (Heller, 2014). In conclusion, considering all performance metrics, the RNN model was not exceptional but had faster prediction times than other models and produced similar results. Therefore, among the three models evaluated in the wind speed forecasting study, the RNN model was the most accurate. Additionally, combining more low-performing models into the ensemble model can significantly improve its results as well.

4. TRANSACTIVE ENERGY OPERATIONS IN WWTP FACILITY

4.1 Transactive Energy Trading as Emerging Market

4.1.1 Transactive Energy Market Mechanism

Transactive Energy (TE) is a distributed energy management system that facilitates two-way energy flow and trading between prosumers, such as roof-top solar panels, distributed energy storage, and electric vehicles. The TE market works on the basis of price signaling to balance power supply and demand in real time, utilizing modern communication and automation technology. Utility firms and customers participate in the energy exchange process known as "transactive energy" in order to build a more dependable and efficient power supply. For instance, traditional users now can produce power using solar panels on a building's roof and exchange that energy on the grid in the transactive energy market. Another illustration would be deploying smart devices to reduce energy use during costly peak hours. The U.S. Department of Energy's GridWise Architecture Council defines transactive energy (TE) as "a system of economic and control mechanisms that allows the dynamic balance of supply and demand across the entire electrical infrastructure using value as a key operational parameter" in its Transactive Energy Framework (Transactive Energy, 2017).

TE is often composed of multiple components, such as a market platform with which candidates communicate with one another either in the presence of a centralized authority or direct peer-to-peer trading. This communication is required to determine the price of energy. In energy markets, information regarding power demand and supply can be obtained either directly via member interactions or through the use of information technology. To better understand how a TE network works, we will now go over its major components (Sioshansi, 2014).

- **Participants:** Participants in the TE market include energy users, producers, and grid operators, all of whom can sell or buy electricity at a given price point. These participants may also be

distributed energy resources (DER) owners, with the ability to bid on or sell energy to the TE market.

- **Communication and control:** To enable participants to interact with one another and with the grid, the TE market employs modern communication and control technology. Real-time price signals, automated bidding and dispatch, smart meters, and sensors that monitor energy usage and generation are examples of these technologies.
- **Pricing Indication:** The TE market employs price signals to balance power supply and demand in real time. Pricing is established based on the marginal cost of generating or power usage, with prices rising during peak hours and falling during low demand periods.
- **Optimization:** The TE market employs optimization algorithms to reduce energy costs while fulfilling demand and preserving grid stability. These algorithms include aspects including generating capacity, energy storage capacity, distribution capacity, and environmental restrictions.
- **Agreement:** Transactions between participants in the TE market are settled in the day ahead or in real time, with payments and energy transfers occurring automatically. The prices and quantities agreed upon by the participants serve as the basis for settlement.

According to recent studies (Odeh and Watts, 2019; Pfeifer et al., 2019), the increasing use of renewable energy resources such as solar panels and wind turbines, along with distributed storage and advanced information and communication technologies (ICT) devices (Saad al-sumaiti et al., 2014), is leading to the transformation of the traditional energy market into a new peer-to-peer (P2P) trading market. In this new system, energy market participants can generate and share surplus energy with other consumers. Individuals who own renewable energy resources can act as buyer or seller in a transactive energy network are commonly referred to as "prosumers" (Silva et

al., 2022; Zafar et al., 2018). Namely, the entity can behave as a producer and consumer.

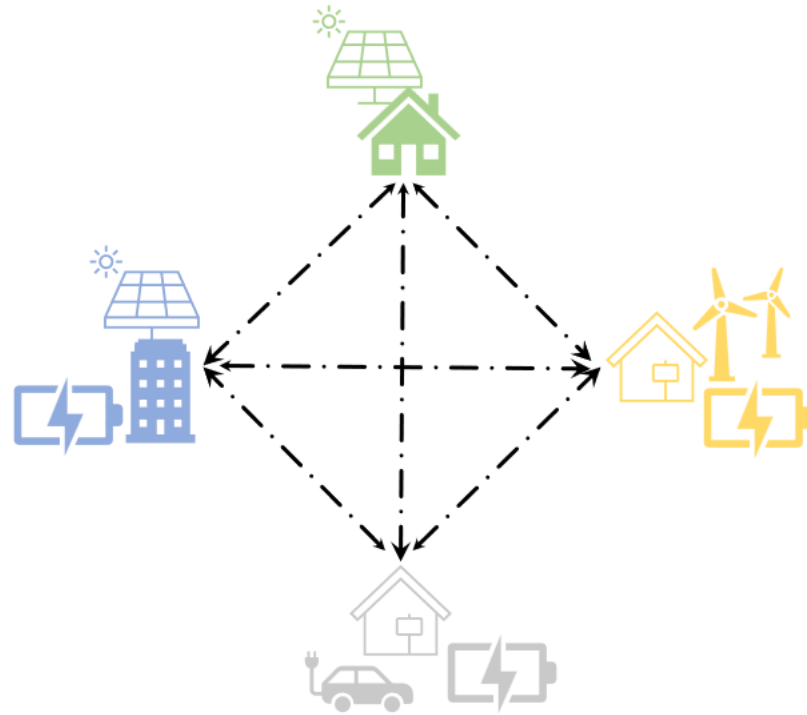


Figure 4.1 A transactive energy setup involving prosumers

4.1.2 Best industry practices

The energy crisis coupled with climate change is a critical topic that has gained a lot of attention recently. Rising global energy demand has intensified the depletion of fossil resources such as oil, natural gas, and coal. Various studies, as discussed below, have shown that transactive energy may be utilized for energy trading, reducing the requirement for fossil fuels. Worrall et al. (2016) implement Transactive Energy Market Information Exchange, a decentralized network management and automated energy transaction effort. This project involved the development of energy trading software. The study by Rahimi and Ipakchi (2012) describes the development of a project called Open Access Technology International, Inc. Microgrid Center, which includes advanced control and optimization software for microgrids. A multi-campus experiment for transactive control and TE management was built as part of the Clean Energy and Transactive

Campus project (Lian et al., 2018). There were several projects involved in this, including the Clean Energy and Transactive Campus project, the Olympic Peninsula Grid-Wise project, and the PowerMatcher project. The Clean Energy and Transactive Campus project conducted a multicampus experiment for transactive control and TE management, while the Olympic Peninsula Grid-Wise project implemented automatic load response to price variations in a very short timeframe. The PowerMatcher project, on the other hand, developed a smart grid coordination mechanism that takes distributed energy resources and flexible loads into account. The Vandebrom project in the Netherlands investigated P2P energy trading from both the provider and client viewpoints (Vandebrom, 2023). Germany's peer energy cloud initiative has resulted in the development of a cloud-based infrastructure for local energy trading and smart homes (Software Cluster, 2023).

4.2 Estimating Onsite Wind Turbine Power Generation

On-site wind generation could be a realistic solution for powering wastewater treatment plant (WWTP) or water treatment facility looking to decrease their energy expenditures and environmental imprint. Estimating onsite wind generation entails various procedures which are elaborated below.

The first stage is to evaluate the wind speed profile of the location where the turbine will be potentially positioned. This entails assessing the wind resource at the location, including wind speed, wind direction, and seasonal variation. The site evaluation can be carried out using a mix of ground-based and remote sensing techniques such as anemometers, wind vanes, and lidar. After assessing the wind resource, the appropriate wind turbine may be chosen depending on the wind conditions at the site. The turbine power curve, rotor diameter, cut-in and cut-out wind speeds, and rated power output are all factors to consider when choosing a turbine. The wind turbine's power

output may be approximated using the turbine power curve and the measured wind speed at the site. Power output may be calculated using a variety of approaches, including the cubic function or the Weibull cubic function, as discussed in Chapter 3.

The next stage in evaluating onsite wind turbine output is to examine the WWTP's load profile. The load profile study entails analyzing the plant's power demand trends, including peak and average energy demand, as well as demand variation during the course of a year.

The last stage is to connect the wind turbine to the WWTP's current power generation infrastructure. This entails maximizing the turbine output to fulfill the plant's energy requirement while minimizing the consumption of grid electricity.

The most significant factor that affects wind turbine power production is wind speed. As per the Department of Energy, the average rotor diameter, or the width of the circle swept by the blades, was 127.5 meters (418 feet) in 2021, which is greater than the length of a football field (Hartman, 2022). The rotor swept areas have increased by approximately 600% since 1998-1999 because of the ability to collect more wind at lower wind speeds, which can increase the number of locations across the country suitable for wind energy development (Hartman, 2022).

Wind turbine power output is also governed by its design features such as cut-in speed, which is the minimum wind speed required for the wind turbine to begin delivering electric power, rated wind speed, the wind speed above which the machine delivers the rated power output, and cut-out speed, the maximum wind speed the machine is allowed to deliver power (Manwell et al., 2010).

Here for research purposes, we assume the rated power or the turbine capacity, P_m of 1 MW is installed on site. The wind speed data has been adjusted to a standard reference height of 80 meters, which is commonly used as the hub height of wind turbines. The power law equation

has been applied to extrapolate the wind speed to this height (Abbes and Belhadj, 2012). That is

$$V_2 = V_1 \times \left(\frac{h_2}{h_1}\right)^\alpha, \quad (5.1)$$

where V_1 is ground level wind speed, V_2 is the wind speed at the desired height, h_1 is the height at which V_1 is measured, usually at 10 meters from ground level, h_2 is the wind turbine tower height, in this case 80 meters and α is the wind shear exponent, typically between 0.1 and 0.4 for wind speeds in the range of interest for wind turbine power calculations. The wind shear exponent can differ greatly due to various factors, such as the vegetation coverage, terrain, and climate. Table 5.1 illustrates the approximate annual wind shear exponent ranges in different regions and site conditions across the country.

Table 4.1 Approximate annual wind shear exponent range in the USA (Roeth, 2010)

Region	Site condition	Range of α
Central US/Great Plains	Open, relatively flat	0.16-0.19
Eastern US	Cleared, sharp ridgeline	0.18 - 0.25
	Wooded, broad ridgeline	0.22 - 0.30
	Wooded valley or plain	0.25 - 0.40
Pacific Northwest	Open ridgelines	0.05 - 0.15
Southern California	Grassland and desert	0.00 - 0.15
New Mexico/ Arizona	Open, rolling	0.12 - 0.20
Hawaii, Southern Coastal	Open coastal or island	0.08 - 0.20
Tropical Offshore	Warm water	0.07 - 0.10
Temperate Offshore	Cold water	0.12 - 0.15

Texas is a large state with diverse geographical features. The wind shear exponent for Texas could vary depending on the specific location within the state. However, based on the information provided in the table, the wind shear exponent for Texas is most likely to fall within the range of 0.12 - 0.20, which is the approximate range for the New Mexico/Arizona region. This is because the terrain in the western and southern parts of Texas is similar to New Mexico and Arizona, with open, rolling terrain. We will use the average value of this range, 0.16, as the wind shear exponent

for our calculations, which is calculated by taking average as follows,

$$\alpha = \frac{0.12 + 0.20}{2} = 0.16$$

The output power generation for 24 hours of wind speeds on 03/16/2018 has been calculated with the help of a Python regression model using the cubic wind power Equation 3.1 for $P_w(v)$ shown in equation 1, with $v_c=3$ m/s, $v_r=12$ m/s, and $v_s=25$ m/s. Table 5.2 shows the output power for the three models namely RNN, LSTM and ensemble with their extrapolated wind speed at 80 m height.

Table 4.2 Output power of RNN, LSTM and ensemble models on 03/16/2018 with 1 MW WT

Hours	Wind Speed (m/s) RNN	$P_w(v)$ RNN	Wind Speed (m/s) LSTM	$P_w(v)$ LSTM	Wind Speed (m/s) Ensemble	$P_w(v)$ Ensemble
1:00	9.1531	0.4437	8.9586	0.4160	9.0558	0.4297
2:00	9.5954	0.5112	8.4610	0.3505	9.0282	0.4258
3:00	8.0419	0.3009	7.1409	0.2107	7.5914	0.2531
4:00	7.6774	0.2618	7.3428	0.2291	7.5101	0.2451
5:00	7.8634	0.2813	7.5843	0.2524	7.7239	0.2666
6:00	8.7392	0.3862	8.7026	0.3814	8.7209	0.3838
7:00	9.0425	0.4278	9.0111	0.4234	9.0268	0.4256
8:00	7.3577	0.2305	7.4896	0.2431	7.4236	0.2367
9:00	5.9828	0.1239	6.0814	0.1301	6.0321	0.1270
10:00	5.0142	0.0729	5.1930	0.0810	5.1036	0.0769
11:00	4.1411	0.0410	4.7191	0.0608	4.4301	0.0503
12:00	4.6724	0.0590	5.3595	0.0890	5.0160	0.0730
13:00	5.6594	0.1049	6.0441	0.1277	5.8518	0.1159
14:00	4.8646	0.0666	5.3649	0.0893	5.1148	0.0774
15:00	2.6751	0	3.4512	0.0237	3.0631	0.0166
16:00	5.0254	0.0734	5.3758	0.0899	5.2006	0.0814
17:00	6.3618	0.1490	6.4370	0.1543	6.3994	0.1516
18:00	4.0984	0.0398	4.3001	0.0460	4.1992	0.0428
19:00	6.0749	0.1297	5.7746	0.1114	5.9247	0.1203
20:00	4.6666	0.0588	4.5261	0.0536	4.5964	0.0561
21:00	5.3382	0.0880	5.1422	0.0786	5.2402	0.0832
22:00	4.9456	0.0700	4.8407	0.0656	4.8932	0.0678
23:00	5.4331	0.0928	5.4423	0.0932	5.4377	0.0930
24:00	5.5447	0.0986	5.5870	0.1009	5.5658	0.0997
	$\sum P_w(\text{RNN})$	4.1118	$\sum P_w(\text{LSTM})$	3.9017	$\sum P_w(\text{Enbl.})$	3.9994

Table 4.3 Output power of RNN, LSTM and ensemble models on 03/16/2018 with 3 MW WT

Hours	Wind Speed (m/s) RNN	$P_w(v)$ RNN	Wind Speed (m/s) LSTM	$P_w(v)$ LSTM	Wind Speed (m/s) Ensemble	$P_w(v)$ Ensemble
1:00	9.1531	1.331322	8.9586	1.248259	9.0558	1.289345
2:00	9.5954	1.533808	8.4610	1.051595	9.0282	1.277574
3:00	8.0419	0.902953	7.1409	0.632179	7.5914	0.759541
4:00	7.6774	0.78564	7.3428	0.687351	7.5101	0.735401
5:00	7.8634	0.844155	7.5843	0.757413	7.7239	0.800001
6:00	8.7392	1.158795	8.7026	1.14427	8.7209	1.151516
7:00	9.0425	1.283676	9.0111	1.270348	9.0268	1.277001
8:00	7.3577	0.691533	7.4896	0.729391	7.4236	0.710294
9:00	5.9828	0.371792	6.0814	0.390478	6.0321	0.381059
10:00	5.0142	0.218875	5.1930	0.243135	5.1036	0.230792
11:00	4.1411	0.123293	4.7191	0.182466	4.4301	0.150952
12:00	4.6724	0.177097	5.3595	0.267281	5.0160	0.219105
13:00	5.6594	0.314704	6.0441	0.383346	5.8518	0.347897
14:00	4.8646	0.199867	5.3649	0.268093	5.1148	0.232313
15:00	2.6751	0	3.4512	0.071366	3.0631	0.0499
16:00	5.0254	0.220349	5.3758	0.269723	5.2006	0.244205
17:00	6.3618	0.447011	6.4370	0.463058	6.3994	0.454987
18:00	4.0984	0.119519	4.3001	0.138045	4.1992	0.12856
19:00	6.0749	0.389221	5.7746	0.334306	5.9247	0.361068
20:00	4.6666	0.176439	4.5261	0.160981	4.5964	0.168592
21:00	5.3382	0.264109	5.1422	0.236067	5.2402	0.249826
22:00	4.9456	0.210015	4.8407	0.196936	4.8932	0.203406
23:00	5.4331	0.278436	5.4423	0.279851	5.4377	0.279143
24:00	5.5447	0.295952	5.5870	0.302777	5.5658	0.299352
$\sum P_w(\text{RNN})$		12.3386	$\sum P_w(\text{LSTM})$	11.4059	$\sum P_w(\text{Enbl.})$	12.0018

Based on the information presented in Tables 5.2 and 5.3, it can be inferred that the RNN model provides the largest power output compared to the LSTM model in which the predicted wind speeds result in the least output power. The ensemble model's power output falls in between the power outputs of the RNN and LSTM models. As wind energy generation is unpredictable, using the RNN power predictions P_w would result in an optimistic estimate, while the LSTM model's predictions would be pessimistic. Therefore, using the ensemble power predictions would provide a more realistic estimation for further calculations.

4.3 Transactive Energy Trading over 24 Hours in WWTP of Melbourne

Transactive energy trading allows prosumers to purchase and sell energy in a marketplace using an automated system. It allows for direct contract between the buyer and seller or in a so-called P2P mode. The technology matches energy demand with supply in real time and allows transactions between the two parties. After estimating the power production of a wind turbine installed in a WWTP, the following procedures can be adopted to engage in transactive energy trading:

The first step is to analyze the WWTP's historical energy consumption data to establish its energy demands. This data may be used to calculate the amount of surplus energy that can be sold in the market. The marketplace determines the price of energy based on demand and supply. The cost varies according to the time of day, season, and location. As a result, it is critical to watch the market in order to determine the ideal time to sell energy and the greatest price. The next stage is to enter the market through a transactive energy platform. The software would make energy trading easier by automatically matching supply and demand and conducting deals.

Table 4.4 Power load of different WWTP

WWTP	Country	Treatment Capacity (×1000 m³/day)	Power Demand (Load) (MW)
WWTP in Eastern China	China	725.748	26.77
ACUA	US	151.416	5.59
Browning WWTP	US	0.9464	0.0349
Boulder WWTP	US	77.602	2.86
Oroville WWTP	US	40.202	1.48
Melbourne WWTP(East)	Australia	440	16.23
SMAT	Italy	615	22.68

Table 4.4 shows the energy consumption data of several WWTP (ACUA, n.d.-a; Browning Montana, n.d.; City of Boulder, 2007; Melbourne Water, 2021; Panepinto et al., 2016; SCOR,

2022; Xu et al., 2017). To examine the energy usage pattern, the information obtained from Melbourne WWTP will be utilized and compared to the energy produced by wind turbines of 1 MW and 3 MW, respectively, for the month of April, 2018. Figure 5.2 displays the assessment of the energy usage in Melbourne WWTP as well as the energy produced by the 1 MW turbine over one-month period.

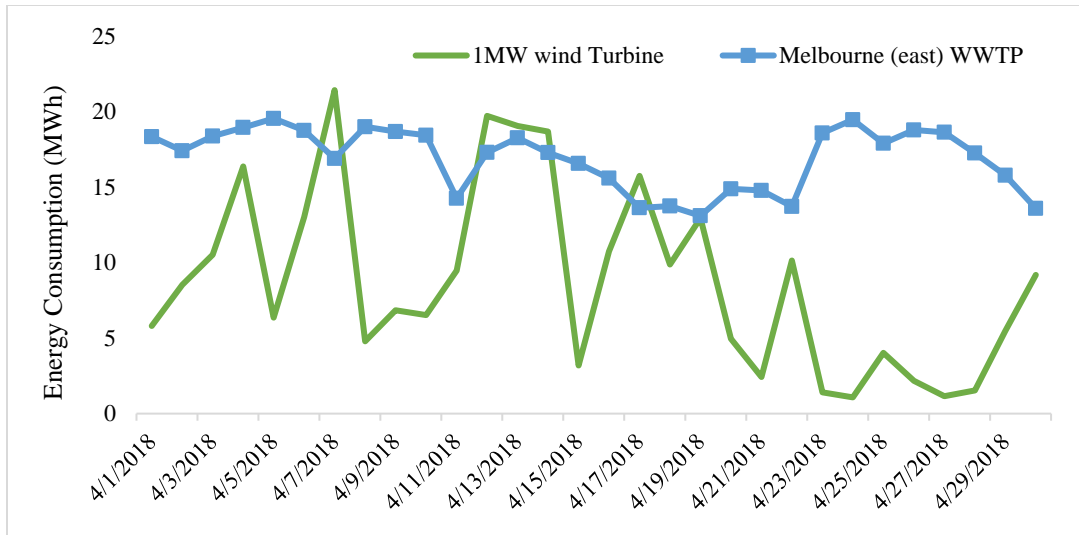


Figure 4.2 Daily energy consumption Analysis with 1MW turbine (April 2018)

Figure 4.2 indicates that the 1 MW wind turbine falls short of meeting the energy demands of the plant. The annual energy production of a 1 MW turbine is around 1459.78 MWh, less than the plant’s requirement of 6220.65 MWh. However, if we were to install three or four 1 MW wind turbines, the plant's energy requirements could be easily met. Nevertheless, this may not always be feasible due to land or space constraints. Therefore, an alternative approach is to increase the capacity of single turbine to generate more energy with fewer turbines. To investigate this, a 3 MW wind turbine was used and examine its energy production in comparison to the energy consumption patterns at Melbourne WWTP. Figure 4.3 depicts the daily energy usage and the WT generation.

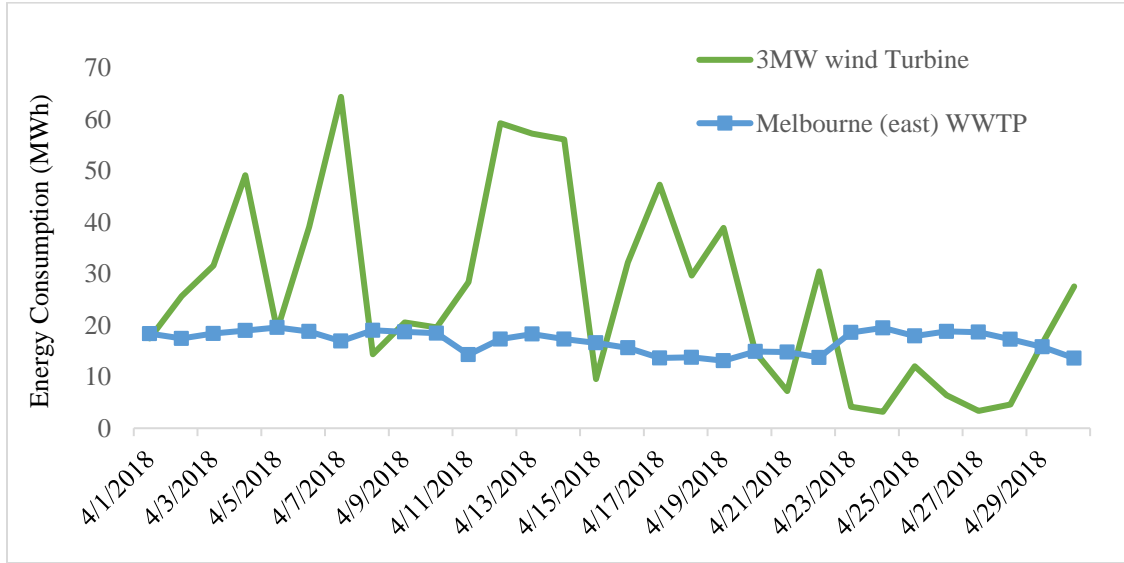


Figure 4.3 Daily energy consumption Analysis with 3 MW turbine (April 2018)

As seen from Figure 4.3 the power generated from one 3 MW turbine will be sufficient to meet the energy requirement of the Melbourne WWTP. There are some mild peaks in the energy consumption of the WWTP in the last week of the month. However, the power generated from the turbine is much higher than the required energy for the most days of the month, therefore the extra energy can be easily sold to the grid to earn the revenue.

Determining whether the energy produced will meet the peak demand during the peak months of the year is crucial. The data analysis revealed that the highest demand occurs between March and August every year. These peak demand months in the Melbourne WWTP, spanning from March to August of 2019, is presented in Figure 4.4.

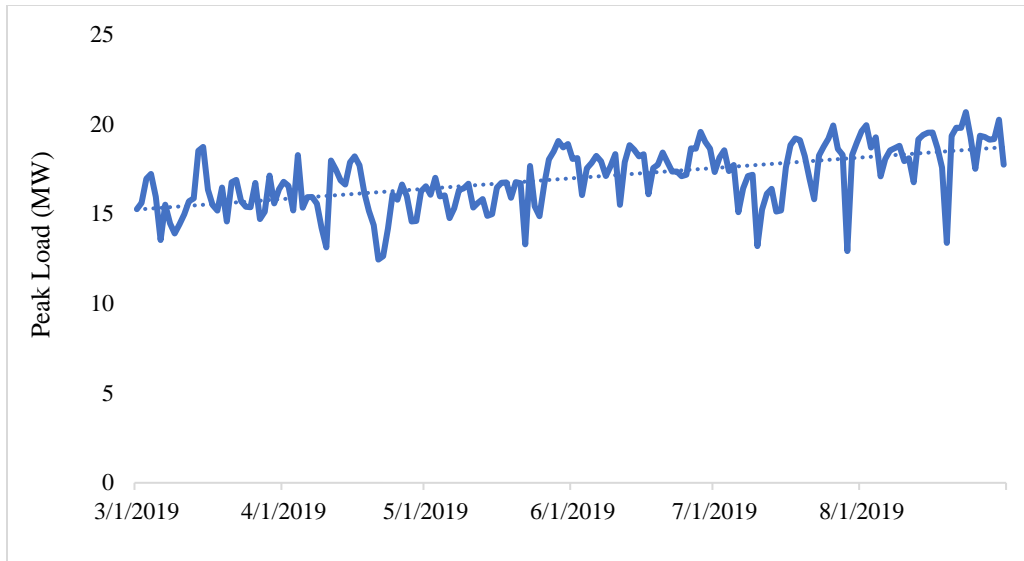


Figure 4.4 Peak Load in Melbourne WWTP

As observed in Figure 4.4 for Melbourne WWTP, there are a few peak demands occurred in the period of six months from April 2018 to September 2018. There is no fixed pattern for these peak demands as the first peak demand occurred on 5 April 2018, the next occurred on April 24, then on May 10 and lastly on June 16.

By taking into account the installation of a 3 MW wind turbine at the WWTP, along with the predicted hourly energy production and power load of the plant, the amount of energy that can be utilized in the TE market can be approximated. This estimation has been calculated and tabulated in Table 4.5. From Table 4.5 we can state the total energy generated from the wind turbine in a month is about 798.770 MWh and the surplus wind energy that can be used in the transactive energy market for trading is 290.917 MWh per month. From the table it can also be inferred that the average daily energy requirement of the WWTP is about 16.929 MWh which the plant needs to purchase daily in order to overcome the uncertainty in demand and supply in the renewable energy market.

Table 4.5 Estimated surplus energy from 3 MW wind turbine for April, 2018 (Unit: MWh)

Date	3 MW Turbine (MWh)	Melbourne (east) WWTP	Surplus energy (MWh)
4/1	17.42	18.35	-0.93
4/2	25.62	17.42	8.20
4/3	31.57	18.39	13.18
4/4	49.11	18.96	30.15
4/5	19.04	19.56	-0.52
4/6	39.10	18.77	20.33
4/7	64.33	16.91	47.41
4/8	14.35	19.01	-4.66
4/9	20.55	18.69	1.85
4/10	19.57	18.45	1.12
4/11	28.37	14.27	14.10
4/12	59.20	17.31	41.89
4/13	57.20	18.27	38.93
4/14	56.08	17.30	38.78
4/15	9.56	16.58	-7.02
4/16	32.18	15.60	16.57
4/17	47.28	13.64	33.64
4/18	29.64	13.76	15.89
4/19	38.88	13.11	25.78
4/20	14.77	14.90	-0.13
4/21	7.20	14.79	-7.59
4/22	30.45	13.73	16.72
4/23	4.16	18.60	-14.44
4/24	3.19	19.48	-16.29
4/25	12.02	17.91	-5.89
4/26	6.41	18.80	-12.39
4/27	3.37	18.65	-15.28
4/28	4.59	17.27	-12.68
4/29	16.45	15.80	0.65
4/30	27.53	13.60	13.93
ΣEnergy=	789.17	507.86	281.31

Moreover, the average power produced by the wind turbine is about 26.63 MWh for this month.

Now, if the wind turbine is able to produce sufficient energy during the peak months, it can easily

provide energy during the other times of the year if the wind speed profiles are similar. To analyze this, the wind turbine power generation data has been compared with the power consumption of the Melbourne WWTP over the period of 6 months from March, 2019 to August, 2019 (peak months) as shown in Figure 4.5.

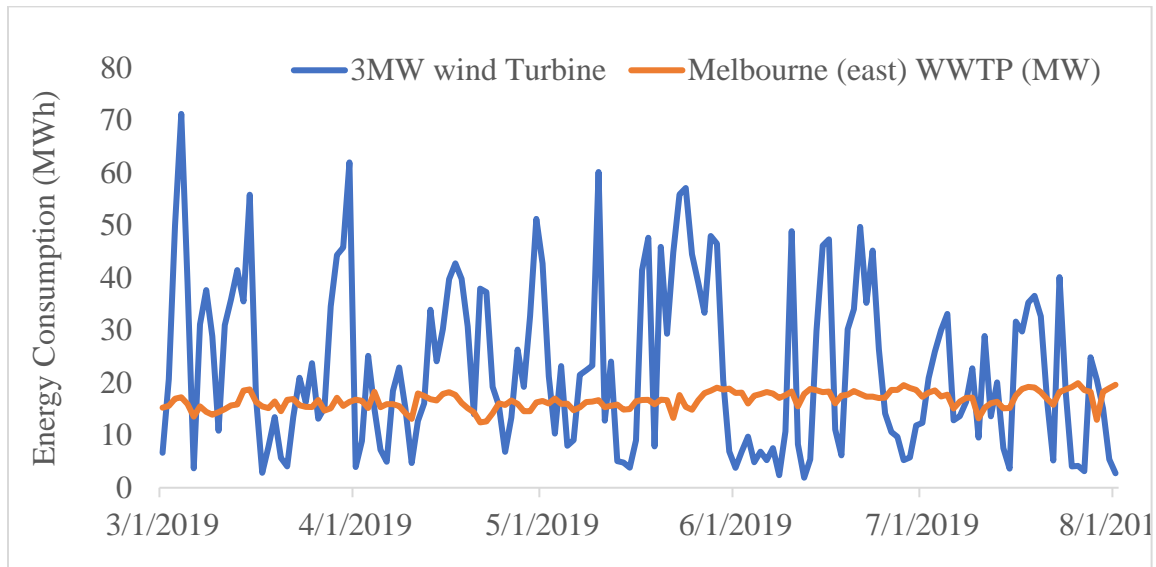


Figure 4.5 Daily Energy consumption Analysis with 3 MW turbine

In Figure 4.5 the power produced from WT can easily provide surplus energy to the WWTP as seen over the peak months of 2019 from March to August. Moreover, the annual energy requirement of the WWTP was about 6220.65 MWh for the year 2019. The net annual energy produced by wind turbines was about 7469.77 MWh for 2019. On average the plant will have around 1249.12 MWh of surplus energy which will be available for sale in the TE market.

4.4 Transactive Energy Trading for San Marcos Water Treatment Plant

To gain a deeper insight into energy use, the energy consumption of the San Marcos water treatment plant (SM WTP) is taken into account. This facility is responsible for treating and supplying safe drinking water to the local community and commercial establishments. Notably, the plant has been recognized by the Texas Commission on Environmental Quality (TCEQ) for

eight consecutive years, as it has consistently demonstrated outstanding performance in meeting regulatory benchmarks for water quality and environmental standards (GBRA, 2022). Recently, the City of San Marcos has invested in upgrading the plant capacity to handle 79,290 m³ per day (GBRA, 2023). After analyzing the power consumption data of the water treatment plant during the peak months of spring and summer, fluctuations in demand were observed, with intermittent occurrences of high and low demands. Notably, a comparison between the energy consumption pattern of the plant and that of a 3 MW wind turbine indicated distinct peaks in the graph throughout the year. These peaks were observed between May and June, as well as between August and December, as shown in Figure 4.6.

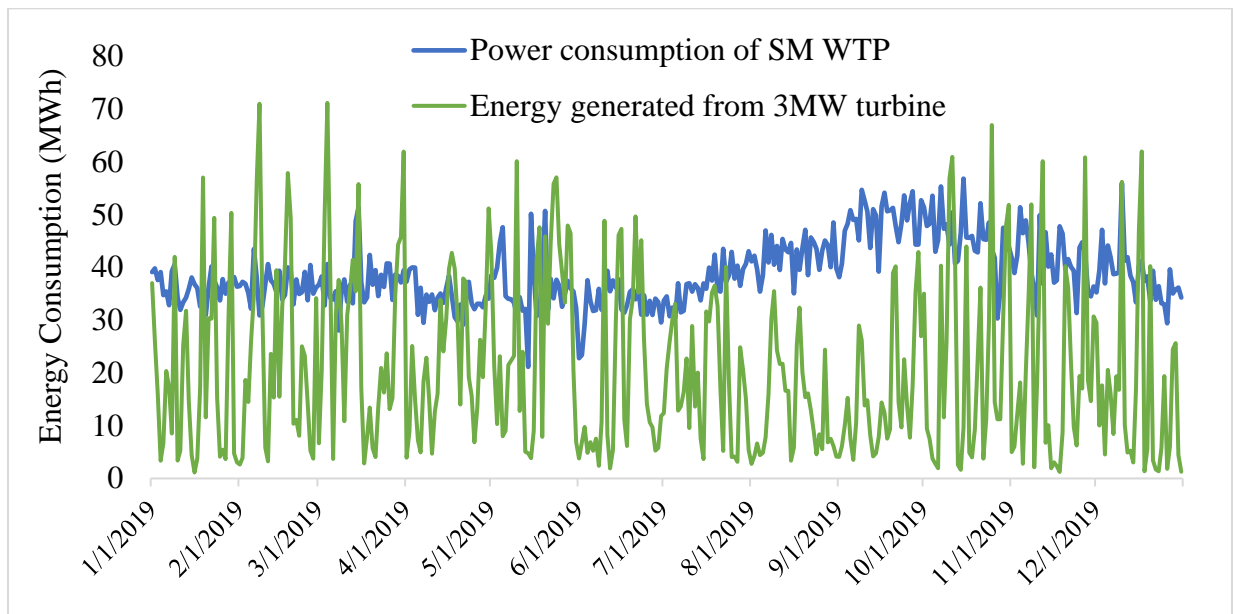


Figure 4.6 Daily Energy consumption Analysis of San Marcos WTP with a 3 MW turbine (2019)

It is noteworthy that the 3 MW turbine provided insufficient energy to fulfill the energy demand of the plant, particularly during the peak demand months of August to October. The water treatment plant required a total of approximately 14,210 MWh, while the turbine produced only 7,461 MWh of energy over the course of the year. Various factors could potentially account for

the observed peaks in power consumption at the water treatment plant, including seasonal variations that are typically experienced during the hot summer months, augmented water usage for irrigation or other purposes, shifts in population, maintenance or repair activities, and modifications to equipment or processes. Interestingly, the 3 MW turbine was barely able to cover up the energy requirement of the plant. Especially in the peak demand months of August to October the wind turbine fell short in providing energy to the plant. The total requirement of the plant was around 14,210MWh but the turbine barely produced 7,461 MWh of energy throughout the year. There are several potential factors that could contribute to the observed peaks in power consumption at the water treatment plant, such as seasonal variations that commonly occur during hot summer months, increased water usage for irrigation or other activities, changes in population, maintenance or repair activities, and equipment or process modifications.

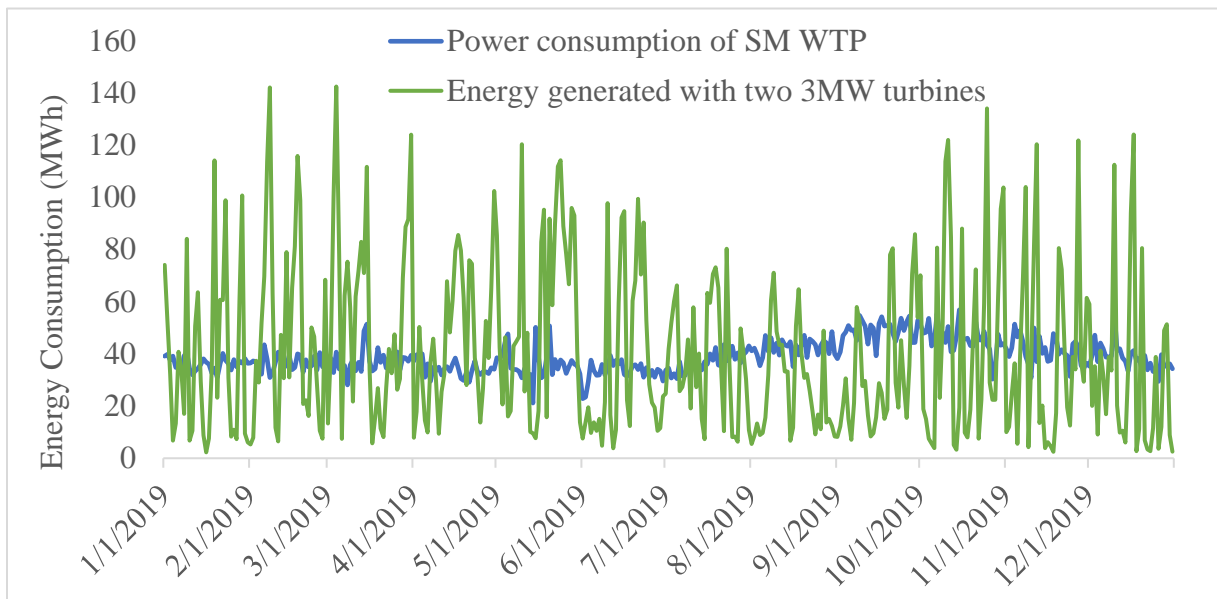


Figure 4.7 Daily Energy consumption Analysis of San Marcos WTP with two 3 MW turbine (2019)

Conversely, when the energy consumption of the plant was compared to that of two 3 MW turbines operating in tandem to provide energy to the plant, as shown in Figure 4.7, it was discovered that

the turbines were capable of effortlessly supplying surplus energy to the plant all year round. The two turbines generated a total of approximately 14,922 MWh of energy throughout the year, surpassing the electricity requirements of the San Marcos plant and generating around 712 MWh of excess energy. This superfluous energy can be profitably channeled back into the grid, potentially producing revenue for the plant.

4.5 Carbon footprint analysis

In the context of conducting a life cycle assessment (LCA) for a wind turbine, the carbon footprint is a significant environmental impact that must be taken into account. The carbon footprint of a wind turbine encompasses both direct and indirect emissions. Direct emissions result from the use of fossil fuels during the manufacturing, transportation, and installation of the wind turbine, as well as emissions generated during its operation and maintenance. Indirect emissions arise from the energy sources used in the production of materials and components. To calculate the carbon footprint of a wind turbine, an LCA methodology can be applied, involving a comprehensive analysis of the environmental impacts associated with the wind turbine throughout its entire life cycle. This includes identifying the raw materials used, the energy sources utilized in manufacturing and transportation, and the end-of-life disposal or recycling options.

4.5.1 Calculation of carbon footprint of 3 MW wind turbine

To determine the carbon footprint of a 3 MW wind turbine manufactured by Enercon, using data from their website, calculations would need to consider the expected operational lifespan of 20 years and the projected annual electricity generation of 7,469.77 MWh as forecasted above. The carbon footprint assessment would encompass multiple factors and emissions associated with the manufacturing, transportation, installation, operations, and maintenance of the wind turbine throughout its entire lifespan.

Manufacturing Emissions: As per the manufacturer's data, the production of the wind turbine emits 30 tons of carbon dioxide equivalent (CO_{2e}). This includes emissions associated with the manufacturing process, such as energy use, raw material extraction, and manufacturing operations.

Transportation Emissions: Based on industry data, the transportation of the components required for the wind turbine results in emissions of 5 tons of CO_{2e}. This includes emissions from transporting the turbine components from the manufacturing facility to the wind farm site.

Installation Emissions: The construction and installation of the wind turbine at the wind farm site emits 20 tons of CO_{2e}. This includes emissions associated with the on-site installation process, including transportation of heavy machinery, construction materials, and installation operations.

Carbon Offset: Based on the expected electricity generation of 7,469.77 MWh per year and assuming that the electricity is replacing electricity generated by a natural gas power plant, the wind turbine is estimated to offset 4,979.85 tons of CO_{2e} per year. This is calculated based on the assumption that the wind turbine generates clean energy that would have otherwise been generated by a natural gas power plant, thereby reducing greenhouse gas emissions.

Net Carbon Footprint: To calculate the net carbon footprint of the wind turbine, we subtract the amount of carbon offset by the wind turbine (from electricity generation) from the total emissions associated with its manufacturing, transportation, and installation (Kaldellis & Apostolou, 2017). This provides an overall estimate of the net carbon footprint of the wind turbine, taking into account both its emissions and its offsetting effects.

$$\text{Total emissions} = 30 + 5 + 20 = 55 \text{ ton}$$

$$\text{CO}_2\text{e Total offset} = 2,000 \text{ ton}$$

$$\text{CO}_2\text{e per year} \times 20 \text{ years} = 40,000 \text{ tons CO}_2\text{e}$$

$$\text{Net carbon footprint} = 55 \text{ tons CO}_2\text{e} - 40,000 \text{ tons CO}_2\text{e} = \mathbf{-39,945 \text{ tons CO}_2\text{e}}$$

Based on the calculations mentioned above, it is evident that the 3 MW wind turbine has a negative carbon footprint. This means that the wind turbine is estimated to offset more carbon emissions than it generates throughout its entire lifecycle. This is primarily due to the carbon offset achieved through the generation of clean electricity, which is expected to offset significant amounts of emissions that would have otherwise been produced by a natural gas power plant.

4.5.2 Calculation of carbon footprint of 1 MW wind turbine

$$\text{Total emissions} = 30 + 5 + 20 = 55 \text{ tons}$$

Based on the projected annual electricity generation of 1459.78 MWh and assuming that the electricity generated by the wind turbine is replacing electricity generated by a natural gas power plant, the wind turbine is estimated to offset approximately 1000 tons of CO_{2e} emissions per year.

$$\text{CO}_{2e} \text{ Total offset} = 1000 \text{ tons}$$

$$\text{CO}_{2e} \text{ per year} \times 20 \text{ years} = 20,000 \text{ tons CO}_{2e}$$

$$\text{Net carbon footprint} = 55 \text{ tons CO}_{2e} - 20,000 \text{ tons CO}_{2e} = \mathbf{-19,945 \text{ tons CO}_{2e}}$$

As per the calculations provided above, it is clear that the 1MW wind turbine has a negative carbon footprint, meaning that it offsets more carbon emissions than it generates over its entire lifecycle (Bi et al., 2022). This can be attributed to several factors, including the relatively low emissions associated with the manufacturing, transportation, and installation of the wind turbine, as well as the significant amount of clean electricity generated during its operational lifespan. This underscores the potential of wind energy as a renewable and sustainable source of electricity, with the capacity to effectively contribute to climate change mitigation by reducing carbon emissions.

4.6 Present Worth Analysis

To facilitate the buying or selling of electricity to the grid, it is necessary to compare the cost of onsite generation with the electricity from utility provider. Now, to calculate the energy cost the energy consumption of the WWTP will be multiplied by the cost of electricity. In addition, when

selling surplus energy back to the grid, the feed-in-tariff (FIT) price is utilized, assuming the FIT rate of \$0.05/kWh, for selling the renewable energy to the grid. FIT typically requires contracts that are long-term, ranging from 10 to 20 years.

The present worth analysis typically involves four distinct phases, each aimed at providing a comprehensive evaluation of the financial aspects of the wind turbine project.

Manufacturing Phase: This phase encompasses the production of wind turbine components, such as the blades, tower, and nacelle. It also includes the cost of transporting these components to the installation site.

Installation Phase: During this phase, the wind turbine components are assembled and set up at the installation site. The costs associated with the installation process, including labor, equipment, and materials, are included in this phase.

Operation and Maintenance Phase: Once the wind turbine is installed and operational, there are ongoing costs for monitoring its performance, repairing any faults, and replacing components as needed. This phase includes the expenses incurred in operating and maintaining the wind turbine throughout its operational lifespan.

Salvage Value: The salvage value in wind turbine installation refers to the estimated residual value or residual worth of the wind turbine and its components at the end of their useful life. It is the estimated value that the wind turbine and its components can still hold after depreciation and wear and tear over time. Salvage value is typically expressed as a percentage of the original cost of the wind turbine or its components, and it is used in financial calculations. The salvage value can vary depending on factors such as the condition of the wind turbine, technological advancements, market demand for used wind turbines, and other relevant factors.

It is important to consider all these phases and their associated costs when conducting a

comprehensive present worth analysis (PWA) of a wind turbine. This analysis helps evaluate the total cost of ownership of the turbine over its entire lifespan, including not only the upfront costs of manufacturing and installation, but also the ongoing operation, maintenance, revenue generation of energy trading, and eventual salvage value costs.

In the context of cost analysis for wind farms, various factors are taken into consideration. These factors typically include the rating of the wind turbines, capital expenditures, fixed charge rates, operational expenditures, net annual energy production, and the leveled cost of energy. These parameters are used to evaluate the costs associated with the entire life cycle of a wind farm, including both upfront and ongoing expenses, and to determine the overall economic feasibility and financial performance of the project.

Identification of cost elements:

- Initial capital cost (purchase price and installation cost)
- Operating and maintenance costs (including regular maintenance, unscheduled repairs, and replacement of parts)
- Fuel costs (in this study, wind is the fuel with no cost)
- Salvage value

4.6.1 Quantification of cost elements

1. Initial capital cost: There are various **incentives and tax rebate schemes** which are available for renewable projects by the government. Assuming our project will satisfy the new wage and apprenticeship requirements, Texas provides 10 percent of the total capital cost of the project under Franchise tax credit for clean energy project (Hegar, 2023)

Also as seen from few studies the cost of installing an on-shore 1 MW of wind turbine cost around \$ 1.5 million (ACUA, n.d.; EPA Fact Sheet, 2013). The total cost of installation of a 3 MW turbine will be approximately \$ 4.5 million plus the Government will cover 10% of this

cost. Thus, we have

$$\begin{aligned} \text{Total installation cost} &= \$4.5 \text{ million} - (10\% \text{ of } \$4.5 \text{ million}) \\ &= \$3.87 \text{ million} = \$3,870,000 \end{aligned}$$

2. Operating and maintenance costs: \$30,000 per year (assuming a 20-year lifespan for the turbine) (Stehly & Duffy, 2022)
3. Fuel costs: \$0 (since wind is the fuel, there is no fuel cost)
4. Salvage Value: As salvage value are typically estimated as a percentage of the installation cost, so assume a range of 10-15% for the Salvage Value in our case:

Salvage Value = 10-15% of installation cost

Salvage Value = 12.5% of \$4.32 million (taking average value of 10 and 15%)

Salvage Value (estimated) = $0.125 * \$4,320,000$

Salvage Value = \$540,000 (approximately)

In order to determine the present value of costs, it is necessary to incorporate a discount rate that considers the concept of time value of money. Assuming a discount rate of 7%.

$$\text{Present Value (PV)} = C / (1 + r)^n$$

Where, C = initial capital cost, r =discount rate and n = service life of turbine

$$\text{Total PV cost} = \$1.00 \text{ million}$$

The capital expenditures (CapEx) associated with a wind turbine project can fluctuate due to various factors, including turbine size, location, site preparation, transmission infrastructure, and ancillary equipment. A larger turbine with a higher capacity is likely to entail higher CapEx costs. For instance, according to Puglia (2013), the estimated CapEx for a 3 MW wind turbine ranges from \$2.5 million to \$4.5 million. As the wind turbine project has a capacity of 3 MW, the CapEx in \$/kW would be:

$$\text{For a CapEx of } \$4.5 \text{ million: } \$4.5 \text{ million} / 3,000 \text{ kW} = \$1,500/\text{kW}$$

Fixed charge rate (FCR)= 5.88 % (Stehly & Duffy, 2022)

Operational expenditures (OpEx)= \$30 kW/yr

For making the present worth analysis, we have initial investment cost of \$3,870,000, Operations & Maintenance cost is \$30,000/year, the expected annual income is around \$373,488.5 considering a FIT rate of \$0.05/kWh to the grid.

So here we can calculate the PW as

$$PW = P_1 + A \left[\frac{((1+i)^n - 1)}{i(1+i)^n} \right] + \left[\frac{F}{(1+i)^n} \right]$$

Putting the initial investment, $P_1 = 3,870,000$, net earnings, $A = (373,488.5 - 20,000) = 353,488.5$, $i = 7\%$ and $n = 20$ years, we will get

$$PW = \$ 226,388.91$$

A positive PW means that the project or investment is expected to generate more revenue than the initial investment cost, taking into account the time value of money. In other words, the project is expected to be profitable and generate a positive return on investment. This is a favorable result, as it indicates that the project is financially viable and worth pursuing.

4.6.2 Payback period

To determine the amount of time it will take for the profit generated from the wind turbine to cover the overall investment, a financial metric called the payback period can be used. The payback period is the amount of time required for the cumulative cash inflows from a project to equal the initial cash outflow or investment. In other words, it is the time duration it takes for the project to pay for itself.

The installation cost of the wind turbine is \$3,870,000, and the annual revenue generated will be around \$353,488.5, Using an interest rate of 7%, the total PW is \$ 226,388.91. To determine the payback period, the net cash flow for each year needs to be calculated by subtracting the annual

revenue from the installation cost until it gives a positive value.

i.e., Year 1: $-3,670,000 + 353,488.5 = -3,316,511.5$

Year 2: $-3,316,511.5 + 353,488.5 = -2,963,023$ till we get a positive value.

Upon further analysis, it has been determined that the payback period for the initial investment cost of the wind turbine is approximately 10.38 years.

However, it is worth noting that there are different rebate schemes and programs offered in various states that can potentially reduce the initial investment cost of the turbines, leading to a more expedited recovery of the initial investment. These rebate schemes and programs can significantly impact the payback period and make the investment in wind turbines more financially feasible.

4.7 Wind turbine spacing

The spacing of wind turbines is a critical aspect of wind farm design that has a significant impact on its performance and efficiency. Multiple factors, such as the wind turbine size and capacity, the land topography, wind speed and direction, and environmental impact, determine the spacing between two turbines (Talinli et al., 2011). The primary objective of optimizing wind turbine spacing is to maximize energy production while minimizing negative effects on the environment and surrounding communities.

The minimum spacing between turbines depends on the wind turbine size and rotor diameter. Generally, turbines are placed six or seven times the diameter of the rotor apart from each other to avoid wake effects and turbulence, which can hinder the energy production of downstream turbines. Recent studies suggest that doubling the distance between turbines would prove more cost-effective (Ali et al., 2018; Clayton, 2022). Wind turbine capacity also affects

spacing requirements, where a 3 MW turbine demands more spacing than a 2 MW turbine due to its larger rotor diameter.

The spacing between two turbines has an impact on the wind farm's land requirement, and decreased spacing between turbines can lead to negative environmental effects, such as noise pollution and disturbance of local wildlife. Reduced spacing can also cause wake effects, where the wind flow behind one turbine interferes with the wind flow of another turbine downstream. This interference significantly reduces the energy output of downstream turbines and causes turbulence that can damage the turbines over time (Ali et al., 2018). Therefore, maintaining sufficient spacing between turbines is critical to avoid such problems.

To overcome these issues, wind farm designers use advanced computer models and optimization methods to simulate wake effects and optimize the spacing between turbines (Baker et al., n.d.; Zhao et al., 2022). Various factors such as land topography, wind speed and direction, and other environmental factors are considered to minimize the negative impact of the wind farm. Moreover, the use of new technologies, such as adjustable blade wind turbines, can reduce wake effects and optimize turbine spacing (Upadhaya et al., 2014).

5. CONCLUSION AND FUTURE WORK

5.1 Conclusion

Wastewater treatment plant (WWTP) requires a large amount of electric power due to the different treatment procedures involved, such as aeration, which alone uses around 60% of the plant's electricity. Also, behind personnel, energy is the second most expensive component of WWTP operation. In addition to large electricity costs, most WWTP facilities in the world still rely on the power grid for their daily operations. Since 60-70% of today's grid power is generated by burning fossil fuels, operations of WWTP also result in huge amounts of greenhouse gas emissions.

However, there are several techniques for lowering energy use in WWTPs. One way is to increase the efficiency of the treatment processes themselves, such as via the use of more advanced aeration systems or by the optimization of biological nutrient removal. Another alternative is to install energy recovery systems, such as utilizing biogas created from anaerobic digestion of wastewater solids to power turbines or cogeneration systems. Additional energy-saving techniques include improving equipment maintenance schedule and introducing energy-efficient lighting.

Using renewable power production sources, such as wind energy, is an emerging technology for lowering WWTP energy usage and dependency on the grid. According to surveys, Texas is presently one of the top wind-producing states in the United States, which motivated this research. Since wind speed is inconsistent and unpredictable, it is difficult to produce trustworthy generation forecasts. Nevertheless, machine learning (ML) is a powerful interdisciplinary field that may be utilized to enhance wind speed predictions. In recent decades, ML has been widely utilized to solve time series issues, with neural network (NN) models being the most preferred technique since NN have shown in previous research that they are capable of analyzing time series data. Additionally, regression models like as LSTM and RNN have proven to be more accurate

than conventional statistical models for modeling time series data in a variety of domains, yielding outstanding results, which is why these models were chosen for this study. We highlight the accomplishments of this thesis work from five aspects as follows.

- 1) This thesis looked at the power consumption trends of WWTP and WTP. The power consumption trends show that the energy demand of various processes and equipment in wastewater and water treatment varies greatly. This gives insight into WWTP and WTP's power load profile and underlines the significance of monitoring power demand to guarantee stable operations and equipment performance. This conclusion further emphasizes the need to implement targeted energy-saving strategies to optimize power use and save expenses.
- 2) To forecast time series wind speeds, several machine learning models such as RNN, LSTM, and ensemble models were used. The ensemble model was also used to test if it can potentially improve the accuracy of two or more NN models. Based on various error scores, learning curves, prediction speeds, and accuracy, the study discovered that the RNN model was the most successful for wind speed forecasting. It was also shown that including more low-performing models into the ensemble model might greatly enhance its outcomes.
- 3) The analysis of transactive energy demonstrated how contemporary communication and automation technologies may be used to balance power supply and demand through price signaling. TE has been used in a number of projects, demonstrating that it may be a viable solution for energy trading and management in a variety of sectors, including WWTP. The analysis of transactive energy also highlighted that the integration of these two technologies can enable peer-to-peer energy trading, where energy transactions can take place directly between prosumers and consumers without the need for intermediaries. This can potentially reduce transaction costs and increase the efficiency of the energy market. The power output

of the proposed turbine calculated with the help of a regression model and the analysis of its results for the year 2019 also revealed that one 3 MW turbine can generate enough electricity to run the WWTP.

- 4) Upon conducting a rigorous carbon footprint analysis, it has been determined that wind turbines exhibit a negative carbon footprint, signifying that their environmental impact in terms of greenhouse gas emissions is lower compared to energy generated from fossil fuel sources. This finding suggests that wind energy generation has the potential to contribute positively towards reversing the climate change.
- 5) Based on the current analysis, the payback period for the wind turbine is estimated to be approximately 10.38 years. However, further investigation is warranted to fully ascertain the potential impact of rebate schemes and other discount programs that may be available in the specific location. These programs have the potential to significantly reduce the initial investment cost of the turbine, resulting in a shorter payback period. Additional research is needed to comprehensively evaluate the available rebate schemes and discount programs and their potential impact on the payback period of the wind turbine project.

5.2 Future Work

The potential area for future research is a more comprehensive analysis of water treatment plants, with a focus on calculating their power consumption. Additionally, while the study determined that RNN models were the most effective for predicting wind speed, further research could investigate the potential of other machine learning models, such as CNNs, for improving wind speed forecasting accuracy. Future studies could also examine the practical implementation of blockchain and transactive energy in WWTPs, assessing the potential benefits and identifying any obstacles that may impede their adoption, such as technological limitations, regulatory challenges,

or stakeholder resistance.

In addition, we can also use blockchain technology for real-time energy trading in our future studies. Blockchain can be used to track and manage the distribution of energy, enabling P2P energy trading, and ensuring the integrity of the grid. Blockchain technology has various potential uses in the energy business. Blockchain can facilitate P2P trading by allowing individuals and organizations to buy and sell energy directly with one another without the use of mediators or aggregators (Thukral, 2021). This can assist to enhance energy access, lower prices, and encourage the expansion of distributed renewable energy systems. Blockchain technology may be used to track the production and use of renewable energy certificates, which are intended to validate the source and quality of renewable energy (Bao et al., 2021; Westphall and Martina, 2022; Zhang et al., 2020). This can serve to promote openness and confidence in the renewable energy market while also promoting the expansion of renewable energy systems.

In addition, the utilization of smart contracts can facilitate automation of energy transactions and enforcement of agreements between parties (Bao et al., 2021; Wu and Tran, 2018). To illustrate, a smart contract can be deployed to pay renewable energy producers automatically for the energy they contribute to the grid. Also, blockchain technology can assist in managing energy grids by improving the efficiency and security of grid assets and data management. An example of this is the use of blockchain-based solutions to balance energy demand and supply, monitor grid performance, and manage energy storage systems.

APPENDIX

Table 1 Output power of RNN, LSTM and ensemble models in Peak demand month of March 2019 with 3 MW WT

Date	Ensemble Wind Speed (m/s)	Ensemble Pw	LSTM Wind Speed (m/s)	LSTM Pw	RNN Wind Speed (m/s)	RNN Pw
3/1/2019 0:53	6.96	0.59	6.92	0.57	7.00	0.60
3/1/2019 1:53	6.04	0.38	6.17	0.41	5.91	0.36
3/1/2019 2:53	5.04	0.22	5.21	0.25	4.88	0.20
3/1/2019 3:53	7.04	0.61	7.25	0.66	6.83	0.55
3/1/2019 4:53	6.07	0.39	6.15	0.40	6.00	0.37
3/1/2019 5:53	6.92	0.57	7.10	0.62	6.73	0.53
3/1/2019 6:53	7.22	0.65	7.36	0.69	7.08	0.62
3/1/2019 7:53	6.49	0.48	6.54	0.49	6.45	0.47
3/1/2019 8:53	5.71	0.32	5.76	0.33	5.66	0.32
3/1/2019 9:53	6.34	0.44	6.47	0.47	6.22	0.42
3/1/2019 10:53	7.05	0.61	7.07	0.61	7.03	0.60
3/1/2019 11:53	5.80	0.34	5.82	0.34	5.77	0.33
3/1/2019 12:53	5.58	0.30	5.66	0.31	5.49	0.29
3/1/2019 13:55	4.50	0.16	4.73	0.18	4.27	0.14
3/1/2019 14:53	3.45	0.07	3.82	0.10	3.08	0.05
3/1/2019 15:53	4.64	0.17	4.79	0.19	4.48	0.16
3/1/2019 16:53	3.72	0.09	4.03	0.11	3.41	0.07
3/1/2019 17:53	3.25	0.06	3.49	0.07	3.02	0.05
3/1/2019 18:53	2.31	0.00	2.57	0.00	2.05	0.00
3/1/2019 19:53	3.08	0.05	3.26	0.06	2.89	0.00
3/1/2019 20:53	2.30	0.00	2.54	0.00	2.07	0.00
3/1/2019 21:53	1.99	0.00	2.16	0.00	1.81	0.00
3/1/2019 22:53	1.97	0.00	2.04	0.00	1.90	0.00
3/1/2019 23:53	4.59	0.17	4.70	0.18	4.47	0.16
3/2/2019 0:53	2.48	0.00	2.72	0.00	2.25	0.00
3/2/2019 1:53	2.08	0.00	2.26	0.00	1.91	0.00
3/2/2019 2:53	7.84	0.84	8.08	0.91	7.61	0.76
3/2/2019 3:53	5.18	0.24	5.15	0.24	5.21	0.25
3/2/2019 4:53	6.43	0.46	6.18	0.41	6.69	0.52
3/2/2019 5:53	6.27	0.43	6.10	0.39	6.45	0.46
3/2/2019 6:53	8.51	1.07	8.04	0.90	8.98	1.26
3/2/2019 7:53	7.35	0.69	7.11	0.62	7.59	0.76
3/2/2019 8:53	8.41	1.03	8.40	1.03	8.42	1.04
3/2/2019 9:53	8.73	1.15	8.50	1.06	8.96	1.25
3/2/2019 10:53	8.59	1.10	8.17	0.95	9.02	1.27
3/2/2019 11:53	9.60	1.53	9.09	1.31	10.10	1.79
3/2/2019 12:53	7.30	0.68	6.79	0.54	7.82	0.83

3/2/2019 13:53	7.53	0.74	7.35	0.69	7.71	0.80
3/2/2019 14:53	6.97	0.59	6.69	0.52	7.25	0.66
3/2/2019 15:53	7.43	0.71	7.27	0.67	7.59	0.76
3/2/2019 16:53	7.52	0.74	7.32	0.68	7.73	0.80
3/2/2019 17:53	7.47	0.72	7.32	0.68	7.61	0.77
3/2/2019 18:53	6.93	0.58	6.69	0.52	7.16	0.64
3/2/2019 19:53	7.45	0.72	7.27	0.67	7.63	0.77
3/2/2019 20:53	9.64	1.56	9.51	1.49	9.78	1.62
3/2/2019 21:53	9.14	1.32	8.99	1.26	9.29	1.39
3/2/2019 22:53	10.45	1.98	10.40	1.95	10.51	2.02
3/2/2019 23:53	10.06	1.77	10.06	1.77	10.06	1.77
3/3/2019 0:53	9.34	1.41	9.37	1.43	9.31	1.40
3/3/2019 1:53	10.03	1.75	9.89	1.68	10.18	1.83
3/3/2019 2:53	11.94	2.96	11.89	2.92	11.99	2.99
3/3/2019 3:53	8.29	0.99	8.07	0.91	8.52	1.07
3/3/2019 4:53	6.83	0.55	6.98	0.59	6.68	0.52
3/3/2019 5:53	8.84	1.20	8.96	1.25	8.73	1.15
3/3/2019 6:53	7.06	0.61	7.07	0.61	7.06	0.61
3/3/2019 7:53	6.39	0.45	6.60	0.50	6.17	0.41
3/3/2019 8:53	8.53	1.08	8.53	1.08	8.52	1.07
3/3/2019 9:53	7.98	0.88	7.95	0.87	8.02	0.90
3/3/2019 10:53	7.50	0.73	7.45	0.72	7.56	0.75
3/3/2019 11:53	9.24	1.37	9.27	1.38	9.22	1.36
3/3/2019 12:53	12.74	3.00	12.66	3.00	12.81	3.00
3/3/2019 13:53	15.16	3.00	15.16	3.00	15.16	3.00
3/3/2019 14:53	16.58	3.00	16.64	3.00	16.51	3.00
3/3/2019 15:53	17.05	3.00	17.13	3.00	16.97	3.00
3/3/2019 16:53	17.56	3.00	17.61	3.00	17.52	3.00
3/3/2019 17:53	17.85	3.00	17.80	3.00	17.90	3.00
3/3/2019 18:53	18.28	3.00	18.27	3.00	18.29	3.00
3/3/2019 19:53	17.89	3.00	17.85	3.00	17.93	3.00
3/3/2019 20:53	17.35	3.00	17.17	3.00	17.52	3.00
3/3/2019 21:53	16.56	3.00	16.27	3.00	16.85	3.00
3/3/2019 22:53	15.31	3.00	14.94	3.00	15.68	3.00
3/3/2019 23:53	15.14	3.00	14.67	3.00	15.61	3.00
3/4/2019 0:53	15.09	3.00	14.62	3.00	15.57	3.00
3/4/2019 1:53	12.43	3.00	11.56	2.68	13.31	3.00
3/4/2019 2:53	11.84	2.88	11.76	2.83	11.91	2.94
3/4/2019 3:53	12.85	3.00	12.86	3.00	12.85	3.00
3/4/2019 4:53	14.22	3.00	14.21	3.00	14.24	3.00
3/4/2019 5:53	16.02	3.00	16.18	3.00	15.87	3.00
3/4/2019 6:53	16.73	3.00	17.04	3.00	16.42	3.00
3/4/2019 7:53	13.81	3.00	13.68	3.00	13.93	3.00

3/4/2019 8:53	15.52	3.00	15.59	3.00	15.45	3.00
3/4/2019 9:53	16.64	3.00	16.92	3.00	16.36	3.00
3/4/2019 10:53	16.51	3.00	16.71	3.00	16.31	3.00
3/4/2019 11:53	14.86	3.00	15.18	3.00	14.53	3.00
3/4/2019 12:53	13.42	3.00	13.95	3.00	12.90	3.00
3/4/2019 13:53	13.71	3.00	13.97	3.00	13.45	3.00
3/4/2019 14:53	13.17	3.00	13.41	3.00	12.92	3.00
3/4/2019 15:53	12.41	3.00	12.74	3.00	12.09	3.00
3/4/2019 16:53	11.26	2.48	11.46	2.61	11.05	2.34
3/4/2019 17:53	12.71	3.00	12.89	3.00	12.52	3.00
3/4/2019 18:53	14.11	3.00	14.09	3.00	14.14	3.00
3/4/2019 19:53	12.73	3.00	12.89	3.00	12.56	3.00
3/4/2019 20:53	12.23	3.00	12.41	3.00	12.04	3.00
3/4/2019 21:53	11.78	2.84	12.00	3.00	11.56	2.68
3/4/2019 22:53	13.89	3.00	14.11	3.00	13.68	3.00
3/4/2019 23:53	12.21	3.00	12.39	3.00	12.02	3.00
3/5/2019 0:53	11.18	2.42	11.45	2.60	10.91	2.25
3/5/2019 1:53	11.42	2.58	11.67	2.76	11.17	2.42
3/5/2019 2:53	7.65	0.78	7.48	0.73	7.82	0.83
3/5/2019 3:53	7.78	0.82	7.96	0.88	7.60	0.76
3/5/2019 4:53	6.89	0.57	7.11	0.62	6.66	0.51
3/5/2019 5:53	5.99	0.37	5.91	0.36	6.07	0.39
3/5/2019 6:53	5.74	0.33	6.06	0.39	5.42	0.28
3/5/2019 7:53	6.56	0.49	6.71	0.53	6.41	0.46
3/5/2019 8:53	6.53	0.48	6.68	0.52	6.37	0.45
3/5/2019 9:53	6.45	0.47	6.66	0.51	6.24	0.42
3/5/2019 10:53	9.40	1.44	9.65	1.56	9.15	1.33
3/5/2019 11:53	10.33	1.92	10.53	2.03	10.13	1.81
3/5/2019 12:53	11.79	2.84	12.03	3.00	11.54	2.67
3/5/2019 13:53	12.48	3.00	12.65	3.00	12.32	3.00
3/5/2019 14:53	14.62	3.00	14.72	3.00	14.53	3.00
3/5/2019 15:53	14.10	3.00	14.35	3.00	13.85	3.00
3/5/2019 16:53	13.75	3.00	13.89	3.00	13.61	3.00
3/5/2019 17:53	11.60	2.71	11.66	2.75	11.55	2.67
3/5/2019 18:53	11.73	2.80	11.91	2.93	11.56	2.68
3/5/2019 19:53	9.89	1.68	9.97	1.72	9.81	1.64
3/5/2019 20:53	10.72	2.14	10.81	2.19	10.62	2.08
3/5/2019 21:53	9.40	1.44	9.26	1.38	9.53	1.50
3/5/2019 22:53	6.96	0.58	6.91	0.57	7.00	0.59
3/5/2019 23:53	4.86	0.20	4.78	0.19	4.94	0.21
3/6/2019 0:53	2.27	0.00	2.26	0.00	2.28	0.00
3/6/2019 1:53	2.80	0.00	2.92	0.00	2.67	0.00
3/6/2019 2:53	8.06	0.91	7.63	0.77	8.48	1.06

3/6/2019 3:53	3.23	0.06	2.67	0.00	3.78	0.09
3/6/2019 4:53	1.26	0.00	0.92	0.00	1.59	0.00
3/6/2019 5:53	1.30	0.00	1.03	0.00	1.58	0.00
3/6/2019 6:53	1.34	0.00	0.98	0.00	1.69	0.00
3/6/2019 7:53	1.23	0.00	0.87	0.00	1.58	0.00
3/6/2019 8:53	1.44	0.00	1.18	0.00	1.71	0.00
3/6/2019 9:53	1.59	0.00	1.44	0.00	1.74	0.00
3/6/2019 10:53	2.81	0.00	2.79	0.00	2.84	0.00
3/6/2019 11:53	6.91	0.57	7.45	0.72	6.37	0.45
3/6/2019 12:53	5.76	0.33	6.01	0.38	5.50	0.29
3/6/2019 13:53	5.92	0.36	5.90	0.36	5.93	0.36
3/6/2019 14:53	8.79	1.18	8.84	1.20	8.75	1.16
3/6/2019 15:53	9.91	1.69	9.75	1.61	10.07	1.77
3/6/2019 16:53	10.98	2.30	10.98	2.30	10.99	2.30
3/6/2019 17:53	11.99	2.99	12.11	3.00	11.88	2.91
3/6/2019 18:53	10.47	1.99	10.60	2.07	10.34	1.92
3/6/2019 19:53	9.91	1.69	9.95	1.71	9.87	1.67
3/6/2019 20:53	8.31	0.99	8.30	0.99	8.32	1.00
3/6/2019 21:53	7.33	0.68	7.30	0.68	7.36	0.69
3/6/2019 22:53	6.98	0.59	6.85	0.56	7.10	0.62
3/6/2019 23:53	10.20	1.84	10.05	1.76	10.34	1.92
3/7/2019 0:53	10.46	1.99	10.04	1.76	10.88	2.24
3/7/2019 1:53	9.70	1.58	8.35	1.01	11.05	2.34
3/7/2019 2:53	9.48	1.48	9.35	1.42	9.60	1.54
3/7/2019 3:53	7.62	0.77	7.54	0.74	7.70	0.79
3/7/2019 4:53	8.79	1.18	8.73	1.16	8.84	1.20
3/7/2019 5:53	8.00	0.89	8.02	0.90	7.98	0.88
3/7/2019 6:53	7.24	0.66	7.25	0.66	7.22	0.65
3/7/2019 7:53	5.87	0.35	5.94	0.36	5.80	0.34
3/7/2019 8:53	4.53	0.16	4.65	0.17	4.40	0.15
3/7/2019 9:53	4.73	0.18	4.85	0.20	4.62	0.17
3/7/2019 10:53	5.65	0.31	5.64	0.31	5.67	0.32
3/7/2019 11:53	4.91	0.21	4.98	0.21	4.84	0.20
3/7/2019 12:53	5.60	0.31	5.77	0.33	5.44	0.28
3/7/2019 13:53	9.41	1.45	9.59	1.53	9.23	1.37
3/7/2019 14:53	11.45	2.61	11.40	2.57	11.51	2.65
3/7/2019 15:53	13.97	3.00	13.98	3.00	13.97	3.00
3/7/2019 16:53	14.55	3.00	14.69	3.00	14.42	3.00
3/7/2019 17:53	14.00	3.00	14.04	3.00	13.96	3.00
3/7/2019 18:53	13.68	3.00	13.59	3.00	13.76	3.00
3/7/2019 19:53	11.48	2.62	11.49	2.63	11.46	2.61
3/7/2019 20:53	9.66	1.56	9.72	1.59	9.60	1.53
3/7/2019 21:53	6.15	0.40	6.51	0.48	5.80	0.34

3/7/2019 22:53	4.87	0.20	5.14	0.24	4.60	0.17
3/7/2019 23:53	5.09	0.23	5.41	0.28	4.76	0.19
3/8/2019 0:53	5.68	0.32	5.87	0.35	5.50	0.29
3/8/2019 1:53	8.10	0.92	7.96	0.88	8.24	0.97
3/8/2019 2:53	10.50	2.01	9.92	1.69	11.09	2.37
3/8/2019 3:53	9.67	1.57	9.26	1.38	10.07	1.78
3/8/2019 4:53	10.51	2.01	10.35	1.92	10.67	2.11
3/8/2019 5:53	10.01	1.74	9.81	1.64	10.22	1.85
3/8/2019 6:53	9.84	1.65	9.72	1.59	9.96	1.71
3/8/2019 7:53	9.81	1.64	9.74	1.60	9.88	1.67
3/8/2019 8:53	7.61	0.76	7.62	0.77	7.59	0.76
3/8/2019 9:53	7.71	0.80	7.77	0.81	7.66	0.78
3/8/2019 10:53	7.29	0.67	7.37	0.69	7.22	0.65
3/8/2019 11:53	7.79	0.82	8.03	0.90	7.55	0.75
3/8/2019 12:53	8.95	1.25	9.12	1.32	8.78	1.17
3/8/2019 13:53	10.63	2.09	10.82	2.20	10.44	1.98
3/8/2019 14:53	10.51	2.01	10.56	2.04	10.45	1.98
3/8/2019 15:53	11.87	2.90	11.78	2.83	11.96	2.97
3/8/2019 16:53	12.87	3.00	12.72	3.00	13.02	3.00
3/8/2019 17:53	11.55	2.68	11.33	2.53	11.77	2.83
3/8/2019 18:53	11.15	2.41	11.01	2.32	11.29	2.50
3/8/2019 19:53	8.37	1.02	8.07	0.91	8.67	1.13
3/8/2019 20:53	7.26	0.66	7.20	0.65	7.31	0.68
3/8/2019 21:53	9.20	1.35	9.18	1.35	9.21	1.36
3/8/2019 22:53	9.08	1.30	9.04	1.28	9.11	1.31
3/8/2019 23:53	10.57	2.05	10.70	2.13	10.45	1.98
3/9/2019 0:53	11.11	2.38	11.21	2.44	11.02	2.33
3/9/2019 1:53	10.65	2.10	10.64	2.09	10.66	2.10
3/9/2019 2:53	7.39	0.70	6.17	0.41	8.61	1.11
3/9/2019 3:53	10.42	1.96	10.36	1.93	10.48	2.00
3/9/2019 4:53	10.49	2.00	10.43	1.97	10.55	2.04
3/9/2019 5:53	10.78	2.17	10.28	1.88	11.28	2.49
3/9/2019 6:53	10.67	2.11	10.80	2.18	10.54	2.03
3/9/2019 7:56	8.21	0.96	8.59	1.10	7.84	0.84
3/9/2019 8:53	9.11	1.31	9.10	1.31	9.12	1.32
3/9/2019 9:53	11.15	2.41	11.31	2.51	11.00	2.31
3/9/2019 10:53	10.99	2.30	11.01	2.32	10.96	2.28
3/9/2019 11:53	7.35	0.69	7.55	0.75	7.15	0.63
3/9/2019 12:53	6.66	0.51	6.95	0.58	6.37	0.45
3/9/2019 13:53	9.35	1.42	9.53	1.50	9.16	1.34
3/9/2019 14:53	10.15	1.81	10.26	1.88	10.03	1.75
3/9/2019 15:53	7.55	0.75	7.66	0.78	7.43	0.71
3/9/2019 16:53	7.16	0.64	7.29	0.67	7.03	0.60

3/9/2019 17:53	6.49	0.47	6.37	0.45	6.61	0.50
3/9/2019 18:53	5.77	0.33	5.78	0.33	5.77	0.33
3/9/2019 19:53	7.45	0.72	7.53	0.74	7.37	0.69
3/9/2019 20:53	6.01	0.38	5.90	0.36	6.12	0.40
3/9/2019 21:53	4.90	0.20	4.97	0.21	4.82	0.19
3/9/2019 22:53	6.30	0.43	6.30	0.43	6.29	0.43
3/9/2019 23:53	3.44	0.07	3.37	0.07	3.50	0.07
3/10/2019 0:53	2.15	0.00	2.14	0.00	2.17	0.00
3/10/2019 1:53	2.22	0.00	2.69	0.00	1.76	0.00
3/10/2019 2:53	2.13	0.00	2.58	0.00	1.68	0.00
3/10/2019 3:53	2.01	0.00	2.50	0.00	1.52	0.00
3/10/2019 4:53	1.90	0.00	2.19	0.00	1.60	0.00
3/10/2019 5:53	1.85	0.00	2.03	0.00	1.67	0.00
3/10/2019 6:53	2.90	0.00	3.03	0.05	2.76	0.00
3/10/2019 7:53	4.18	0.13	4.25	0.13	4.10	0.12
3/10/2019 8:53	5.72	0.32	5.60	0.31	5.83	0.34
3/10/2019 9:53	3.42	0.07	3.41	0.07	3.43	0.07
3/10/2019 10:55	6.19	0.41	5.95	0.37	6.43	0.46
3/10/2019 11:53	5.36	0.27	5.22	0.25	5.51	0.29
3/10/2019 12:53	5.37	0.27	5.26	0.25	5.48	0.29
3/10/2019 13:53	7.11	0.62	6.96	0.58	7.26	0.66
3/10/2019 14:53	7.70	0.79	7.48	0.73	7.91	0.86
3/10/2019 15:53	7.64	0.78	7.60	0.76	7.69	0.79
3/10/2019 16:53	7.55	0.75	7.57	0.75	7.54	0.74
3/10/2019 17:53	7.18	0.64	7.12	0.63	7.25	0.66
3/10/2019 18:53	9.38	1.43	9.03	1.28	9.74	1.60
3/10/2019 19:53	7.64	0.77	7.04	0.60	8.25	0.97
3/10/2019 20:53	6.22	0.42	5.78	0.33	6.66	0.51
3/10/2019 21:53	5.27	0.25	4.72	0.18	5.81	0.34
3/10/2019 22:53	9.17	1.34	8.89	1.22	9.46	1.47
3/10/2019 23:53	9.73	1.60	9.40	1.44	10.07	1.77
3/11/2019 0:53	6.85	0.56	6.62	0.50	7.08	0.62
3/11/2019 1:53	7.35	0.69	7.21	0.65	7.48	0.73
3/11/2019 2:53	5.78	0.33	5.56	0.30	5.99	0.37
3/11/2019 3:53	6.66	0.51	6.49	0.47	6.84	0.55
3/11/2019 4:53	6.89	0.57	6.69	0.52	7.09	0.62
3/11/2019 5:53	7.48	0.73	7.39	0.70	7.58	0.76
3/11/2019 6:53	7.57	0.75	7.57	0.75	7.57	0.75
3/11/2019 7:53	7.09	0.62	7.06	0.61	7.12	0.63
3/11/2019 8:53	7.68	0.79	7.74	0.81	7.62	0.77
3/11/2019 9:53	10.52	2.02	10.42	1.96	10.63	2.09
3/11/2019 10:53	11.03	2.33	10.96	2.29	11.09	2.37
3/11/2019 11:53	10.68	2.12	10.76	2.16	10.60	2.07

3/11/2019 12:53	10.12	1.80	10.18	1.83	10.06	1.77
3/11/2019 13:53	9.92	1.69	9.97	1.72	9.87	1.67
3/11/2019 14:53	10.39	1.95	10.41	1.96	10.37	1.94
3/11/2019 15:53	9.44	1.46	9.50	1.49	9.38	1.43
3/11/2019 16:53	10.17	1.82	10.25	1.87	10.08	1.78
3/11/2019 17:53	7.65	0.78	7.48	0.73	7.81	0.83
3/11/2019 18:53	8.71	1.15	8.69	1.14	8.72	1.15
3/11/2019 19:53	9.37	1.43	9.14	1.33	9.60	1.54
3/11/2019 20:53	9.70	1.59	9.73	1.60	9.68	1.57
3/11/2019 21:53	10.15	1.82	10.08	1.78	10.22	1.85
3/11/2019 22:53	10.15	1.82	9.91	1.69	10.40	1.95
3/11/2019 23:53	9.88	1.67	9.81	1.64	9.94	1.71
3/12/2019 0:53	8.16	0.94	8.01	0.89	8.30	0.99
3/12/2019 1:53	7.25	0.66	7.20	0.65	7.29	0.67
3/12/2019 2:53	7.15	0.63	7.17	0.64	7.12	0.63
3/12/2019 3:53	6.55	0.49	6.52	0.48	6.59	0.50
3/12/2019 4:53	5.69	0.32	5.69	0.32	5.70	0.32
3/12/2019 5:53	5.59	0.30	5.66	0.32	5.51	0.29
3/12/2019 6:53	4.46	0.15	4.68	0.18	4.25	0.13
3/12/2019 7:53	5.61	0.31	5.93	0.36	5.30	0.26
3/12/2019 8:53	5.15	0.24	5.34	0.26	4.97	0.21
3/12/2019 9:53	4.87	0.20	5.09	0.23	4.65	0.17
3/12/2019 10:53	4.30	0.14	4.50	0.16	4.10	0.12
3/12/2019 11:53	5.49	0.29	5.53	0.29	5.45	0.28
3/12/2019 12:53	8.92	1.23	8.88	1.22	8.96	1.25
3/12/2019 13:53	10.45	1.98	10.09	1.78	10.82	2.20
3/12/2019 14:53	10.07	1.77	10.08	1.78	10.07	1.77
3/12/2019 15:53	10.86	2.22	10.91	2.26	10.81	2.19
3/12/2019 16:53	13.65	3.00	13.61	3.00	13.69	3.00
3/12/2019 17:53	15.40	3.00	15.39	3.00	15.41	3.00
3/12/2019 18:53	15.07	3.00	15.13	3.00	15.02	3.00
3/12/2019 19:53	16.16	3.00	16.18	3.00	16.14	3.00
3/12/2019 20:53	15.34	3.00	15.32	3.00	15.36	3.00
3/12/2019 21:53	12.36	3.00	11.90	2.93	12.81	3.00
3/12/2019 22:53	14.95	3.00	14.44	3.00	15.45	3.00
3/12/2019 23:53	13.70	3.00	13.09	3.00	14.30	3.00
3/13/2019 0:53	12.34	3.00	11.66	2.75	13.02	3.00
3/13/2019 1:53	14.07	3.00	13.12	3.00	15.02	3.00
3/13/2019 2:53	12.85	3.00	12.05	3.00	13.65	3.00
3/13/2019 3:53	15.57	3.00	14.31	3.00	16.84	3.00
3/13/2019 4:53	15.54	3.00	14.70	3.00	16.37	3.00
3/13/2019 5:53	16.58	3.00	16.51	3.00	16.64	3.00
3/13/2019 6:53	14.74	3.00	14.37	3.00	15.11	3.00

3/13/2019 7:53	12.83	3.00	12.94	3.00	12.72	3.00
3/13/2019 8:53	11.47	2.62	11.60	2.71	11.35	2.54
3/13/2019 9:53	9.83	1.65	10.09	1.78	9.57	1.52
3/13/2019 10:53	6.86	0.56	6.23	0.42	7.48	0.73
3/13/2019 11:53	7.66	0.78	7.71	0.80	7.61	0.76
3/13/2019 12:53	4.86	0.20	4.70	0.18	5.03	0.22
3/13/2019 13:53	5.13	0.23	5.31	0.26	4.95	0.21
3/13/2019 14:53	4.75	0.19	4.79	0.19	4.71	0.18
3/13/2019 15:53	5.47	0.28	5.60	0.30	5.34	0.26
3/13/2019 16:53	7.43	0.71	7.60	0.76	7.26	0.66
3/13/2019 17:53	9.55	1.51	9.30	1.40	9.80	1.63
3/13/2019 18:53	10.72	2.14	10.61	2.07	10.83	2.21
3/13/2019 19:53	12.44	3.00	12.50	3.00	12.39	3.00
3/13/2019 20:53	10.35	1.92	10.55	2.04	10.14	1.81
3/13/2019 21:53	6.95	0.58	7.23	0.66	6.67	0.51
3/13/2019 22:53	6.14	0.40	6.29	0.43	5.98	0.37
3/13/2019 23:53	7.27	0.67	7.61	0.76	6.92	0.58
3/14/2019 0:53	7.21	0.65	7.34	0.69	7.08	0.62
3/14/2019 1:53	9.93	1.70	10.30	1.90	9.57	1.52
3/14/2019 2:53	8.24	0.97	8.41	1.03	8.07	0.91
3/14/2019 3:53	7.87	0.85	7.93	0.87	7.81	0.83
3/14/2019 4:53	7.22	0.65	7.19	0.64	7.26	0.67
3/14/2019 5:53	5.93	0.36	5.87	0.35	5.98	0.37
3/14/2019 6:53	8.89	1.22	8.83	1.20	8.95	1.24
3/14/2019 7:53	6.66	0.51	6.35	0.44	6.98	0.59
3/14/2019 8:53	4.52	0.16	4.24	0.13	4.80	0.19
3/14/2019 9:53	6.15	0.40	6.07	0.39	6.23	0.42
3/14/2019 10:53	6.94	0.58	6.89	0.57	7.00	0.59
3/14/2019 11:53	7.49	0.73	7.64	0.77	7.34	0.69
3/14/2019 12:53	10.14	1.81	10.21	1.85	10.07	1.77
3/14/2019 13:53	12.35	3.00	12.53	3.00	12.16	3.00
3/14/2019 14:53	13.16	3.00	13.32	3.00	13.00	3.00
3/14/2019 15:53	11.44	2.60	11.57	2.69	11.30	2.51
3/14/2019 16:53	13.63	3.00	13.53	3.00	13.73	3.00
3/14/2019 17:53	11.16	2.42	11.14	2.40	11.18	2.43
3/14/2019 18:53	11.50	2.64	11.31	2.51	11.69	2.77
3/14/2019 19:53	9.81	1.64	9.71	1.59	9.90	1.69
3/14/2019 20:53	10.56	2.04	10.56	2.04	10.55	2.04
3/14/2019 21:53	11.53	2.66	11.32	2.52	11.74	2.81
3/14/2019 22:53	8.70	1.14	8.61	1.11	8.80	1.18
3/14/2019 23:53	7.49	0.73	7.62	0.77	7.37	0.69
3/15/2019 0:53	9.18	1.34	9.05	1.28	9.31	1.40
3/15/2019 1:53	7.42	0.71	7.19	0.64	7.65	0.78

3/15/2019 2:53	8.97	1.25	8.82	1.19	9.12	1.32
3/15/2019 3:53	10.79	2.18	10.50	2.01	11.08	2.36
3/15/2019 4:53	13.43	3.00	13.17	3.00	13.70	3.00
3/15/2019 5:53	14.74	3.00	13.99	3.00	15.49	3.00
3/15/2019 6:53	13.42	3.00	13.16	3.00	13.67	3.00
3/15/2019 7:53	13.19	3.00	13.11	3.00	13.28	3.00
3/15/2019 8:53	15.15	3.00	15.12	3.00	15.17	3.00
3/15/2019 9:53	16.02	3.00	16.11	3.00	15.93	3.00
3/15/2019 10:53	18.64	3.00	18.70	3.00	18.57	3.00
3/15/2019 11:53	17.96	3.00	18.51	3.00	17.41	3.00
3/15/2019 12:53	17.11	3.00	17.07	3.00	17.15	3.00
3/15/2019 13:53	16.26	3.00	16.04	3.00	16.48	3.00
3/15/2019 14:53	15.36	3.00	15.43	3.00	15.29	3.00
3/15/2019 15:53	15.84	3.00	15.49	3.00	16.18	3.00
3/15/2019 16:53	12.86	3.00	12.48	3.00	13.24	3.00
3/15/2019 17:53	11.64	2.74	11.59	2.71	11.69	2.78
3/15/2019 18:53	10.66	2.10	10.55	2.04	10.77	2.17
3/15/2019 19:53	12.08	3.00	12.12	3.00	12.03	3.00
3/15/2019 20:53	9.89	1.68	9.90	1.68	9.88	1.68
3/15/2019 21:53	7.68	0.79	7.89	0.85	7.47	0.72
3/15/2019 22:53	6.16	0.40	6.20	0.41	6.11	0.40
3/15/2019 23:53	7.09	0.62	7.23	0.66	6.95	0.58
3/16/2019 0:53	6.62	0.50	6.79	0.54	6.46	0.47
3/16/2019 1:53	7.02	0.60	7.22	0.65	6.82	0.55
3/16/2019 2:53	6.58	0.49	6.69	0.52	6.47	0.47
3/16/2019 3:53	5.13	0.23	5.19	0.24	5.06	0.23
3/16/2019 4:53	5.66	0.31	5.76	0.33	5.56	0.30
3/16/2019 5:53	7.22	0.65	7.64	0.77	6.80	0.55
3/16/2019 6:53	6.11	0.40	6.30	0.43	5.92	0.36
3/16/2019 7:53	7.55	0.75	7.86	0.84	7.25	0.66
3/16/2019 8:53	9.00	1.27	9.21	1.35	8.80	1.18
3/16/2019 9:53	9.06	1.29	9.21	1.36	8.92	1.23
3/16/2019 10:53	10.15	1.81	10.33	1.91	9.97	1.72
3/16/2019 11:53	9.45	1.47	9.62	1.54	9.29	1.39
3/16/2019 12:53	10.31	1.90	10.40	1.95	10.23	1.86
3/16/2019 13:53	8.47	1.05	8.55	1.08	8.38	1.02
3/16/2019 14:53	7.88	0.85	7.89	0.85	7.87	0.85
3/16/2019 15:53	8.85	1.20	8.90	1.22	8.81	1.19
3/16/2019 16:53	6.35	0.45	6.44	0.46	6.27	0.43
3/16/2019 17:53	7.01	0.60	7.18	0.64	6.84	0.55
3/16/2019 18:53	6.38	0.45	6.29	0.43	6.47	0.47
3/16/2019 19:53	4.95	0.21	4.81	0.19	5.10	0.23
3/16/2019 20:53	4.63	0.17	4.47	0.16	4.80	0.19

3/16/2019 21:53	4.03	0.11	3.95	0.11	4.12	0.12
3/16/2019 22:53	4.57	0.17	4.62	0.17	4.52	0.16
3/16/2019 23:53	4.85	0.20	4.82	0.19	4.88	0.20
3/17/2019 0:53	4.77	0.19	4.76	0.19	4.77	0.19
3/17/2019 1:53	4.68	0.18	4.67	0.18	4.68	0.18
3/17/2019 2:53	4.73	0.18	4.66	0.18	4.80	0.19
3/17/2019 3:53	3.46	0.07	3.55	0.08	3.37	0.07
3/17/2019 4:53	2.23	0.00	2.39	0.00	2.06	0.00
3/17/2019 5:53	1.98	0.00	2.12	0.00	1.84	0.00
3/17/2019 6:53	2.02	0.00	2.16	0.00	1.87	0.00
3/17/2019 7:53	2.98	0.00	3.09	0.05	2.86	0.00
3/17/2019 8:53	2.21	0.00	2.43	0.00	1.99	0.00
3/17/2019 9:53	3.01	0.05	3.15	0.05	2.87	0.00
3/17/2019 10:53	4.92	0.21	4.94	0.21	4.89	0.20
3/17/2019 11:53	7.07	0.61	6.84	0.56	7.31	0.68
3/17/2019 12:53	5.57	0.30	5.41	0.27	5.73	0.33
3/17/2019 13:53	4.66	0.18	4.59	0.17	4.73	0.18
3/17/2019 14:53	5.36	0.27	5.26	0.25	5.46	0.28
3/17/2019 15:53	4.45	0.15	4.51	0.16	4.39	0.15
3/17/2019 16:53	3.46	0.07	3.66	0.08	3.27	0.06
3/17/2019 17:53	2.23	0.00	2.51	0.00	1.95	0.00
3/17/2019 18:53	4.46	0.15	4.62	0.17	4.30	0.14
3/17/2019 19:53	4.27	0.14	4.31	0.14	4.23	0.13
3/17/2019 20:53	3.18	0.06	3.29	0.06	3.07	0.05
3/17/2019 21:53	3.02	0.05	2.98	0.00	3.05	0.05
3/17/2019 22:53	2.14	0.00	2.08	0.00	2.21	0.00
3/17/2019 23:53	2.84	0.00	2.73	0.00	2.95	0.00
3/18/2019 0:53	1.93	0.00	1.76	0.00	2.11	0.00
3/18/2019 1:53	1.55	0.00	1.25	0.00	1.85	0.00
3/18/2019 2:53	1.49	0.00	1.04	0.00	1.93	0.00
3/18/2019 3:53	2.46	0.00	2.00	0.00	2.93	0.00
3/18/2019 4:53	2.73	0.00	2.39	0.00	3.06	0.05
3/18/2019 5:53	1.88	0.00	1.68	0.00	2.08	0.00
3/18/2019 6:53	1.77	0.00	1.54	0.00	2.00	0.00
3/18/2019 7:53	1.91	0.00	1.80	0.00	2.03	0.00
3/18/2019 8:53	2.11	0.00	2.27	0.00	1.96	0.00
3/18/2019 9:53	2.16	0.00	2.38	0.00	1.94	0.00
3/18/2019 10:53	2.19	0.00	2.44	0.00	1.94	0.00
3/18/2019 11:53	3.98	0.11	4.02	0.11	3.94	0.11
3/18/2019 12:53	5.07	0.23	4.87	0.20	5.27	0.25
3/18/2019 13:53	7.34	0.69	7.08	0.62	7.60	0.76
3/18/2019 14:53	8.24	0.97	7.84	0.84	8.64	1.12
3/18/2019 15:53	6.27	0.43	6.04	0.38	6.51	0.48

3/18/2019 16:53	6.34	0.44	6.32	0.44	6.37	0.45
3/18/2019 17:53	8.41	1.03	8.16	0.94	8.67	1.13
3/18/2019 18:53	9.90	1.69	9.32	1.40	10.49	2.00
3/18/2019 19:53	9.20	1.35	8.68	1.13	9.73	1.60
3/18/2019 20:53	7.00	0.60	6.52	0.48	7.48	0.73
3/18/2019 21:53	4.72	0.18	4.32	0.14	5.12	0.23
3/18/2019 22:53	3.87	0.10	3.35	0.07	4.39	0.15
3/18/2019 23:53	1.93	0.00	1.80	0.00	2.06	0.00
3/19/2019 0:53	1.51	0.00	1.32	0.00	1.70	0.00
3/19/2019 1:53	2.51	0.00	2.07	0.00	2.95	0.00
3/19/2019 2:53	1.65	0.00	1.42	0.00	1.89	0.00
3/19/2019 3:53	1.44	0.00	1.21	0.00	1.66	0.00
3/19/2019 4:53	1.46	0.00	1.13	0.00	1.79	0.00
3/19/2019 5:53	1.40	0.00	1.00	0.00	1.80	0.00
3/19/2019 6:53	2.28	0.00	1.69	0.00	2.86	0.00
3/19/2019 7:53	1.58	0.00	1.15	0.00	2.00	0.00
3/19/2019 8:53	1.52	0.00	1.06	0.00	1.97	0.00
3/19/2019 9:53	1.70	0.00	1.39	0.00	2.01	0.00
3/19/2019 10:53	1.83	0.00	1.66	0.00	2.01	0.00
3/19/2019 11:53	1.92	0.00	1.85	0.00	1.99	0.00
3/19/2019 12:53	1.99	0.00	1.97	0.00	2.01	0.00
3/19/2019 13:53	8.86	1.21	9.11	1.31	8.61	1.11
3/19/2019 14:53	11.82	2.87	11.68	2.77	11.97	2.97
3/19/2019 15:53	10.24	1.86	9.94	1.70	10.54	2.03
3/19/2019 16:53	10.59	2.06	10.51	2.02	10.68	2.11
3/19/2019 17:53	9.67	1.57	9.56	1.52	9.77	1.62
3/19/2019 18:53	9.73	1.60	9.63	1.55	9.82	1.65
3/19/2019 19:53	9.48	1.48	9.37	1.43	9.59	1.53
3/19/2019 20:53	6.33	0.44	5.90	0.36	6.75	0.53
3/19/2019 21:53	4.91	0.21	4.40	0.15	5.41	0.28
3/19/2019 22:53	3.32	0.06	3.17	0.06	3.48	0.07
3/19/2019 23:53	3.71	0.09	3.60	0.08	3.82	0.10
3/20/2019 0:53	4.07	0.12	3.78	0.09	4.36	0.14
3/20/2019 1:53	2.32	0.00	2.24	0.00	2.39	0.00
3/20/2019 2:53	1.62	0.00	1.60	0.00	1.63	0.00
3/20/2019 3:53	1.61	0.00	1.39	0.00	1.83	0.00
3/20/2019 4:53	1.51	0.00	1.32	0.00	1.71	0.00
3/20/2019 5:53	1.38	0.00	1.06	0.00	1.71	0.00
3/20/2019 6:53	1.36	0.00	0.96	0.00	1.76	0.00
3/20/2019 7:53	1.38	0.00	0.96	0.00	1.80	0.00
3/20/2019 8:53	2.40	0.00	1.93	0.00	2.86	0.00
3/20/2019 9:53	1.74	0.00	1.48	0.00	2.01	0.00
3/20/2019 10:53	2.81	0.00	2.58	0.00	3.04	0.05

3/20/2019 11:53	2.21	0.00	2.27	0.00	2.15	0.00
3/20/2019 12:53	4.74	0.19	4.72	0.18	4.76	0.19
3/20/2019 13:53	2.74	0.00	3.05	0.05	2.44	0.00
3/20/2019 14:53	5.30	0.26	5.24	0.25	5.35	0.27
3/20/2019 15:53	3.90	0.10	4.07	0.12	3.73	0.09
3/20/2019 16:53	3.47	0.07	3.68	0.09	3.27	0.06
3/20/2019 17:53	2.45	0.00	2.82	0.00	2.07	0.00
3/20/2019 18:53	6.72	0.53	6.60	0.50	6.83	0.55
3/20/2019 19:53	8.45	1.05	7.49	0.73	9.41	1.45
3/20/2019 20:53	9.12	1.31	7.82	0.83	10.41	1.96
3/20/2019 21:53	9.68	1.57	8.87	1.21	10.49	2.00
3/20/2019 22:53	6.16	0.40	5.29	0.26	7.02	0.60
3/20/2019 23:53	3.78	0.09	3.17	0.06	4.39	0.15
3/21/2019 0:53	6.48	0.47	6.03	0.38	6.93	0.58
3/21/2019 1:53	6.58	0.49	6.12	0.40	7.03	0.60
3/21/2019 2:53	5.28	0.26	4.92	0.21	5.64	0.31
3/21/2019 3:53	3.40	0.07	3.19	0.06	3.61	0.08
3/21/2019 4:53	4.07	0.12	3.67	0.09	4.47	0.16
3/21/2019 5:53	5.16	0.24	4.51	0.16	5.81	0.34
3/21/2019 6:53	4.19	0.13	3.88	0.10	4.51	0.16
3/21/2019 7:53	2.13	0.00	1.97	0.00	2.29	0.00
3/21/2019 8:53	2.58	0.00	2.33	0.00	2.82	0.00
3/21/2019 9:53	4.30	0.14	4.04	0.11	4.56	0.16
3/21/2019 10:53	4.13	0.12	4.06	0.12	4.19	0.13
3/21/2019 11:53	3.07	0.05	3.11	0.05	3.03	0.05
3/21/2019 12:53	3.86	0.10	3.87	0.10	3.85	0.10
3/21/2019 13:53	2.36	0.00	2.24	0.00	2.47	0.00
3/21/2019 14:53	5.08	0.23	5.09	0.23	5.08	0.23
3/21/2019 15:53	4.47	0.15	4.47	0.15	4.47	0.15
3/21/2019 16:53	4.18	0.13	4.28	0.14	4.07	0.12
3/21/2019 17:53	5.91	0.36	5.72	0.33	6.10	0.39
3/21/2019 18:53	3.96	0.11	4.07	0.12	3.86	0.10
3/21/2019 19:53	6.54	0.49	6.29	0.43	6.80	0.54
3/21/2019 20:53	5.75	0.33	5.41	0.28	6.08	0.39
3/21/2019 21:53	3.68	0.09	3.57	0.08	3.79	0.09
3/21/2019 22:53	2.41	0.00	2.64	0.00	2.17	0.00
3/21/2019 23:53	2.00	0.00	2.15	0.00	1.85	0.00
3/22/2019 0:53	1.86	0.00	1.97	0.00	1.75	0.00
3/22/2019 1:53	1.70	0.00	1.78	0.00	1.62	0.00
3/22/2019 2:53	1.72	0.00	1.80	0.00	1.63	0.00
3/22/2019 3:53	1.69	0.00	1.68	0.00	1.71	0.00
3/22/2019 4:53	2.62	0.00	2.46	0.00	2.78	0.00
3/22/2019 5:53	1.63	0.00	1.34	0.00	1.93	0.00

3/22/2019 6:53	1.52	0.00	1.13	0.00	1.91	0.00
3/22/2019 7:53	1.90	0.00	1.81	0.00	2.00	0.00
3/22/2019 8:53	1.81	0.00	1.62	0.00	1.99	0.00
3/22/2019 9:53	1.75	0.00	1.51	0.00	2.00	0.00
3/22/2019 10:53	1.90	0.00	1.77	0.00	2.02	0.00
3/22/2019 11:53	1.99	0.00	1.96	0.00	2.02	0.00
3/22/2019 12:53	4.15	0.12	4.19	0.13	4.10	0.12
3/22/2019 13:53	9.16	1.33	8.77	1.17	9.55	1.51
3/22/2019 14:53	9.65	1.56	8.88	1.21	10.43	1.97
3/22/2019 15:53	7.71	0.79	7.24	0.66	8.17	0.95
3/22/2019 16:53	9.12	1.32	8.90	1.22	9.35	1.42
3/22/2019 17:53	9.80	1.63	9.70	1.58	9.90	1.69
3/22/2019 18:53	9.54	1.51	9.48	1.48	9.60	1.54
3/22/2019 19:53	8.36	1.01	7.68	0.79	9.04	1.28
3/22/2019 20:53	7.25	0.66	6.68	0.52	7.81	0.83
3/22/2019 21:53	6.79	0.54	6.22	0.42	7.36	0.69
3/22/2019 22:53	9.24	1.37	8.70	1.14	9.78	1.62
3/22/2019 23:53	9.77	1.62	9.18	1.34	10.36	1.93
3/23/2019 0:53	9.45	1.47	9.03	1.28	9.88	1.67
3/23/2019 1:53	8.89	1.22	8.66	1.13	9.11	1.31
3/23/2019 2:53	7.84	0.84	7.59	0.76	8.09	0.92
3/23/2019 3:53	7.11	0.63	6.95	0.58	7.28	0.67
3/23/2019 4:53	6.47	0.47	6.36	0.45	6.59	0.50
3/23/2019 5:53	4.08	0.12	4.11	0.12	4.04	0.11
3/23/2019 6:53	4.60	0.17	4.34	0.14	4.86	0.20
3/23/2019 7:53	3.39	0.07	3.17	0.06	3.60	0.08
3/23/2019 8:53	4.12	0.12	3.95	0.11	4.28	0.14
3/23/2019 9:53	3.21	0.06	2.96	0.00	3.45	0.07
3/23/2019 10:53	3.83	0.10	3.89	0.10	3.78	0.09
3/23/2019 11:53	7.50	0.73	7.65	0.78	7.36	0.69
3/23/2019 12:53	9.69	1.58	9.61	1.54	9.76	1.61
3/23/2019 13:53	11.82	2.86	11.69	2.77	11.95	2.96
3/23/2019 14:53	10.50	2.01	10.63	2.08	10.38	1.94
3/23/2019 15:53	8.49	1.06	8.51	1.07	8.48	1.06
3/23/2019 16:53	9.05	1.29	9.01	1.27	9.10	1.31
3/23/2019 17:53	7.54	0.74	7.59	0.76	7.49	0.73
3/23/2019 18:53	9.21	1.36	9.27	1.38	9.15	1.33
3/23/2019 19:53	9.13	1.32	9.17	1.34	9.08	1.30
3/23/2019 20:53	6.43	0.46	6.67	0.52	6.20	0.41
3/23/2019 21:53	6.51	0.48	6.67	0.51	6.34	0.44
3/23/2019 22:53	5.27	0.25	5.37	0.27	5.18	0.24
3/23/2019 23:53	9.62	1.54	9.60	1.54	9.63	1.55
3/24/2019 0:53	9.71	1.59	9.30	1.40	10.12	1.80

3/24/2019 1:53	7.84	0.84	7.49	0.73	8.19	0.95
3/24/2019 2:53	6.25	0.42	6.03	0.38	6.46	0.47
3/24/2019 3:53	6.06	0.39	5.67	0.32	6.45	0.47
3/24/2019 4:53	5.00	0.22	4.76	0.19	5.25	0.25
3/24/2019 5:53	4.99	0.22	4.56	0.16	5.43	0.28
3/24/2019 6:56	4.64	0.17	4.40	0.15	4.89	0.20
3/24/2019 7:53	6.14	0.40	6.16	0.41	6.11	0.40
3/24/2019 8:53	5.81	0.34	5.99	0.37	5.62	0.31
3/24/2019 9:53	5.81	0.34	6.01	0.38	5.61	0.31
3/24/2019 10:53	8.69	1.14	8.93	1.23	8.45	1.05
3/24/2019 11:53	8.19	0.95	8.35	1.01	8.03	0.90
3/24/2019 12:53	9.74	1.61	9.72	1.59	9.77	1.62
3/24/2019 13:53	8.22	0.97	8.26	0.98	8.18	0.95
3/24/2019 14:53	7.84	0.84	7.86	0.84	7.81	0.83
3/24/2019 15:53	7.79	0.82	7.78	0.82	7.79	0.82
3/24/2019 16:53	6.68	0.52	6.72	0.53	6.65	0.51
3/24/2019 17:53	9.09	1.31	9.10	1.31	9.09	1.30
3/24/2019 18:53	7.40	0.70	7.29	0.67	7.52	0.74
3/24/2019 19:53	6.38	0.45	6.18	0.41	6.57	0.49
3/24/2019 20:53	6.85	0.56	6.78	0.54	6.92	0.57
3/24/2019 21:53	6.68	0.52	6.80	0.54	6.57	0.49
3/24/2019 22:53	5.69	0.32	5.72	0.33	5.65	0.31
3/24/2019 23:53	7.32	0.68	7.28	0.67	7.36	0.69
3/25/2019 0:53	7.05	0.61	6.80	0.55	7.29	0.67
3/25/2019 1:53	5.16	0.24	5.10	0.23	5.22	0.25
3/25/2019 2:53	7.25	0.66	7.25	0.66	7.25	0.66
3/25/2019 3:53	5.94	0.36	5.85	0.35	6.03	0.38
3/25/2019 4:53	8.31	1.00	8.37	1.02	8.25	0.97
3/25/2019 5:53	7.26	0.66	7.24	0.66	7.28	0.67
3/25/2019 6:53	6.32	0.44	6.19	0.41	6.44	0.46
3/25/2019 7:53	8.48	1.06	8.50	1.06	8.47	1.06
3/25/2019 8:53	7.46	0.72	7.52	0.74	7.40	0.70
3/25/2019 9:53	4.59	0.17	4.43	0.15	4.75	0.19
3/25/2019 10:53	2.70	0.00	3.03	0.05	2.36	0.00
3/25/2019 11:53	3.11	0.05	3.28	0.06	2.93	0.00
3/25/2019 12:53	3.31	0.06	3.55	0.08	3.07	0.05
3/25/2019 13:53	4.49	0.16	4.72	0.18	4.27	0.13
3/25/2019 14:53	8.30	0.99	8.45	1.05	8.15	0.94
3/25/2019 15:53	8.20	0.96	8.00	0.89	8.40	1.03
3/25/2019 16:53	8.89	1.22	8.77	1.17	9.00	1.27
3/25/2019 17:53	12.15	3.00	12.26	3.00	12.05	3.00
3/25/2019 18:53	12.17	3.00	12.27	3.00	12.07	3.00
3/25/2019 19:53	11.55	2.68	11.54	2.67	11.57	2.69

3/25/2019 20:53	10.74	2.15	10.68	2.12	10.80	2.19
3/25/2019 21:53	10.44	1.98	10.47	1.99	10.42	1.96
3/25/2019 22:53	8.43	1.04	8.36	1.02	8.51	1.07
3/25/2019 23:53	6.67	0.52	6.74	0.53	6.61	0.50
3/26/2019 0:53	6.58	0.49	6.65	0.51	6.51	0.48
3/26/2019 1:53	7.09	0.62	7.15	0.63	7.03	0.60
3/26/2019 2:53	8.47	1.06	8.39	1.03	8.55	1.09
3/26/2019 3:53	9.55	1.51	9.20	1.35	9.89	1.68
3/26/2019 4:53	7.27	0.67	6.97	0.59	7.57	0.75
3/26/2019 5:53	4.97	0.21	4.85	0.20	5.09	0.23
3/26/2019 6:53	4.08	0.12	3.88	0.10	4.29	0.14
3/26/2019 7:53	1.92	0.00	1.80	0.00	2.05	0.00
3/26/2019 8:53	4.17	0.13	4.13	0.12	4.21	0.13
3/26/2019 9:53	4.84	0.20	4.64	0.17	5.04	0.22
3/26/2019 10:53	8.86	1.21	9.16	1.34	8.56	1.09
3/26/2019 11:53	9.28	1.39	9.30	1.40	9.26	1.38
3/26/2019 12:53	7.56	0.75	7.63	0.77	7.50	0.73
3/26/2019 13:53	6.05	0.38	6.11	0.40	6.00	0.37
3/26/2019 14:53	5.16	0.24	5.26	0.25	5.07	0.23
3/26/2019 15:53	3.02	0.05	3.42	0.07	2.62	0.00
3/26/2019 16:53	7.00	0.60	7.45	0.72	6.55	0.49
3/26/2019 17:53	5.11	0.23	5.08	0.23	5.15	0.24
3/26/2019 18:53	6.47	0.47	6.39	0.45	6.55	0.49
3/26/2019 19:53	8.49	1.06	8.53	1.08	8.45	1.05
3/26/2019 20:53	7.93	0.86	7.94	0.87	7.92	0.86
3/26/2019 21:53	6.63	0.51	6.75	0.53	6.52	0.48
3/26/2019 22:53	5.75	0.33	5.83	0.34	5.68	0.32
3/26/2019 23:53	3.13	0.05	3.36	0.07	2.89	0.00
3/27/2019 0:53	2.17	0.00	2.55	0.00	1.78	0.00
3/27/2019 1:53	2.17	0.00	2.36	0.00	1.97	0.00
3/27/2019 2:53	1.86	0.00	2.08	0.00	1.63	0.00
3/27/2019 3:53	1.75	0.00	1.93	0.00	1.56	0.00
3/27/2019 4:53	1.62	0.00	1.62	0.00	1.62	0.00
3/27/2019 5:53	1.69	0.00	1.68	0.00	1.71	0.00
3/27/2019 6:53	1.82	0.00	1.89	0.00	1.75	0.00
3/27/2019 7:53	1.78	0.00	1.73	0.00	1.83	0.00
3/27/2019 8:53	2.15	0.00	2.39	0.00	1.90	0.00
3/27/2019 9:53	2.09	0.00	2.22	0.00	1.95	0.00
3/27/2019 10:53	2.05	0.00	2.12	0.00	1.99	0.00
3/27/2019 11:53	4.14	0.12	4.11	0.12	4.17	0.13
3/27/2019 12:53	7.72	0.80	7.43	0.71	8.00	0.89
3/27/2019 13:53	9.70	1.58	9.27	1.38	10.13	1.81
3/27/2019 14:53	8.60	1.10	8.08	0.92	9.12	1.32

3/27/2019 15:53	6.96	0.58	6.78	0.54	7.13	0.63
3/27/2019 16:53	9.64	1.56	9.56	1.52	9.72	1.59
3/27/2019 17:53	10.82	2.20	10.83	2.20	10.80	2.19
3/27/2019 18:53	9.47	1.47	9.62	1.55	9.32	1.40
3/27/2019 19:53	10.91	2.25	10.92	2.26	10.89	2.24
3/27/2019 20:53	9.54	1.51	8.81	1.19	10.26	1.88
3/27/2019 21:53	6.50	0.48	5.76	0.33	7.25	0.66
3/27/2019 22:53	6.79	0.54	6.50	0.48	7.08	0.62
3/27/2019 23:53	8.39	1.02	8.10	0.92	8.67	1.13
3/28/2019 0:53	7.64	0.77	7.35	0.69	7.93	0.87
3/28/2019 1:53	7.33	0.68	7.11	0.62	7.55	0.75
3/28/2019 2:53	6.84	0.56	6.59	0.50	7.09	0.62
3/28/2019 3:53	5.69	0.32	5.39	0.27	5.98	0.37
3/28/2019 4:53	5.27	0.25	5.04	0.22	5.50	0.29
3/28/2019 5:53	3.45	0.07	3.37	0.07	3.54	0.08
3/28/2019 6:53	1.95	0.00	1.92	0.00	1.97	0.00
3/28/2019 7:53	1.67	0.00	1.51	0.00	1.84	0.00
3/28/2019 8:53	1.67	0.00	1.60	0.00	1.74	0.00
3/28/2019 9:53	1.72	0.00	1.79	0.00	1.65	0.00
3/28/2019 10:53	2.87	0.00	2.98	0.00	2.76	0.00
3/28/2019 11:53	5.64	0.31	5.80	0.34	5.47	0.28
3/28/2019 12:53	10.73	2.14	10.31	1.90	11.15	2.41
3/28/2019 13:53	13.38	3.00	12.80	3.00	13.96	3.00
3/28/2019 14:53	13.39	3.00	13.47	3.00	13.30	3.00
3/28/2019 15:53	14.50	3.00	14.54	3.00	14.46	3.00
3/28/2019 16:53	13.03	3.00	12.99	3.00	13.06	3.00
3/28/2019 17:53	12.30	3.00	12.30	3.00	12.30	3.00
3/28/2019 18:53	11.90	2.93	11.98	2.99	11.82	2.87
3/28/2019 19:53	12.11	3.00	12.26	3.00	11.95	2.97
3/28/2019 20:53	12.48	3.00	12.31	3.00	12.65	3.00
3/28/2019 21:53	12.46	3.00	12.34	3.00	12.59	3.00
3/28/2019 22:53	8.43	1.04	7.70	0.79	9.16	1.34
3/28/2019 23:53	9.42	1.45	9.41	1.44	9.43	1.46
3/29/2019 0:53	9.33	1.41	9.01	1.27	9.66	1.56
3/29/2019 1:53	9.26	1.38	8.45	1.05	10.06	1.77
3/29/2019 2:53	8.39	1.02	8.10	0.92	8.68	1.14
3/29/2019 3:53	9.04	1.28	8.77	1.17	9.31	1.40
3/29/2019 4:53	10.35	1.93	10.31	1.90	10.40	1.95
3/29/2019 5:53	7.07	0.61	7.11	0.62	7.04	0.60
3/29/2019 6:53	6.63	0.51	6.54	0.49	6.71	0.53
3/29/2019 7:53	6.41	0.46	6.38	0.45	6.44	0.46
3/29/2019 8:53	5.14	0.24	5.03	0.22	5.25	0.25
3/29/2019 9:53	8.51	1.07	8.81	1.19	8.22	0.96

3/29/2019 10:53	8.12	0.93	8.38	1.02	7.86	0.84
3/29/2019 11:53	9.94	1.70	10.19	1.84	9.69	1.58
3/29/2019 12:53	10.47	1.99	10.73	2.14	10.20	1.84
3/29/2019 13:53	12.09	3.00	12.31	3.00	11.87	2.90
3/29/2019 14:53	11.57	2.69	11.68	2.76	11.46	2.61
3/29/2019 15:53	12.36	3.00	12.46	3.00	12.27	3.00
3/29/2019 16:53	12.17	3.00	12.19	3.00	12.14	3.00
3/29/2019 17:53	11.50	2.64	11.61	2.72	11.39	2.57
3/29/2019 18:53	11.81	2.86	11.87	2.90	11.75	2.82
3/29/2019 19:53	11.85	2.89	11.91	2.93	11.79	2.85
3/29/2019 20:53	12.67	3.00	12.46	3.00	12.87	3.00
3/29/2019 21:53	11.71	2.79	11.78	2.84	11.65	2.74
3/29/2019 22:53	10.80	2.19	10.84	2.21	10.75	2.16
3/29/2019 23:53	10.03	1.75	10.01	1.74	10.05	1.76
3/30/2019 0:53	8.24	0.97	8.19	0.95	8.29	0.99
3/30/2019 1:53	9.36	1.42	9.37	1.43	9.35	1.42
3/30/2019 2:53	9.03	1.28	8.89	1.22	9.16	1.34
3/30/2019 3:53	9.69	1.58	9.34	1.41	10.05	1.76
3/30/2019 4:53	10.70	2.12	10.53	2.03	10.86	2.22
3/30/2019 5:53	9.98	1.73	9.88	1.68	10.08	1.78
3/30/2019 6:53	9.26	1.38	9.22	1.36	9.30	1.40
3/30/2019 7:53	9.30	1.40	9.40	1.44	9.20	1.35
3/30/2019 8:54	6.57	0.49	6.78	0.54	6.37	0.45
3/30/2019 9:53	5.37	0.27	5.52	0.29	5.21	0.25
3/30/2019 10:53	5.10	0.23	5.34	0.26	4.86	0.20
3/30/2019 11:53	5.01	0.22	5.35	0.27	4.67	0.18
3/30/2019 12:53	5.05	0.22	5.27	0.25	4.84	0.20
3/30/2019 13:53	11.22	2.45	12.27	3.00	10.17	1.82
3/30/2019 14:53	14.28	3.00	14.76	3.00	13.81	3.00
3/30/2019 15:53	16.18	3.00	16.21	3.00	16.15	3.00
3/30/2019 16:53	16.37	3.00	16.78	3.00	15.97	3.00
3/30/2019 17:53	15.88	3.00	16.34	3.00	15.41	3.00
3/30/2019 18:53	18.07	3.00	17.81	3.00	18.33	3.00
3/30/2019 19:53	17.59	3.00	17.71	3.00	17.47	3.00
3/30/2019 20:53	17.20	3.00	17.50	3.00	16.90	3.00
3/30/2019 21:53	14.41	3.00	14.24	3.00	14.58	3.00
3/30/2019 22:53	14.62	3.00	14.53	3.00	14.70	3.00
3/30/2019 23:53	15.91	3.00	15.55	3.00	16.27	3.00
3/31/2019 0:53	16.61	3.00	16.25	3.00	16.97	3.00
3/31/2019 1:53	17.97	3.00	17.58	3.00	18.36	3.00
3/31/2019 2:53	17.13	3.00	16.91	3.00	17.36	3.00
3/31/2019 3:53	16.69	3.00	16.16	3.00	17.23	3.00
3/31/2019 4:53	16.22	3.00	15.60	3.00	16.85	3.00

3/31/2019 5:53	13.59	3.00	13.01	3.00	14.18	3.00
3/31/2019 6:53	13.42	3.00	12.95	3.00	13.89	3.00
3/31/2019 7:53	12.78	3.00	12.83	3.00	12.72	3.00
3/31/2019 8:53	14.29	3.00	14.59	3.00	13.99	3.00
3/31/2019 9:53	13.97	3.00	14.35	3.00	13.59	3.00
3/31/2019 10:53	15.81	3.00	16.31	3.00	15.30	3.00
3/31/2019 11:53	16.03	3.00	16.26	3.00	15.80	3.00
3/31/2019 12:53	13.73	3.00	13.79	3.00	13.67	3.00
3/31/2019 13:53	12.15	3.00	12.26	3.00	12.05	3.00
3/31/2019 14:53	12.14	3.00	12.28	3.00	12.00	3.00
3/31/2019 15:53	12.78	3.00	12.99	3.00	12.57	3.00
3/31/2019 16:53	10.94	2.27	11.30	2.50	10.59	2.06
3/31/2019 17:53	11.05	2.34	11.38	2.56	10.71	2.14
3/31/2019 18:53	12.40	3.00	12.58	3.00	12.23	3.00
3/31/2019 19:53	11.11	2.38	11.33	2.53	10.89	2.24
3/31/2019 20:53	10.88	2.23	11.20	2.44	10.56	2.04
3/31/2019 21:53	8.19	0.95	8.25	0.98	8.13	0.93
3/31/2019 22:53	6.91	0.57	7.00	0.60	6.82	0.55
3/31/2019 23:53	5.02	0.22	5.14	0.24	4.90	0.20

Forecasting model codes

```
# Basic Libraries
import math
import datetime
import numpy as np
import pandas as pd
from time import time
pd.set_option('display.float_format', lambda x: '%.4f' % x)
```

```
#Visualziation
from matplotlib import pyplot as plt
from matplotlib.dates import drange
import matplotlib.ticker as tkr
import seaborn as sns
sns.set_context("paper", font_scale=1.3)
sns.set_style('white')
get_ipython().run_line_magic('matplotlib', 'inline')
```

```
# deep learning libraries
import keras
import tensorflow as tf
from keras.models import Sequential
from keras.layers import Dense
```

```

from keras.layers import LSTM
from keras.layers import Dropout
from keras.layers import *
from keras.layers import SimpleRNN
from sklearn.preprocessing import MinMaxScaler
from sklearn.metrics import mean_squared_error
from sklearn.metrics import mean_absolute_error
from sklearn.metrics import r2_score
from keras.callbacks import EarlyStopping
from scipy import stats
from statsmodels.tsa.stattools import adfuller
from sklearn import preprocessing
from statsmodels.tsa.stattools import pacf

# ignore warnings
import warnings
warnings.filterwarnings("ignore")

### <center><font color="#110896">Load The Dataset</font><center>

# In[3]:

# read the dataset and store in the variable df and see the dataset
df = pd.read_csv('San Marcos wind speed data 2011-2019.csv', parse_dates = ['Date'], index_col
= ['Date'])

# In[4]:

# check the bottom 5 rows of the dataset
df.tail()

# In[5]:

# see the columns
df.columns

# In[6]:

```

```

# dropping the not required columns
df = df.drop(['Temp (F)', 'dew_pt', 'hum (%)', 'Wind Speed (mph)', 'wind_gust ?mph)',
            'pressure', 'precip', 'dir', 'Weather Condition', 'Temp (C)',
            'Date_new', 'Weather State',
            'Codes for weather State'], axis=1)

# In[7]:

# check the information about the dataset
df.info()

# In[8]:

# check the description about the dataset
df.describe()

# # <center><font color="#110896"> Recurrent Neural Network (RNN)

# In[9]:

# making data again to remove inconsistencies
temp = df
dataset = temp['Wind Speed (m/s)'].dropna().values #numpy.ndarray
dataset = dataset.astype('float32')
dataset = np.reshape(dataset, (-1, 1))

###Scaling the data--This helps avoid exploding gradient
scaler = MinMaxScaler(feature_range=(0, 1))
dataset = scaler.fit_transform(dataset)

###Splitting the dataset into training and test part
train_size = 63110          ##data used for training, taking 80% data
test_size = len(dataset) - train_size
train, test = dataset[0:train_size,:], dataset[train_size:len(dataset),:]

#####
###Here 0= start, train size = 0 to train size(63110)
## := step (It is the improvisation/improvement from one step to another)

```

```

##Here X is the time stamp in hrs. and Y is the wind speed in m/s
#####

def create_dataset(dataset, look_back):
    X, Y = [], []
    for i in range(len(dataset)-look_back-1):
        a = dataset[i:(i+look_back), 0]
        X.append(a)
        Y.append(dataset[i + look_back, 0])
    return np.array(X), np.array(Y)

look_back = 24          #it is in hours #can be changed(1-24) to get better prediction values
X_train, Y_train = create_dataset(train, look_back)
X_test, Y_test = create_dataset(test, look_back)

# reshape input to be [samples, time steps, features], RNN models requires 3-dimensional input
data
X_train = np.reshape(X_train, (X_train.shape[0], X_train.shape[1], 1))
X_test = np.reshape(X_test, (X_test.shape[0], X_test.shape[1], 1))
print("Shapes: \nTraining set: {}, Testing set: {}".format(X_train.shape, X_test.shape))
print("Sample from training set: \n{}".format(X_train[0]))

# In[10]:

X_train.shape

# In[11]:

Y_test

# In[12]:

###Building the RNN model with simple RNN

model = Sequential()
model.add(SimpleRNN(units=100, activation="relu", input_shape=(X_train.shape[1],
X_train.shape[2])))
model.add(Dropout(0.2))
model.add(Dense(1))
model.compile(loss='mean_squared_error', optimizer='adam')

```

```

es=EarlyStopping(monitor='val_loss', min_delta=0, patience=10, mode='min')

history = model.fit(X_train, Y_train, epochs=200, batch_size=64, validation_data=(X_test,
Y_test),
                    callbacks=[es],verbose=1, shuffle=False)
model.save('rnn_model.h5')
model.summary()

```

In[13]:

```

plt.figure(figsize=(8,4),dpi=300)
plt.plot(history.history['loss'], label='Training Loss')
plt.plot(history.history['val_loss'], label='Validation Loss')
plt.title('Model loss for RNN - San Marcos')
plt.ylabel('Loss')
plt.xlabel('Epochs')
plt.legend(loc='upper right')
plt.savefig('WindSpeed_RNN_Learning_curve_San_Marcos.png', bbox_inches='tight')
plt.show();

```

In[14]:

```

train_predict_RNN = model.predict(X_train)
test_predict_RNN = model.predict(X_test)
# invert predictions
print(Y_train)
train_predict_RNN = scaler.inverse_transform(train_predict_RNN)
Y_train = scaler.inverse_transform([Y_train])
print(Y_train)
test_predict_RNN = scaler.inverse_transform(test_predict_RNN)
Y_test = scaler.inverse_transform([Y_test])
print('Train Mean Absolute Error:', mean_absolute_error(Y_train[0], train_predict_RNN[:,0]))
print('Train Root Mean Squared Error:',np.sqrt(mean_squared_error(Y_train[0],
train_predict_RNN[:,0])))
print('Test Mean Absolute Error:', mean_absolute_error(Y_test[0], test_predict_RNN[:,0]))
print('Test Root Mean Squared Error:',np.sqrt(mean_squared_error(Y_test[0],
test_predict_RNN[:,0])))

```

 Append the RNN Evalutaion Result

```
# In[15]:
```

```
result = { }
result['RNN']=[np.sqrt(mean_squared_error(Y_test[0], test_predict_RNN[:,0])),
              mean_absolute_error(Y_test[0], test_predict_RNN[:,0]),
              r2_score(Y_test[0], test_predict_RNN[:,0])]
```

```
# In[16]:
```

```
plt.rcParams['font.sans-serif'] = "Times New Roman"
plt.rcParams['font.family'] = "sans-serif"
```

```
plt.figure(figsize=(8,4),dpi=300)
#plt.plot(df['Wind Speed (m/s)'], color="blue", label='History')
plt.plot(Y_test[0], marker='.', label="Actual")
plt.plot(test_predict_RNN[:,0], 'r', label="Prediction")
# plt.tick_params(left=False, labelleft=True) #remove ticks
plt.tight_layout()
sns.despine(top=True)
plt.subplots_adjust(left=0.07)
plt.ylabel("Wind Speed (m/s)", size=15)
plt.xlabel("Time step (hours)", size=15)
plt.legend(fontsize=15)
```

```
plt.savefig('WindSpeed_RNN_Model_San_Marcos.png', bbox_inches='tight')
plt.show();
```

```
# In[17]:
```

```
plt.rcParams['font.sans-serif'] = "Times New Roman"
plt.rcParams['font.family'] = "sans-serif"
```

```
plt.figure(figsize=(8,4),dpi=300)
#plt.plot(df['Wind Speed (m/s)'], color="blue", label='History')
plt.plot(Y_test[0, 15580:], marker='.', label="Actual")
plt.plot(test_predict_RNN[15581:,0], 'r', label="Prediction")
# plt.tick_params(left=False, labelleft=True) #remove ticks
plt.tight_layout()
sns.despine(top=True)
```

```

plt.subplots_adjust(left=0.07)
plt.ylabel("Wind Speed (m/s)", size=15)
plt.xlabel("Time step (hours)", size=15)
plt.legend(fontsize=15)

plt.savefig('WindSpeed_RNN_ZOOM_Model_San_Marcos.png', bbox_inches='tight')
plt.show();

# # <center><font color="#110896"> Long short-term memory (LSTM)
# Long short-term memory is an artificial recurrent neural network architecture used in the field
of deep learning. Unlike standard feedforward neural networks, LSTM has feedback
connections. It can not only process single data points, but also entire sequences of data

# In[18]:

# making data again to remove inconsistencies
temp = df
dataset = temp['Wind Speed (m/s)'].dropna().values #numpy.ndarray
dataset = dataset.astype('float32')
dataset = np.reshape(dataset, (-1, 1))
scaler = MinMaxScaler(feature_range=(0, 1))
dataset = scaler.fit_transform(dataset)
train_size = 63110
test_size = len(dataset) - train_size
train, test = dataset[0:train_size,:], dataset[train_size:len(dataset),:]

def create_dataset(dataset, look_back):
    X, Y = [], []
    for i in range(len(dataset)-look_back-1):
        a = dataset[i:(i+look_back), 0]
        X.append(a)
        Y.append(dataset[i + look_back, 0])
    return np.array(X), np.array(Y)

look_back = 24      #it is in hours #can be changed(1-24) to get better prediction values
X_train, Y_train = create_dataset(train, look_back)
X_test, Y_test = create_dataset(test, look_back)

# reshape input to be [samples, time steps, features],LSTM models requires 3-dimensional input
data
X_train = np.reshape(X_train, (X_train.shape[0], X_train.shape[1], 1))
X_test = np.reshape(X_test, (X_test.shape[0], X_test.shape[1], 1))

```

```
# In[19]:
```

```
##Building the LSTM model
model = Sequential()
model.add(LSTM(units=100, activation="relu", input_shape=(X_train.shape[1],
X_train.shape[2])))
model.add(Dropout(0.2))
model.add(Dense(1))
model.compile(loss='mean_squared_error', optimizer='adam')

es=EarlyStopping(monitor='val_loss', min_delta=0, patience=10, mode='min')

history = model.fit(X_train, Y_train, epochs=200, batch_size=64, validation_data=(X_test,
Y_test),
                    callbacks=[es],verbose=1, shuffle=False)

model.save('lstm_model.h5')
model.summary()
```

```
# In[20]:
```

```
train_predict_LSTM = model.predict(X_train)
test_predict_LSTM = model.predict(X_test)
# invert predictions
train_predict_LSTM = scaler.inverse_transform(train_predict_LSTM)
Y_train = scaler.inverse_transform([Y_train])
test_predict_LSTM = scaler.inverse_transform(test_predict_LSTM)
Y_test = scaler.inverse_transform([Y_test])
print("Train Mean Absolute Error:", mean_absolute_error(Y_train[0], train_predict_LSTM[:,0]))
print("Train Root Mean Squared Error:",np.sqrt(mean_squared_error(Y_train[0],
train_predict_LSTM[:,0])))
print("Test Mean Absolute Error:", mean_absolute_error(Y_test[0], test_predict_LSTM[:,0]))
print("Test Root Mean Squared Error:",np.sqrt(mean_squared_error(Y_test[0],
test_predict_LSTM[:,0])))
```

```
# ### <font color="k"><strong> Append the LSTM Evalutaion Result
```

```
# In[21]:
```

```
result['LSTM']=[np.sqrt(mean_squared_error(Y_test[0], test_predict_LSTM[:,0])),
               mean_absolute_error(Y_test[0], test_predict_LSTM[:,0]),
```

```
r2_score(Y_test[0], test_predict_LSTM[:,0])
```

```
# In[22]:
```

```
plt.figure(figsize=(8,4), dpi=300)
plt.plot(history.history['loss'], label='Training Loss')
plt.plot(history.history['val_loss'], label='Validation Loss')
plt.title('Model loss for LSTM - San Marcos')
plt.ylabel('Loss')
plt.xlabel('Epochs')
plt.legend(loc='upper right')

plt.savefig('WindSpeed_LSTM_Loss_Model_San_Marcos.png', bbox_inches='tight')
plt.show();
```

```
# In[23]:
```

```
plt.rcParams['font.sans-serif'] = "Times New Roman"
plt.rcParams['font.family'] = "sans-serif"

plt.figure(figsize=(8,4),dpi=300)
#plt.plot(df['Wind Speed (m/s)'], color="blue", label='History')
plt.plot(Y_test[0], marker='.', label="Actual")
plt.plot(test_predict_LSTM[:,0], 'r', label="Prediction")
# plt.tick_params(left=False, labelleft=True) #remove ticks
plt.tight_layout()
sns.despine(top=True)
plt.subplots_adjust(left=0.07)
plt.ylabel("Wind Speed (m/s)", size=15)
plt.xlabel("Time step (hours)", size=15)
plt.legend(fontsize=15)

plt.savefig('WindSpeed_LSTM_Model_San_Marcos.png', bbox_inches='tight')
plt.show();
```

```
# In[24]:
```

```
plt.rcParams['font.sans-serif'] = "Times New Roman"
plt.rcParams['font.family'] = "sans-serif"
```

```
plt.figure(figsize=(8,4),dpi=300)
#plt.plot(df['Wind Speed (m/s)'], color="blue", label='History')
plt.plot(Y_test[0, 15580:], marker='.', label="Actual")
plt.plot(test_predict_LSTM[15581:,0], 'r', label="Prediction")
# plt.tick_params(left=False, labelleft=True) #remove ticks
plt.tight_layout()
sns.despine(top=True)
plt.subplots_adjust(left=0.07)
plt.ylabel("Wind Speed (m/s)", size=15)
plt.xlabel("Time step (hours)", size=15)
plt.legend(fontsize=15)

plt.savefig('WindSpeed_LSTM_ZOOM_Model_San_Marcos.png', bbox_inches='tight')
plt.show();
```

```
# In[25]:
```

```
result
```

```
# In[26]:
```

```
output=pd.DataFrame.from_dict(result, orient='index')
output.rename({0: 'MSE', 1: 'MAE', 2: 'R2'}, axis=1, inplace=True)
output
```

```
# In[27]:
```

```
Y_test.shape
```

```
# In[28]:
```

```
test_predict_LSTM.shape
```

```
## <center><font color="#110896"> Ensemble
```

```
# In[29]:
```

```

# making data again to remove inconsistencies
temp = df
dataset = temp['Wind Speed (m/s)'].dropna().values #numpy.ndarray
dataset = dataset.astype('float32')
dataset = np.reshape(dataset, (-1, 1))
scaler = MinMaxScaler(feature_range=(0, 1))
dataset = scaler.fit_transform(dataset)
train_size = 63110
test_size = len(dataset) - train_size
train, test = dataset[0:train_size,:], dataset[train_size:len(dataset),:]

def create_dataset(dataset, look_back):
    X, Y = [], []
    for i in range(len(dataset)-look_back-1):
        a = dataset[i:(i+look_back), 0]
        X.append(a)
        Y.append(dataset[i + look_back, 0])
    return np.array(X), np.array(Y)

look_back = 24      #it is in hours #can be changed(1-24) to get better prediction values
X_train, Y_train = create_dataset(train, look_back)
X_test, Y_test = create_dataset(test, look_back)

# reshape input to be [samples, time steps, features]
X_train = np.reshape(X_train, (X_train.shape[0], X_train.shape[1], 1))
X_test = np.reshape(X_test, (X_test.shape[0], X_test.shape[1], 1))

# In[30]:

rnn_model = tf.keras.models.load_model('rnn_model.h5')
lstm_model = tf.keras.models.load_model('lstm_model.h5')

# In[31]:

#Making the ensembl model

models = [rnn_model, lstm_model]

model_input = tf.keras.Input(shape=(X_train.shape[1], X_train.shape[2]))
model_outputs = [model(model_input) for model in models]
ensembled_output = tf.keras.layers.Average()(model_outputs)

```

```
ensembled_model = tf.keras.Model(inputs=model_input, outputs=ensembled_output)
```

```
# In[32]:
```

```
train_predict_ensembled = ensembled_model.predict(X_train)
test_predict_ensembled = ensembled_model.predict(X_test)
```

```
# In[33]:
```

```
# invert predictions
train_predict_ensembled = scaler.inverse_transform(train_predict_ensembled)
Y_train = scaler.inverse_transform([Y_train])
test_predict_ensembled = scaler.inverse_transform(test_predict_ensembled)
Y_test = scaler.inverse_transform([Y_test])
print("Train Mean Absolute Error:", mean_absolute_error(Y_train[0],
train_predict_ensembled[:,0]))
print("Train Root Mean Squared Error:", np.sqrt(mean_squared_error(Y_train[0],
train_predict_ensembled[:,0])))
print("Test Mean Absolute Error:", mean_absolute_error(Y_test[0], test_predict_ensembled[:,0]))
print("Test Root Mean Squared Error:", np.sqrt(mean_squared_error(Y_test[0],
test_predict_ensembled[:,0])))
```

```
##### <font color="k"><strong> Append the Ensembled Evalutaion Result
```

```
# In[34]:
```

```
result['ensembled']=[np.sqrt(mean_squared_error(Y_test[0,:-1], test_predict_ensembled[1:,0])),
                    mean_absolute_error(Y_test[0,:-1], test_predict_ensembled[1:,0]),
                    r2_score(Y_test[0,:-1], test_predict_ensembled[1:,0])]
```

```
# In[35]:
```

```
plt.rcParams['font.sans-serif'] = "Times New Roman"
plt.rcParams['font.family'] = "sans-serif"
```

```
plt.figure(figsize=(8,4),dpi=300)
#plt.plot(df['Wind Speed (m/s)'], color="blue", label='History')
```

```

plt.plot(Y_test[0], marker='.', label="Actual")
plt.plot(test_predict_ensembled[:,0], 'r', label="Prediction")
# plt.tick_params(left=False, labelleft=True) #remove ticks
plt.tight_layout()
sns.despine(top=True)
plt.subplots_adjust(left=0.07)
plt.ylabel("Wind Speed (m/s)", size=15)
plt.xlabel("Time step (hours)", size=15)
plt.legend(fontsize=15)

plt.savefig('WindSpeed_ensembled_Model_San_Marcos.png', bbox_inches='tight')
plt.show();

```

In[36]:

```

plt.rcParams['font.sans-serif'] = "Times New Roman"
plt.rcParams['font.family'] = "sans-serif"

plt.figure(figsize=(8,4),dpi=300)
#plt.plot(df['Wind Speed (m/s)'], color="blue", label='History')
plt.plot(Y_test[0, 15580:], marker='.', label="Actual")
plt.plot(test_predict_ensembled[15581:,0], 'r', label="Prediction")
# plt.tick_params(left=False, labelleft=True) #remove ticks
plt.tight_layout()
sns.despine(top=True)
plt.subplots_adjust(left=0.07)
plt.ylabel("Wind Speed (m/s)", size=15)
plt.xlabel("Time step (hours)", size=15)
plt.legend(fontsize=15)

plt.savefig('WindSpeed_ensembled_ZOOM_Model_San_Marcos.png', bbox_inches='tight')
plt.show();

```

 Evaluation Result of All Models

In[37]:

```

output=pd.DataFrame.from_dict(result, orient='index')
output.rename({0: 'MSE', 1: 'MAE', 2: 'R2'}, axis=1, inplace=True)
output

```

```
# # <center><font color="#110896"> All the 3 prediction graphs on a single plot to compare them easily
```

```
# In[38]:
```

```
output.plot(kind = "bar", figsize = (8,6))
plt.xlabel("Algorithm", fontsize = 16)
plt.xticks(rotation = 0,fontsize = 16)
plt.yticks(rotation = 0,fontsize = 16)
plt.ylabel("Score", fontsize = 16)
plt.title("Evaluation Result of All Models", fontsize = 20)
plt.legend(frameon = False, loc = 'best')
plt.show()
```

```
# In[39]:
```

```
plt.rcParams['font.sans-serif'] = "Times New Roman"
plt.rcParams['font.family'] = "sans-serif"
```

```
fig, (ax1, ax2, ax3) = plt.subplots(nrows=3, ncols=1, figsize=(12,16),dpi=300)
```

```
# Plot for RNN
```

```
ax1.plot(Y_test[0, 15580:], marker='.', label="Actual")
ax1.plot(test_predict_RNN[15581:,0], 'green', label="RNN Prediction")
ax1.set_xlabel("Time step (hours)", size=12)
ax1.set_ylabel("Wind Speed (m/s)", size=12)
ax1.legend(fontsize=8)
ax1.tick_params(left=False, labelleft=True)
ax1.set_title("RNN prediction Graph", fontsize=12)
```

```
# Plot for LSTM
```

```
ax2.plot(Y_test[0, 15580:], marker='.', label="Actual")
ax2.plot(test_predict_LSTM[15581:,0], 'purple', label="LSTM Prediction")
ax2.set_xlabel("Time step (hours)", size=12)
ax2.set_ylabel("Wind Speed (m/s)", size=12)
ax2.legend(fontsize=8)
ax2.tick_params(left=False, labelleft=True)
ax2.set_title("LSTM prediction Graph", fontsize=12)
```

```
# Plot for Ensembled
```

```
ax3.plot(Y_test[0, 15580:], marker='.', label="Actual")
ax3.plot(test_predict_ensembled[15581:,0], 'orange', label="Ensembled Prediction")
```

```

ax3.set_xlabel('Time step (hours)', size=12)
ax3.set_ylabel("Wind Speed (m/s)", size=12)
ax3.legend(fontsize=8)
ax3.tick_params(left=False, labelleft=True)
ax3.set_title("Ensembled prediction Graph", fontsize=12)
sns.despine(top=True)
plt.subplots_adjust(left=0.07)
plt.xlabel('Time Step (hours)', size=12)
plt.savefig('WindSpeed_Model_San_Marcos.png', bbox_inches='tight')
plt.show()

```

```
# In[40]:
```

```

plt.rcParams['font.sans-serif'] = "Times New Roman"
plt.rcParams['font.family'] = "sans-serif"

```

```
fig, (ax1) = plt.subplots(nrows=1, ncols=1, figsize=(8,4),dpi=300)
```

```
# Plot for RNN
```

```

ax1.plot(Y_test[0, 15580:], marker='.', label="Actual")
ax1.plot(test_predict_RNN[15581:,0], 'green', label="RNN Prediction")

```

```
# Plot for LSTM
```

```
ax1.plot(test_predict_LSTM[15581:,0], 'purple', label="LSTM Prediction")
```

```
# Plot for Ensembled
```

```
ax1.plot(test_predict_ensembled[15581:,0], 'orange', label="Ensembled Prediction")
```

```
ax1.set_ylabel("Wind Speed (m/s)", fontsize = 20)
```

```
ax1.legend(fontsize=11)
```

```
ax1.tick_params(left=False, labelleft=True)
```

```
sns.despine(top=True)
```

```
plt.subplots_adjust(left=0.07)
```

```
plt.xlabel('Time step (hours)', fontsize = 20)
```

```
plt.savefig('Combined_WindSpeed_All_Models_San_Marcos.png', bbox_inches='tight')
```

```
plt.show()
```

```
### <font color="k"><strong> saving the predicted wind speed in a csv
```

```
# In[41]:
```

```
# Creating a DataFrame to store the predicted wind speeds
predictions_df = pd.DataFrame({'Actual': Y_test[0:],
                              'RNN_Predictions': test_predict_RNN[:,0],
                              'LSTM_Predictions': test_predict_LSTM[:,0],
                              'Ensembled_Predictions': test_predict_ensembled[:,0]})

# Saving the DataFrame to a CSV file
predictions_df.to_csv('predicted_wind_speed1_HIGH_accuracy.csv', index=False)
```

REFERENCES

- Abbes, M., & Belhadj, J. (2012). Wind resource estimation and wind park design in El-Kef region, Tunisia. *Energy*, 40(1), 348–357. <https://doi.org/10.1016/j.energy.2012.01.061>
- ACUA. (n.d.-a). *ACUA - Wastewater Treatment and Disposal*. Retrieved March 26, 2023, from <https://www.acua.com/Services/Service-Directory/Wastewater-Disposal.aspx>
- ACUA. (n.d.-b). *Jersey-Atlantic Wind Farm Fact Sheet*. Atlantic County Utilities Authority. <https://www.acua.com/ACUA/media/Acua/Project/WindFarm.pdf>
- ACUA. (2011). *Atlantic County Utilities Authority, Green Initiatives*. https://www.njcleanenergy.com/files/file/success_stories/ACUA%202006%20Project%20of%20Year%20Award.pdf (Accessed 02.15.2022)
- Aditionu. (2020, May 10). Understanding of LSTM Networks. *GeeksforGeeks*. <https://www.geeksforgeeks.org/understanding-of-lstm-networks/>
- Akhoundi, A., & Nazif, S. (2018). Sustainability assessment of wastewater reuse alternatives using the evidential reasoning approach. *Journal of Cleaner Production*, 195, 1350–1376. <https://doi.org/10.1016/j.jclepro.2018.05.220>
- AlHajri, M., & El-Hawary, M. (2007). *Optimal Distribution Generation Sizing via Fast Sequential Quadratic Programming*. 63–66. <https://doi.org/10.1109/LESCPE.2007.4437354>
- Alhamid, M. (2022, May 12). *Ensemble Models: What Are They and When Should You Use Them? | Built In*. <https://builtin.com/machine-learning/ensemble-model>
- AmeriGEOSS Community Platform Datahub. (2019, July 27). *Monroe Water Treatment Plant Energy Consumption*. <https://data.amerigeoss.org/ca/dataset/monroe-water-treatment-plant-energy-and-water-consumption> (Accessed 05.12.2022)
- Antonopoulos, A. M. (2014). *Mastering Bitcoin: Unlocking Digital Cryptocurrencies*. O'Reilly Media, Inc.

- Asano, T., Maeda, M., & Takaki, M. (1996). Wastewater reclamation and reuse in Japan: Overview and implementation examples. *Water Science and Technology*, 34(11), 219–226.
[https://doi.org/10.1016/S0273-1223\(96\)00841-4](https://doi.org/10.1016/S0273-1223(96)00841-4)
- Bachmann, N., & La Cour, J. J. (2015). *Sustainable biogas production in municipal wastewater treatment plants* (p. 20). IEA Bioenergy.
- Bao, J., He, D., Luo, M., & Choo, K.-K. R. (2021). A Survey of Blockchain Applications in the Energy Sector. *IEEE Systems Journal*, 15(3), 3370–3381. <https://doi.org/10.1109/JSYST.2020.2998791>
- Bazen, E. F., & Brown, M. A. (2009). Feasibility of solar technology (photovoltaic) adoption: A case study on Tennessee’s poultry industry. *Renewable Energy*, 34(3), 748–754.
<https://doi.org/10.1016/j.renene.2008.04.003>
- Beaufays, F. (2015, August 11). *The neural networks behind Google Voice transcription* [Google research]. Googleblog.Com. <https://ai.googleblog.com/2015/08/the-neural-networks-behind-google-voice.html>
- Bertanza, G., Canato, M., & Laera, G. (2018). Towards energy self-sufficiency and integral material recovery in waste water treatment plants: Assessment of upgrading options. *Journal of Cleaner Production*, 170, 1206–1218. <https://doi.org/10.1016/j.jclepro.2017.09.228>
- Bi, X., Yang, J., & Yang, S. (2022). LCA-Based Regional Distribution and Transference of Carbon Emissions from Wind Farms in China. *Energies*, 15(1), Article 1.
<https://doi.org/10.3390/en15010198>
- Boulder. (2012). *City of Boulder, Colorado, wastewater facility solar electric system*.
http://www.bouldercolorado.gov/index.php?option¼com_content&view¼article&id¼8763&Itemid¼43482 (Accessed 03.6.2022).
- Bousquet, C., Samora, I., Manso, P., Rossi, L., Heller, P., & Schleiss, A. J. (2017). Assessment of hydropower potential in wastewater systems and application to Switzerland. *Renewable Energy*, 113, 64–73. <https://doi.org/10.1016/j.renene.2017.05.062>

- Breuel, T. M., Ul-Hasan, A., Al-Azawi, M. A., & Shafait, F. (2013). High-Performance OCR for Printed English and Fraktur Using LSTM Networks. *2013 12th International Conference on Document Analysis and Recognition*, 683–687. <https://doi.org/10.1109/ICDAR.2013.140>
- Brooklyn Microgrid | Community Powered Energy. (n.d.). Brooklyn Microgrid. Retrieved February 26, 2023, from <https://www.brooklyn.energy/about>
- Browning. (2001). *Wind power for the wastewater treatment plant*.
<http://www.browningmontana.com/wind.html> (Accessed 20.8.2022)
- Browning Montana. (n.d.). *Browning Montana—Wind Energy for the Wastewater Treatment Plant*. Retrieved March 26, 2023, from <http://www.browningmontana.com/wind.html>
- Bukhary, S., Batista, J., & Ahmad, S. (2020). An Analysis of Energy Consumption and the Use of Renewables for a Small Drinking Water Treatment Plant. *Water*, 12(1), Article 1.
<https://doi.org/10.3390/w12010028>
- Chae, K.-J., & Kang, J. (2013). Estimating the energy independence of a municipal wastewater treatment plant incorporating green energy resources. *Energy Conversion and Management*, 75, 664–672.
<https://doi.org/10.1016/j.enconman.2013.08.028>
- City of Boulder. (2007). *City of Boulder Wastewater Treatment Plant Master Plan*.
<https://bouldercolorado.gov/sites/default/files/2021-06/boulder-wastewater-treatment-plant-master-plan.pdf>
- City of San Marcos. (2023). *Electric Rates and Fees | City of San Marcos, TX*.
<https://www.sanmarcostx.gov/1434/Electric-Rates>
- Crawford, G. V. (2010). *Technology Roadmap for Sustainable Wastewater Treatment Plants in a Carbon-Constrained World*. <https://doi.org/10.2166/9781780403366>
- Crites, R., & Tchobanoglous, G. (1998). *Small and decentralized wastewater management systems*. McGraw Hill.
- Davis, M. L., & Cornwell, D. A. (2008). *Introduction to environmental engineering*. McGraw-Hill.
<https://entrospace.nilebasin.org/handle/20.500.12351/421>

- Donges, N. (2022, August). *What Are Recurrent Neural Networks? | Built In*. BuiltIn.
<https://builtin.com/data-science/recurrent-neural-networks-and- lstm>
- Dontas, G., & Glorfindel. (2010). *machine learning—What’s the difference between feed-forward and recurrent neural networks?* Cross Validated.
<https://stats.stackexchange.com/questions/2213/whats-the-difference-between-feed-forward-and-recurrent-neural-networks>
- Eftekhari, H., Al-Obaidi, A. S. M., & Eftekhari, S. (2022). Aerodynamic Performance of Vertical and Horizontal Axis Wind Turbines: A Comparison Review. *Indonesian Journal of Science and Technology*, 7(1), Article 1. <https://doi.org/10.17509/ijost.v7i1.43161>
- Energy and Food Nexus. (2019). *Renewable Energy in the Water, Energy and Food Nexus*. International Renewable Energy Agency (IRENA). https://www.irena.org/-/media/Files/IRENA/Agency/Publication/2019/Apr/IRENA_RE_Water_Energy_Food_2019.pdf
- EPA Fact Sheet. (2013). *Renewable Energy Fact Sheet: Wind Turbines*. United States Environmental Protection Agency. https://www.epa.gov/sites/default/files/2019-08/documents/wind_turbines_fact_sheet_p100il8k.pdf
- GBRA. (2022, February 22). San Marcos Water Treatment Plant Earns Eighth-Consecutive TCEQ Award. *Guadalupe-Blanco River Authority*. <https://www.gbra.org/news/2022/02/san-marcos-water-treatment-plant-earns-eighth-consecutive-tceq-award/>
- GBRA. (2023, March 21). Water Treatment. *Guadalupe-Blanco River Authority*.
<https://www.gbra.org/operations/water-treatment/>
- Giungato, P., Rana, R., Tarabella, A., & Tricase, C. (2017). Current Trends in Sustainability of Bitcoins and Related Blockchain Technology. *Sustainability*, 9(12), Article 12.
<https://doi.org/10.3390/su9122214>
- Gomes, J. F. P., & Cardoso, P. M. (2011). Notice on a Case Study on the Utilization of Wind Energy Potential on a Remote and Isolated Small Wastewater Treatment Plant. *Smart Grid and Renewable Energy*, 2011. <https://doi.org/10.4236/sgre.2011.23033>

- Greff, K., Srivastava, R. K., Koutník, J., Steunebrink, B. R., & Schmidhuber, J. (2017). LSTM: A Search Space Odyssey. *IEEE Transactions on Neural Networks and Learning Systems*, 28(10), 2222–2232. <https://doi.org/10.1109/TNNLS.2016.2582924>
- Gu, Y., Li, Y., Li, X., Luo, P., Wang, H., Wang, X., Wu, J., & Li, F. (2017). Energy Self-sufficient Wastewater Treatment Plants: Feasibilities and Challenges. *Energy Procedia*, 105, 3741–3751. <https://doi.org/10.1016/j.egypro.2017.03.868>
- Hartman, L. (2022, August 16). *Wind Turbines: The Bigger, the Better*. Energy.Gov. <https://www.energy.gov/eere/articles/wind-turbines-bigger-better>
- Hegar, G. (2023). *Franchise Tax Credit for Clean Energy Projects*. <https://comptroller.texas.gov/taxes/franchise/clean-energy.php>
- Heller, A. (2014, April). *Predicting Wind Power with Greater Accuracy*. <https://str.llnl.gov/april-2014/miller>
- Ikehata, K., Zhao, Y., Kulkarni, H. V., Li, Y., Snyder, S. A., Ishida, K. P., & Anderson, M. A. (2018). Water Recovery from Advanced Water Purification Facility Reverse Osmosis Concentrate by Photobiological Treatment Followed by Secondary Reverse Osmosis. *Environmental Science & Technology*, 52(15), 8588–8595. <https://doi.org/10.1021/acs.est.8b00951>
- Jasper, J. T., Nguyen, M. T., Jones, Z. L., Ismail, N. S., Sedlak, D. L., Sharp, J. O., Luthy, R. G., Horne, A. J., & Nelson, K. L. (2013). Unit Process Wetlands for Removal of Trace Organic Contaminants and Pathogens from Municipal Wastewater Effluents. *Environmental Engineering Science*, 30(8), 421–436. <https://doi.org/10.1089/ees.2012.0239>
- Jin, T., Ikehata, K., & Zhu, E. (2021). Advanced Potable Water Reuse Integrating with Renewal Energy: A Data-Driven Study for San Marcos. *Proposal Submitted to Office of Research and Sponsored Program, Texas State University*.
- Jin, T., & Tian, Z. (2010). Uncertainty analysis for wind energy production with dynamic power curves. *2010 IEEE 11th International Conference on Probabilistic Methods Applied to Power Systems*, 745–750. <https://doi.org/10.1109/PMAPS.2010.5528405>

- Jin, Y., Maleky, N., Kramer, N. A., & Ikehata, K. (2013). Health Effects Associated with Wastewater Treatment, Reuse, and Disposal. *Water Environment Research*, 85(10), 1954–1977.
<https://doi.org/10.2175/106143013X13698672323029>
- Kaldellis, J. K., & Apostolou, D. (2017). Life cycle energy and carbon footprint of offshore wind energy. Comparison with onshore counterpart. *Renewable Energy*, 108, 72–84.
<https://doi.org/10.1016/j.renene.2017.02.039>
- Kapalko, R. (2019, November 7). Predictive Model Ensembles: Pros and Cons / Blogs / Perficient. *Perficient Blogs*. <https://blogs.perficient.com/2019/11/07/predictive-model-ensembles-pros-and-cons/>
- Le, Ho, Lee, & Jung. (2019). Application of Long Short-Term Memory (LSTM) Neural Network for Flood Forecasting. *Water*, 11(7), 1387. <https://doi.org/10.3390/w11071387>
- Lemar, P. (2017). *Energy Data Management Manual for the Wastewater Treatment Sector* (p. 35). U.S. Department of Energy.
https://www.energy.gov/sites/prod/files/2018/01/f46/WastewaterTreatmentDataGuide_Final_0118.pdf
- Li, Y., Luo, X., Huang, X., Wang, D., & Zhang, W. (2013). Life Cycle Assessment of a municipal wastewater treatment plant: A case study in Suzhou, China. *Journal of Cleaner Production*, 57, 221–227. <https://doi.org/10.1016/j.jclepro.2013.05.035>
- Li, Z., Wu, D., Hu, C., & Terpenney, J. (2019). An ensemble learning-based prognostic approach with degradation-dependent weights for remaining useful life prediction. *Reliability Engineering & System Safety*, 184, 110–122. <https://doi.org/10.1016/j.ress.2017.12.016>
- Lian, J., Zhang, W., Sun, Y., Marinovici, L. D., Kalsi, K., & Widergren, S. E. (2018). *Transactive System: Part I: Theoretical Underpinnings of Payoff Functions, Control Decisions, Information Privacy, and Solution Concepts* (PNNL-27235_Part_1). Pacific Northwest National Lab. (PNNL), Richland, WA (United States). <https://doi.org/10.2172/1530612>

- Lindtner, S., Schaar, H., & Kroiss, H. (2008). Benchmarking of large municipal wastewater treatment plants treating over 100,000 PE in Austria. *Water Science and Technology*, 57(10), 1487–1493. <https://doi.org/10.2166/wst.2008.214>
- Liu, H., Mi, X., & Li, Y. (2018). Wind speed forecasting method based on deep learning strategy using empirical wavelet transform, long short-term memory neural network and Elman neural network. *Energy Conversion and Management*, 156, 498–514. <https://doi.org/10.1016/j.enconman.2017.11.053>
- Ma, Q. (2020). Comparison of ARIMA, ANN and LSTM for Stock Price Prediction. *E3S Web of Conferences*, 218, 01026. <https://doi.org/10.1051/e3sconf/202021801026>
- Madan, R., & Mangipudi, P. S. (2018). Predicting Computer Network Traffic: A Time Series Forecasting Approach Using DWT, ARIMA and RNN. *2018 Eleventh International Conference on Contemporary Computing (IC3)*, 1–5. <https://doi.org/10.1109/IC3.2018.8530608>
- Maisch, M. (2018, December 6). *Fremantle residents to trade solar energy using blockchain*. Pv Magazine Australia. <https://www.pv-magazine-australia.com/2018/12/06/fremantle-residents-to-trade-solar-energy-using-blockchain/>
- Manwell, J. F., McGowan, J. G., & Rogers, A. L. (2010). *Wind Energy Explained: Theory, Design and Application*. John Wiley & Sons.
- Marner, S. T., Schröter, D., & Jardin, N. (2016). Towards energy neutrality by optimising the activated sludge process of the WWTP Bochum-Ölbachtal. *Water Science and Technology*, 73(12), 3057–3063. <https://doi.org/10.2166/wst.2016.142>
- Masłoń, A., Wójcik, M., & Chmielowski, K. (2018). Efficient use of energy in wastewater treatment plants. *Energy Policy Studies*, No. 1 (2). <http://yadda.icm.edu.pl/baztech/element/bwmeta1.element.baztech-9d1d33a5-3ae6-4a9e-8e47-81a8b971946f>

- Mehr, A. S., MosayebNezhad, M., Lanzini, A., Yari, M., Mahmoudi, S. M. S., & Santarelli, M. (2018). Thermodynamic assessment of a novel SOFC based CCHP system in a wastewater treatment plant. *Energy*, *150*, 299–309. <https://doi.org/10.1016/j.energy.2018.02.102>
- Melbourne Water. (2021). *Melbourne Water*. <https://www.melbournewater.com.au/about/what-we-do/annual-report>
- Melbourne water database. (2021, April 9). *Melbourne Wastewater Treatment (East)—Daily Grid Electricity Consumption*. <https://data-melbournewater.opendata.arcgis.com/datasets/melbournewater::melbourne-wastewater-treatment-east-daily-grid-electricity-consumption/about> (Accessed 8.10.2022)
- Memarzadeh, G., & Keynia, F. (2020). A new short-term wind speed forecasting method based on fine-tuned LSTM neural network and optimal input sets. *Energy Conversion and Management*, *213*, 112824. <https://doi.org/10.1016/j.enconman.2020.112824>
- Mengelkamp, E., Gärttner, J., Rock, K., Kessler, S., Orsini, L., & Weinhardt, C. (2018). Designing microgrid energy markets: A case study: The Brooklyn Microgrid. *Applied Energy*, *210*, 870–880. <https://doi.org/10.1016/j.apenergy.2017.06.054>
- Moss, R. L., Tzimas, E., Kara, H., Willis, P., & Kooroshy, J. (2013). The potential risks from metals bottlenecks to the deployment of Strategic Energy Technologies. *Energy Policy*, *55*, 556–564. <https://doi.org/10.1016/j.enpol.2012.12.053>
- Muttamara, S. (1996). Wastewater characteristics. *Resources, Conservation and Recycling*, *16*(1), 145–159. [https://doi.org/10.1016/0921-3449\(95\)00052-6](https://doi.org/10.1016/0921-3449(95)00052-6)
- Odeh, R. P., & Watts, D. (2019). Impacts of wind and solar spatial diversification on its market value: A case study of the Chilean electricity market. *Renewable and Sustainable Energy Reviews*, *111*, 442–461. <https://doi.org/10.1016/j.rser.2019.01.015>

- Orsini, L., Kessler, S., Wei, J., & Field, H. (2019). 10—How the Brooklyn Microgrid and TransActive Grid are paving the way to next-gen energy markets. In W. Su & A. Q. Huang (Eds.), *The Energy Internet* (pp. 223–239). Woodhead Publishing. <https://doi.org/10.1016/B978-0-08-102207-8.00010-2>
- Pan, S.-Y., Snyder, S. W., Packman, A. I., Lin, Y. J., & Chiang, P.-C. (2018). Cooling water use in thermoelectric power generation and its associated challenges for addressing water-energy nexus. *Water-Energy Nexus*, *1*(1), 26–41. <https://doi.org/10.1016/j.wen.2018.04.002>
- Panepinto, D., Fiore, S., Zappone, M., Genon, G., & Meucci, L. (2016). Evaluation of the energy efficiency of a large wastewater treatment plant in Italy. *Applied Energy*, *161*, 404–411. <https://doi.org/10.1016/j.apenergy.2015.10.027>
- Parry, D. L. (2014). *Co-Digestion of Organic Waste Products with Wastewater Solids: Final Report with Economic Model*. <https://doi.org/10.2166/9781780405384>
- Pfeifer, A., Krajačić, G., Ljubas, D., & Duić, N. (2019). Increasing the integration of solar photovoltaics in energy mix on the road to low emissions energy system – Economic and environmental implications. *Renewable Energy*, *143*, 1310–1317. <https://doi.org/10.1016/j.renene.2019.05.080>
- Power, C., McNabola, A., & Coughlan, P. (2014). Development of an evaluation method for hydropower energy recovery in wastewater treatment plants: Case studies in Ireland and the UK. *Sustainable Energy Technologies and Assessments*, *7*, 166–177. <https://doi.org/10.1016/j.seta.2014.06.001>
- Powerledger. (2018, February 15). Project Update: Fremantle Smart City Development. *Powerledger*. <https://medium.com/power-ledger/project-update-fremantle-smart-city-development-b16ccce2eb8f>
- Puglia, G. L. O. R. I. A. (2013). *Lifw cycle cost analysis on wind turbines* [Chalmers University of Technology]. <https://publications.lib.chalmers.se/records/fulltext/179861/179861.pdf>
- Qasim, S. R. (2017). *Wastewater Treatment Plants: Planning, Design, and Operation, Second Edition* (2nd ed.). Routledge. <https://doi.org/10.1201/9780203734209>

- Qiao, J., & Zhang, W. (2018). Dynamic multi-objective optimization control for wastewater treatment process. *Neural Computing and Applications*, 29(11), 1261–1271.
<https://doi.org/10.1007/s00521-016-2642-8>
- Rahimi, F. A., & Ipakchi, A. (2012). Transactive Energy Techniques: Closing the Gap between Wholesale and Retail Markets. *The Electricity Journal*, 25(8), 29–35.
<https://doi.org/10.1016/j.tej.2012.09.016>
- Ren, B. (2020). The use of machine translation algorithm based on residual and LSTM neural network in translation teaching. *PLOS ONE*, 15(11), e0240663.
<https://doi.org/10.1371/journal.pone.0240663>
- Rodrigues Moreno, S., Gomes da Silva, R., Cocco Mariani, V., & dos Santos Coelho, L. (2020). Multi-step wind speed forecasting based on hybrid multi-stage decomposition model and long short-term memory neural network. *Energy Conversion and Management*, 213, 112869.
<https://doi.org/10.1016/j.enconman.2020.112869>
- Roeth, J. (2010). *WIND RESOURCE ASSESSMENT HANDBOOK* (NYSERDA Report 10-30 NYSERDA 9998; pp. 1–203). New York State energy research and development authority.
- Rott, E., Kuch, B., Lange, C., Richter, P., Kugele, A., & Minke, R. (2018). Removal of Emerging Contaminants and Estrogenic Activity from Wastewater Treatment Plant Effluent with UV/Chlorine and UV/H₂O₂ Advanced Oxidation Treatment at Pilot Scale. *International Journal of Environmental Research and Public Health*, 15(5), Article 5.
<https://doi.org/10.3390/ijerph15050935>
- Saad al-sumaiti, A., Ahmed, M. H., & Salama, M. M. A. (2014). Smart Home Activities: A Literature Review. *Electric Power Components and Systems*, 42(3–4), 294–305.
<https://doi.org/10.1080/15325008.2013.832439>
- Saeed, M. (2022, September 11). Understanding Simple Recurrent Neural Networks in Keras. *Machine Learning Mastery*. <https://machinelearningmastery.com/understanding-simple-recurrent-neural-networks-in-keras/>

- SCOR. (2022). *SC-OR Wastewater Treatment Plant Upgrade Environmental Documents*. Sewerage Commission - Oroville Region. <https://www.sc-or.org/sc-or-wastewater-treatment-plant-upgrade-environmental-documents>
- Secretariat. (2015, May 8). *Wastewater Management—A UN-Water Analytical Brief*. UN-Water. <https://www.unwater.org/publications/wastewater-management-un-water-analytical-brief>
- Sharma, S. (2017, September 6). *Activation Functions in Neural Networks*. Medium. <https://towardsdatascience.com/activation-functions-neural-networks-1cbd9f8d91d6>
- Shen, Y., Linville, J. L., Urgun-Demirtas, M., Mintz, M. M., & Snyder, S. W. (2015). An overview of biogas production and utilization at full-scale wastewater treatment plants (WWTPs) in the United States: Challenges and opportunities towards energy-neutral WWTPs. *Renewable and Sustainable Energy Reviews*, 50, 346–362. <https://doi.org/10.1016/j.rser.2015.04.129>
- Shewalkar, A. (2019). Performance evaluation of deep neural networks applied to speech recognition: RNN, LSTM and GRU. *Journal of Artificial Intelligence and Soft Computing Research*, Vol. 9, No. 4, 235–245. <https://doi.org/10.2478/jaiscr-2019-0006>
- Shizas, I., & Bagley, D. M. (2004). Experimental Determination of Energy Content of Unknown Organics in Municipal Wastewater Streams. *Journal of Energy Engineering*, 130(2), 45–53. [https://doi.org/10.1061/\(ASCE\)0733-9402\(2004\)130:2\(45\)](https://doi.org/10.1061/(ASCE)0733-9402(2004)130:2(45))
- Shumway, R. H., & Stoffer, D. S. (1982). An Approach to Time Series Smoothing and Forecasting Using the Em Algorithm. *Journal of Time Series Analysis*, 3(4), 253–264. <https://doi.org/10.1111/j.1467-9892.1982.tb00349.x>
- Silva, W. N., Henrique, L. F., Silva, A. F. P. da C., Dias, B. H., & Soares, T. A. (2022). Market models and optimization techniques to support the decision-making on demand response for prosumers. *Electric Power Systems Research*, 210, 108059. <https://doi.org/10.1016/j.epsr.2022.108059>
- Singhal, G. (2020). *Introduction to LSTM Units in RNN | Pluralsight*. <https://www.pluralsight.com/guides/introduction-to-lstm-units-in-rnn>

- Sioshansi, F. (2014). *Distributed Generation and its Implications for the Utility Industry*. Academic Press.
- Smagulova, K., & James, A. P. (2019). A survey on LSTM memristive neural network architectures and applications. *The European Physical Journal Special Topics*, 228(10), 2313–2324.
<https://doi.org/10.1140/epjst/e2019-900046-x>
- Software Cluster. (2023). *Peer Energy Cloud | software cluster*. <http://software-cluster.org/projects/peer-energy-cloud/> (accessed on 8 Feb 2023)
- SPGSolar. (2012). *Sewerage Commission—Oroville Region*. <http://www.spgsolar.com/markets-served/government-and-education/water-and-sanitation/sewagecommission-oroville-region/>. (Accessed 03.8.2022).
- Stehly, T., & Duffy, P. (2022). *2021 Cost of Wind Energy Review* (NREL Transforming Energy). National Renewable Energy Laboratory.
- Stoltzfus, J. (2022, May 5). *Why are artificial recurrent neural networks often hard to train?* Techopedia.Com. <http://www.techopedia.com/why-are-artificial-recurrent-neural-networks-often-hard-to-train/7/33332>
- Strazzabosco, A., Kenway, S. J., & Lant, P. A. (2019). Solar PV adoption in wastewater treatment plants: A review of practice in California. *Journal of Environmental Management*, 248, 109337.
<https://doi.org/10.1016/j.jenvman.2019.109337>
- Team, K. (n.d.). *Keras documentation: LSTM layer*. Retrieved November 1, 2022, from https://keras.io/api/layers/recurrent_layers/lstm/
- Thukral, M. K. (2021). *Emergence of blockchain-technology application in peer-to-peer electrical-energy trading: A review*. 104–123. <https://doi.org/10.1093/ce/zkaa033>
- Transactive Energy: An Overview*. (2017, April 19). NIST. <https://www.nist.gov/el/smart-grid-menu/hot-topics/transactive-energy-overview>

- Trendewicz, A. A., & Braun, R. J. (2013). Techno-economic analysis of solid oxide fuel cell-based combined heat and power systems for biogas utilization at wastewater treatment facilities. *Journal of Power Sources*, 233, 380–393. <https://doi.org/10.1016/j.jpowsour.2013.01.017>
- Tuller, S. E., & Brett, A. C. (1984). The Characteristics of Wind Velocity that Favor the Fitting of a Weibull Distribution in Wind Speed Analysis. *Journal of Applied Meteorology and Climatology*, 23(1), 124–134. [https://doi.org/10.1175/1520-0450\(1984\)023<0124:TCOWVT>2.0.CO;2](https://doi.org/10.1175/1520-0450(1984)023<0124:TCOWVT>2.0.CO;2)
- Vandebron. (2023). *Vandebron—Duurzame energie van Nederlandse bodem*. Vandebron. <https://vandebron.nl/> (accesses on 8 Feb 2023)
- Wang, C., Zhang, H., & Ma, P. (2020). Wind power forecasting based on singular spectrum analysis and a new hybrid Laguerre neural network. *Applied Energy*, 259, 114139. <https://doi.org/10.1016/j.apenergy.2019.114139>
- Wang, Y., Zhu, S., & Li, C. (2019). Research on Multistep Time Series Prediction Based on LSTM. *2019 3rd International Conference on Electronic Information Technology and Computer Engineering (EITCE)*, 1155–1159. <https://doi.org/10.1109/EITCE47263.2019.9095044>
- Wang, Z., Wang, Y., & Srinivasan, R. S. (2018). A novel ensemble learning approach to support building energy use prediction. *Energy and Buildings*, 159, 109–122. <https://doi.org/10.1016/j.enbuild.2017.10.085>
- Wang, Z., Wang, Y., Zeng, R., Srinivasan, R. S., & Ahrentzen, S. (2018). Random Forest based hourly building energy prediction. *Energy and Buildings*, 171, 11–25. <https://doi.org/10.1016/j.enbuild.2018.04.008>
- Westphall, J., & Martina, J. E. (2022). Blockchain Privacy and Scalability in a Decentralized Validated Energy Trading Context with Hyperledger Fabric. *Sensors*, 22(12), Article 12. <https://doi.org/10.3390/s22124585>

- Worrall, J. M., Cazalet, E. G., Cox, W. T., Rajagopal, N., Nudell, T. R., & Heitmann, P. D. (2016). *Transactive Energy Challenge Energy Management in Microgrid Systems* (pp. 1–5). http://www.coxsoftwarearchitects.com/Resources/TransactiveSystemsConf2016/tes2016_microgrids_paper_Final.pdf
- Wu, J., & Tran, N. K. (2018). Application of Blockchain Technology in Sustainable Energy Systems: An Overview. *Sustainability*, *10*(9), Article 9. <https://doi.org/10.3390/su10093067>
- Xu, J., Li, Y., Wang, H., Wu, J., Wang, X., & Li, F. (2017). Exploring the feasibility of energy self-sufficient wastewater treatment plants: A case study in eastern China. *Energy Procedia*, *142*, 3055–3061. <https://doi.org/10.1016/j.egypro.2017.12.444>
- Zafar, R., Mahmood, A., Razzaq, S., Ali, W., Naeem, U., & Shehzad, K. (2018). Prosumer based energy management and sharing in smart grid. *Renewable and Sustainable Energy Reviews*, *82*, 1675–1684. <https://doi.org/10.1016/j.rser.2017.07.018>
- Zhang, S., Xuan, J., Lyu, Z., & Fu, Y. (2020). Application Prospect of Blockchain in Renewable Energy Certificates. *Proceedings of the 4th International Conference on Computer Science and Application Engineering*, 1–5. <https://doi.org/10.1145/3424978.3425016>